www.cardiol.br

www.dicsbc.org

ABC Imagem Cardiovascular

Sociedade Brasileira de Cardiologia • ISSN 2675-312X • Volume 35, Nº 3, July/August/September 2022

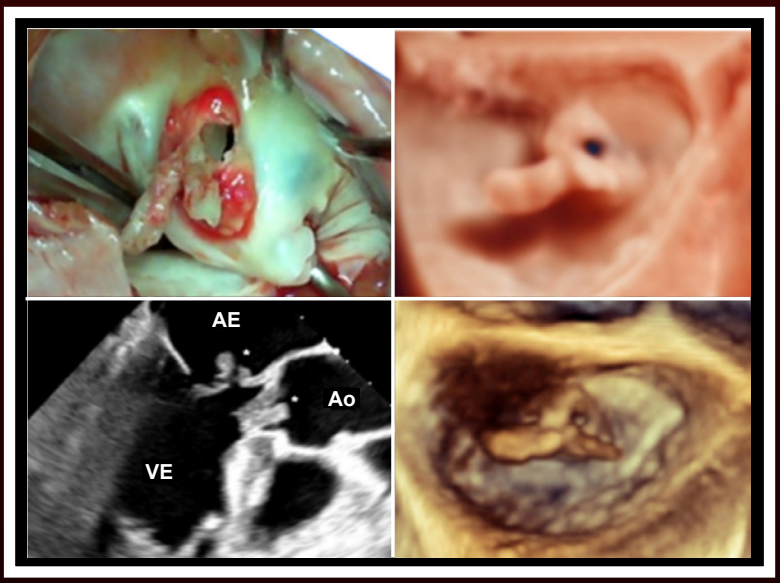

Arquivos Brasileiros de Cardiologia - Imagem Cardiovascular

Volume 35, Nº 3, July/August/September 2022

Indexing source: LILACS - Literatura Latino-Americana e do Caribe em Ciências da Saúde - www.bireme.br, LATINDEX - Sistema Regional de Información en Línea para Revistas Científicas de América Latina, El Caribe, España y Portugal - www.latindex.unam.mx

Department of Cardiovascular Imaging/ Brazilian Society of Cardiology
Rua Barata Ribeiro nº 380 cj.54
01308-000 - São Paulo - SP - Brasil
Fone/Fax: +55 (11) 3259-2988
Fones: +55 (11) 3120-3363
+55 (11) 3259-2988 / +55 (11) 2589-4168

Editorial Coordination
Atha Comunicação e Editora
Rua Machado Bittencourt, 190 - conj. 409
São Paulo, SP, Brasil
Tel.: (11) 50879502

Editorial Support
revista@dicsbc.com

The journal Arquivos Brasileiros de Cardiologia — Imagem Cardiovascular is the official body of the Department of Cardiovascular Imaging of the Brazilian Society of Cardiology.

The articles published here may only be reproduced upon express authorization given by the authors. Paid publications will not be accepted. Reprints of articles must be requested to the Editorial Department and will cost as much as the number of copies requested.

www.cardiol.br
www.dicsbc.org
ABC Imagem Cardiovascular

Contents - *Sumário*

Click on the title to read the article

www.cardiol.br
www.dicsbc.org
ABC Imagem Cardiovascular

www.cardiol.br
www.dicsbc.org
ABC Imagem Cardiovascular

Editorial Board Imagem Cardiovascular

Editor-in-chief
Dra. Daniela do Carmo Rassi Frota - Faculdade de Medicina e Hospital das Clínicas da Universidade Federal de Goiás, Hospital São Francisco de Assis, Goiânia – GO

Previous Editor
Dr. Silvio Henrique Barberato - CardioEco Centro de Diagnóstico Cardiovascular, Curitiba - PR,

Associate Editors

Dr. Alexandre Costa Souza – (Defesa profissional e Formação do Ecocardiografista) - Instituto Dante Pazzanese de Cardiologia, São Paulo - SP e Hospital São Rafael, Bahia - BA

Dra. Karen Saori Shiraishi Sawamura – (Ecocardiografia Pediátrica) - Instituto da Criança, Hospital das Clínicas, Faculdade de Medicina Universidade de São Paulo; Hospital Israelita Albert Einstein; Hospital do Coração; São Paulo - SP

Dr. Leonardo Sara da Silva – (Ressonância) - Centro de Diagnóstico por Imagem, Goiânia - GO

Dr. Marco S. Lofrano Alves – (Inovação e Inteligência Artificial) - Hospital de Clínicas da Universidade Federal do Paraná, Paraná - PR

Dr. Rafael Lopes – (Medicina Nuclear) - Hospital do Coração (Hcor), São Paulo - SP

Dra. Simone Nascimento dos Santos – (Ecocardiografia Vascular) - Hospital DF Star -Rede D'or e Eccos Diagnóstico Cardiovascular, Brasília - DF

Dr. Tiago Senra Garcia dos Santos – (Ressonância e Tomografia) - Instituto Dante Pazzanese de Cardiologia, Instituto do Coração Hospital das Clínicas da Faculdade de Medicina da Universidade de São Paulo (INCOR/FMUSP), São Paulo – SP

Dra. Viviane Tiemi Hotta – (Ecocardiografia Adulto) - Instituto do Coração Hospital das Clínicas da Faculdade de Medicina da Universidade de São Paulo (INCOR/FMUSP) e Fleury Medicina e Saúde, Faculdade de Medicina, Universidade de São Paulo, São Paulo – SP

National Editorial Board

Adelino Parro Junior - Instituto de Moléstias Cardiovasculares, São José do Rio Preto - SP

Adenalva Lima de Souza Beck - Instituto de Cardiologia do DF e Hospital Sirio Libanes de Brasília, Distrito Federal - DF

Adriana Pereira Glavam - Nuclear Medicine Department, Clínica de Diagnóstico Por Imagem - Diagnósticos da América SA (CDPI/DASA), Rio de Janeiro - RJ

Afonso Akio Shiozaki - Centro Diagnóstico do Hospital Paraná e Omega Diagnósticos, Paraná - PR

Afonso Yoshikiro Matsumoto - Fleury Medicina e Saúde, Rio de Janeiro – RJ

Alex dos Santos Félix - Instituto Nacional de Cardiologia, Rio de Janeiro – RJ

Alessandro Cavalcanti Lianza - Instituto da Criança (HC-FMUSP), Hospital Israelita Albert Einstein e Hospital do Coração, São Paulo - SP

Ana Clara Tude Rodrigues - Hospital das Clínicas da Faculdade de Medicina da Universidade de São Paulo (INCOR/FMUSP); Hospital Israelita Albert Einstein, São Paulo – SP

Ana Cláudia Gomes Pereira Petisco - Instituto Dante Pazzanese de Cardiologia, São Paulo - SP

Ana Cristina de Almeida Camarozano Wermelinger - Hospital da Cruz Vermelha, Cruz Vermelha Brasileira, Filial do Estado do Paraná, Curitiba – PR

Ana Cristina Lopes Albricker - Instituto Mineiro de Ultrassonografia e Hospital Universitário São José, Minas Gerais - MG

Ana Gardenia Liberato Ponte Farias - Universidade Federal do Ceará - Hospital Universitário Walter Cantídio, Ceará - CE

Ana Lúcia Martins Arruda - Hospital Sírio-Libanês, São Paulo - SP

André Luiz Cerqueira de Almeida - Santa Casa de Misericórdia de Feira de Santana, Bahia - BA

Andrea de Andrade Vilela - Instituto Dante Pazzanese de Cardiologia, São Paulo - SP

Andrea Maria Gomes Marinho Falcão - Instituto do Coração do Hospital das Clínicas da Faculdade de Medicina da Universidade de São Paulo (INCOR/FMUSP), São Paulo – SP

Andrei Skromov de Albuquerque - Grupo Fleury/Centro de Diagnóstico por Imagem do Hospital Alemão Oswaldo Cruz, São Paulo - SP

Andressa Mussi Soares - Hospital Evangélico de Cachoeiro de Itapemirim, Cachoeiro de Itapemirim, Espirito Santo – ES

Angele Azevedo Alves Mattoso - Hospital Santa Izabel - (SCMBA), Bahia – BA

Antonildes Nascimento Assunção Junior - Instituto do Coração do Hospital das Clínicas da Faculdade de Medicina da Universidade de São Paulo (INCOR/FMUSP), São Paulo – SP

Antônio Carlos Sobral Sousa - Universidade Federal de Sergipe, Sergipe - SE

Aristarco Gonçalves de Siqueira Filho - Universidade Federal do Rio de Janeiro, Rio de Janeiro - RJ

Armando Luis Cantisano - Hospital Barra D'Or - Rede D'Or São Luiz, Rio de Janeiro – RJ

Benedito Carlos Maciel - Faculdade de Medicina de Ribeirão Preto da Universidade de São Paulo, Hospital das Clínicas de Ribeirão Preto, Divisão de Cardiologia, São Paulo - SP

Brivaldo Markman Filho - Hospital das Clínicas da Universidade Federal de Pernambuco – PE

Bruna Morhy Borges Leal Assunção - Hospital Sírio Libanês e Instituto do Câncer do Estado de São Paulo (ICESP), São Paulo - SP

Caio Cesar Jorge Medeiros - Hospital São Luiz, São Paulo - SP

Carlos Eduardo Rochitte - Instituto do Coração do Hospital das Clínicas da Faculdade de Medicina da Universidade de São Paulo (INCOR/FMUSP), São Paulo - SP

Carlos Eduardo Suaide Silva - DASA (Diagnósticos da América) São Paulo - SP

Carlos Eduardo Tizziani Oliveira Lima - Hospital Casa de Saúde de Campinas, Campinas – SP

Cecília Beatriz Bittenciurt Viana Cruz - Instituto do Coração Hospital das Clínicas da Faculdade de Medicina da Universidade de São Paulo (INCOR/FMUSP), Hospital Sírio Libanês e Instituto do Câncer do Estado de São Paulo (ICESP), São Paulo - SP

Cintia Galhardo Tressino - Instituto Dante Pazzanese e Grupo DASA, São Paulo - SP

Claudia Cosentino Gallafrio - Hospital do GRAACC - Universidade Federal de São Paulo/Hospital Israelita Albert Einstein/Grupo DASA São Paulo - Alta diagnósticos, São Paulo – SP

Claudia Pinheiro de Castro Grau - Instituto do Coração Hospital das Clínicas da FMUSP e Hospital e Maternidade São Luiz, São Paulo - SP

Claudia Gianini Monaco - Hospital Israelita Albert Einstein, São Paulo - SP

Cláudio Henrique Fischer – Universidade Federal de São Paulo (UNIFESP) e Hospital Israelita Albert Einstein, São Paulo - SP

Cláudio Leinig Pereira da Cunha - Universidade Federal do Paraná, Curitiba - PR

Claudio Tinoco Mesquita - Universidade Federal Fluminense (UFF), Rio de Janeiro - RJ

Clerio Francisco de Azevedo Filho - Universidade do Estado do Rio de Janeiro (UERJ), Rio de Janeiro – RJ

David Costa de Souza Le Bihan - Instituto Dante Pazzanese da Cardiologia, São Paulo - SP

Djair Brindeiro Filho - Serviço de Ecocardiografia do Recife Ltda. e Real Hospital Português de Beneficência em Pernambuco - PE

Edgar Bezerra Lira Filho - Hospital das Clínicas, FMUSP; Hospital Israelita Albert Einstein, São Paulo – SP

Edgar Daminello - Hospital Israelita Albert Einstein, São Paulo – SP

Eliza de Almeida Gripp - Hospital Pró Cardíaco e do Hospital Universitário Antônio Pedro (UFF), Rio de Janeiro - RJ

Eliza Kaori Uenishi - Instituto do Coração do Hospital das Clínicas da Faculdade de Medicina da Universidade de São Paulo (INCOR/FMUSP), São Paulo - SP

Estela Suzana Kleiman Horowitz - Fundação Universitária de Cardiologia, Porto Alegre – RS

Fabio de Cerqueira Lario - Hospital Alemão Oswaldo Cruz, São Paulo – SP

Fabio Villaça Guimarães Filho - Faculdade de Medicina de Marília/Instituto do Coração de Marília, Marília – SP

Fernando Antônio de Portugal Morcerf - Ecor Ecocardiografia Ltda, Rio de Janeiro – RJ

Frederico José Neves Mancuso - Escola Paulista de Medicina - Universidade Federal de São Paulo (UNIFESP/EPM), São Paulo - SP

Gabriel Leo Blacher Grossman - Hospital Moinhos de Vento e Clínica Cardionuclear, Rio Grande do Sul – RS

Gabriela Liberato - Instituto do Coração do Hospital das Clínicas da Faculdade de Medicina da Universidade de São Paulo (INCOR/FMUSP), São Paulo - SP

Gabriela Nunes Leal - Hospital das Clínicas da Faculdade de Medicina da Universidade de São Paulo (HC-FMUSP), São Paulo - SP

Giordano Bruno de Oliveira Parente - Hospital Agamenon Magalhães, Recife - PE

Gláucia Maria Penha Tavares - Instituto do Coração do Hospital das Clínicas da Faculdade de Medicina da Universidade de São Paulo (INCOR/FMUSP) e Hospital Israelita Albert Einstein, São Paulo - SP

Henry Abensur - Departamento de Ecocardiografia, A Beneficência Portuguesa de São Paulo, São Paulo - SP

Ibraim Masciarelli Francisco Pinto - Instituto Dante Pazzanese de Cardiologia, São Paulo - SP

Ilan Gottlieb - Casa de Saúde São José e Clínica São Vicente, Rio de Janeiro - SP

Iran de Castro - Instituto de Cardiologia do Rio Grande do Sul (IC/FUC), Porto Alegre - RS

Isabel Cristina Britto Guimaraes - Hospital Ana Neri, Universidade Federal da Bahia, Bahia - BA

Ivan Romero Rivera - Universidade Federal de Alagoas, Maceió - AL

Jaime Santos Portugal - Proecho - Cardiologia Serviços Médicos Ltda, Rio de Janeiro - RJ

Jeane Mike Tsutsui - Instituto do Coração do Hospital das Clínicas da Faculdade de Medicina da Universidade de São Paulo (INCOR/FMUSP), Fleury Medicina e Saúde, São Paulo – SP

João Marcos Bemfica Barbosa Ferreira - Universidade do Estado do Amazonas, Amazonas - AM

José de Arimatéia Batista Araujo-Filho - Hospital Sírio-Libanês, São Paulo, Brasil. Memorial Sloan-Kettering Cancer Center, Nova Iorque – Estados Unidos.

José Lázaro de Andrade - Hospital Sírio Libanês, São Paulo – SP

José Luis de Castro e Silva Pretto - Hospital São Vicente de Paulo/Hospital de Clínicas de Passo Fundo, Rio Grade do Sul - RS

José Luiz Barros Pena - Hospital Felício Rocho, Belo Horizonte - MG

José Maria Del Castillo - Pronto Socorro Cardiológico de Pernambuco (PROCAPE - UPE), Recife – PE

José Olimpio Dias Júnior - Hospital Mater Dei, Belo Horizonte - MG

José Sebastião de Abreu - Clinicárdio de Fortaleza e Cardioexata, Fortaleza – PE

José Roberto Matos-Souza - Faculdade de Medicina da UNICAMP, São Paulo - SP

Joselina Luzia Menezes Oliveira - Fundação São Lucas, Aracaju – SE

Jorge Andion Torreão - Hospital Cárdio Pulmonar, Bahia – BA

Juliana Fernandes Kelendjian - CDI Centro de Diagnóstico por Imagem, Goiânia - GC

Laise Antonia Bonfim Guimarães - Sociedade Beneficente Israelita Brasileira de Ensino e Pesquisa Albert Einstein, são Paulo – SP

Lara Cristiane Terra Ferreira Carreira - Cardiologia Nuclear de Curitiba e Hospital Nossa Senhora do Pilar, Curitiba, Paraná – PR

Leina Zorzanelli - Instituto do Coração do Hospital das Clínicas da Faculdade de Medicina da Universidade de São Paulo (INCOR/FMUSP), São Paulo - SP

Lilian Maria Lopes - ECOKIDGRAFIA - Serviços Médicos Ecodoppler, São Paulo – SP

Liz Andréa Baroncini - Hospital da Cruz Vermelha e Instituto Saber e Aprender, Paraná - PR

Luciano Aguiar Filho - Hospital Salvaluz, DIAGMED (Tomografia e Ressonância Cardíaca), Hospital Municipal de Barueri e Instituto Dante Pazzanese de Cardiologia, São Paulo -SP

Luciano Herman Juaçaba Belém - Instituto Nacional de Cardiologia, Rio de Janeiro - RJ

Luiz Darcy Cortez Ferreira - OMNI - CCNI - Medicina Diagnóstica, São Paulo - SP

Luiz Felipe P. Moreira - Instituto do Coração do Hospital das Clínicas da Faculdade de Medicina da Universidade de São Paulo (INCOR/FMUSP), São Paulo - SP

Manuel Adán Gil – Universidade Federal de São Paulo – Escola Paulista de Medicina, São Paulo – SP

Marcela Momesso Peçanha - Instituto Dante Pazzanese de Cardiologia, São Paulo – SP

Marcelo Dantas Tavares - Universidade Federal da Paraíba, Paraíba - PB

Marcelo Haertel Miglioranza - Instituto de Cardiologia do Rio Grande do Sul, Rio Grande do Sul - RS

Marcelo Luiz Campos Vieira - Instituto do Coração do Hospital das Clínicas da Faculdade de Medicina da Universidade de São Paulo (InCor-HCFMUSP) e Hospital Israelita Albert Einstein, São Paulo - SP

Marcelo Souza Hadlich - Instituto Nacional de Cardiologia, INC., Hospital da Unimed-Rio, ACSC - Casa de Saúde São José, RioImagem CDI, Rede D´Or de Hospitais, Rede Labs D'Or, Rio de Janeiro – RJ

Marcia Azevedo Caldas - Faculdade de Medicina de Campos, Rio de Janeiro - RJ

Marcia de Melo Barbosa – ECOCENTER, Belo Horizonte – MG

Marcia Ferreira Alves Barberato - CardioEco – Centro de Diagnóstico Cardiovascular, Curitiba - PR

Márcio Silva Miguel Lima - Instituto do Coração do Hospital das Clínicas da Faculdade de Medicina da Universidade de São Paulo (InCor-HCFMUSP), São Paulo – SP

Marcio Sommer Bittencourt - Hospital Universitário de São Paulo/Hospital Israelita Albert Einstein, São Paulo - SP

Márcio Vinícius Lins de Barros - Faculdade de Saúde e Ecologia Humana FASEH, Vespasiano - MG

Marcos Valério Coimbra de Resende - Hospital Samaritano Paulista, São Paulo – SP

Maria Clementina Di Giorgi - Instituto do Coração do Hospital das Clínicas da Faculdade de Medicina da Universidade de São Paulo (InCor-HCFMUSP), São Paulo – SP

Maria do Carmo Pereira Nunes - Hospital das Clinicas da Faculdade de Medicina da UFMG, Minas Gerais - MG

Maria Eduarda Menezes de Siqueira - Setor de Ressonância Magnética Cardíaca - Universidade Federal de São Paulo (UNIFESP/EPM), São Paulo – SP

Maria Estefânia Bosco Otto - Hospital DF Star, Instituto de Cardiologia e Transplante do DF, Brasília, Distrito Federal - DF

Maria Fernanda Silva Jardim - Instituto de Cardiologia Dante Pazzanese/Hospital Samaritano de São Paulo, São Paulo - SP

Marly Maria Uellendahl Lopes - Serviço de Imagem Cardíaca Delboni-Auriemo/DASA, São Paulo - SP

Miguel Osman Dias Aguiar - Instituto do Coração do Hospital das Clínicas da Faculdade de Medicina da Universidade de São Paulo (InCor-HCFMUSP), São Paulo – SP

Minna Moreira Dias Romano - Faculdade de Medicina de Ribeirão Preto da Universidade de São Paulo, Hospital das Clínicas de Ribeirão Preto, São Paulo – SP

Mirela Frederico de Almeida Andrade - Universidade Federal da Bahia, Bahia – BA

Murillo Antunes - Faculdade de Medicina da Universidade São Francisco/ Instituto do Coração do Hospital das Clínicas da Faculdade de Medicina da Universidade de São Paulo (InCor-HCFMUSP), São Paulo – SP

Nathan Herszkowicz - Instituto de Radiologia do HC/FMUSP, São Paulo - SP

Orlando Campos Filho - Universidade Federal de São Paulo (UNIFESP), São Paulo - SP

Oscar Francisco Sanchez Osella - Universidade Católica de Brasília, Brasília - DF

Oswaldo Cesar de Almeida Filho - Hospital das Clínicas da Faculdade de Medicina de Ribeirão Preto, São Paulo – SP

Otavio Rizzi Coelho Filho - Quanta Diagnóstico por Imagem, Curitiba - PR

Paulo Zielinsky - Instituto de Cardiologia do Rio Grande do Sul - Universidade de Cardiologia Fetal, Porto Alegre – RS

Rafael Bonafim Piveta - Hospital Israelita Albert Einstein, São Paulo – SP

Rafael Borsoi - Quanta Diagnóstico por Imagem, Curitiba – PR

Renato de Aguiar Hortegal - Instituto Dante Pazzanese de Cardiologia/Hospital Beneficência Portuguesa de São Paulo, São Paulo - SP

Reginaldo de Almeida Barros - Hospital Beneficência Portuguesa, Bauru - SP

Roberto Caldeira Cury - Alta Diagnósticos, São Paulo - SP

Roberto Pereira - PROCAPE - Pronto Socorro Cardiológico de Pernambuco - Universidade de Pernambuco, Pernambuco - PE

Rodrigo Alves Barreto - Instituto Dante Pazzanese de Cardiologia, São Paulo – SP

Rodrigo Julio Cerci - Quanta Diagnóstico por Imagem, Curitiba - PR

Samira Saady Morhy - Departamento de Imagem Cardiovascular da Sociedade Brasileira de Cardiologia (DIC/SBC) e Hospital Israelita Albert Einstein, São Paulo - SP

Sandra da Silva Mattos - Real Hospital Português de Beneficência em Pernambuco, Recife – PE

Sandra Marques e Silva - Hospital de Base do Distrito Federal, Brasília - DF

Sandra Nivea dos Reis Saraiva Falcão - Universidade de Fortaleza, Ceara - CE

Sérgio Cunha Pontes Júnior - Instituto Dante Pazzanese de Cardiologia, São Paulo - SP

Silvio Henrique Barberato - CardioEco Centro de Diagnóstico Cardiovascular, Curitiba, PR, Brasil; Quanta Diagnóstico e Terapia, Curitiba, PR, Brasil; Sociedade Brasileira de Cardiologia, Rio de Janeiro – RJ

Simone Cristina Soares Brandão - Universidade Federal de Pernambuco, Pernanbuco - PE

Simone Rolim F. Fontes Pedra - Instituto Dante Pazzanese de Cardiologia, São Paulo – SP

Thais Harada Campos Espirito Santo - Hospital Ana Nery e Diagnoson Grupo Fleury, Bahia - BA

Tamara Cortez Martins - Hospital do Coração, São Paulo - SP

Valdir Ambrósio Moisés - Escola Paulista de Medicina (UNIFESP), São Paulo - SP

Valeria de Melo Moreira - Hospital do Coração / Instituto do Coração, São Paulo - SP - BR

Vera Márcia Lopes Gimenes - Hospital do Coração, São Paulo - SP

Vera Maria Cury Salemi - Faculdade de Medicina da Universidade de São Paulo - InCor/FMUSP, São Paulo – SP

Vicente Nicoliello de Siqueira - Universidade Federal de São Paulo (UNIFESP), São Paulo - SP

Zilma Verçosa Sá Ribeiro - Clínica Humaninhos, Salvador, Bahia - BA

Washington Barbosa de Araújo - Rede Labs D´or, Rio de Janeiro - RJ

Wercules Oliveira - Hospital Israelita Albert Einstein, São Paulo - SP

William Azem Chalela - Instituto do Coração do Hospital das Clínicas da Faculdade de Medicina da Universidade de São Paulo (INCOR/FMUSP), São Paulo - SP

Wilson Mathias Júnior - Instituto do Coração do Hospital das Clínicas da Faculdade de Medicina da Universidade de São Paulo (INCOR/FMUSP), Fleury Medicina e Saúde São Paulo, São Paulo - SP

International Editorial Board

Adelaide Maria Martins Arruda Olson – Mayo Clinic, Rochester, Minnessota – Estados Unidos

Anton E. Becker – Department of Cardiology, Thoraxcenter, Erasmus Medical Center, Rotterdam - Holanda

Daniel Piñeiro - Universidad de Buenos Aires - Argentina

Eduardo Escudero – Hospital Italiano de la Plata, Buenos Aires - Argentina

Eduardo Guevara – Fundación Favaloro, Buenos Aires - Argentina

Fernando Bosch – Policlínica Metropolitana, Caracas - Venezuela

Gustavo Restrepo Molina – Clinica Medillín, Medelín - Colombia

Harry Acquatella – Facultad de Medicina de la Universidad Central de Venezuela - Venezuela

João A.C.Lima – Johns Hopkins University Baltimore, Maryland – Estados Unidos

Jorge Lowenstein – Investigaciones Médicas y Diagnóstico Médico sede Cabildo, Buenos Aires - Argentina

Joseph Kisslo – Department of Medicine, Division of Cardiology, Duke University Hospital, Durham - Estados Unidos

Leopoldo Pérez De Isla – Unidad de Imagen Cardiovascular del Hospital Clínico San Carlos e Facultad de Medicina. Universidad Complutense de Madrid - Espanha

Mani A. Vannan – Structural and Valvular Center of Excellence, Piedmont Heart Institute, Atlanta, GA - Estados Unidos

Laura Mercer-Rosa - Perelman School of Medicine, University of Pennsylvania Children's Hospital of Philadelphia, Estados Unidos

Natesa Pandian – Cardiovascular Imaging Center, Tufts Medical Center, Boston, Massachusetts - Estados Unidos

Navin C. Nanda – Department of Cardiovascular Disease, University of Alabama, Birmingham, AL - Estados Unidos

Nuno Cardim - NOVA Medical School (Universidade Nova de Lisboa – NOVA), Congenital Heart Disease Center (Centro de doenças Cardíacas Hereditárias – CDCH), Hospital da Luz, Lisboa - Portugal

Raffaele De Simone – Department of Cardiac Surgery, Heidelberg University Hospital, Heidelberg, Germany - Alemanha

Ricardo Ronderos – FELLOW en American College of Cardiology, ICBA Instituto Cardiovascula, Instituto de Cardiologia La Plata - Argentina

Vera Rigolin – Department of Medicine/Cardiology, Northwestern University Feinberg School of Medicine, Chicago, Illinois - Estados Unidos

Vitor Coimbra Guerra, University of Toronto - Canadá

Department of Cardiovascular Imaging

President
André Luiz Cerqueira de Almeida - BA

Vice President of Echocardiography
Alex dos Santos Félix - RJ

Vice President of Nuclear Cardiology
Simone Cristina Soares Brandão - PE

Vice President of Vascular Echography
José Aldo Ribeiro Teodoro - SP

Vice President of Magnetic Resonance Imaging
Otávio Rizzi Coelho Filho - SP

Vice President of Computed Tomography
Márcio Sommer Bittencourt - SP

Vice President of Congenital Heart Disease and Pediatric Cardiology
Adriana Mello Rodrigues dos Santos - MG

Managing Director
Silvio Henrique Barberato - PR

Financial Director
Mohamed Hassan Saleh - SP

Journal Director
Daniela do Carmo Rassi Frota - GO

Board of Trustees

President
Fábio Villaça Guimarães Filho - SP

Members
Afonso Akio Shiozaki - PR
Bruna Morhy Borges Leal Assunção - SP
David Costa de Souza Le Bihan - SP
Jorge Andion Torreão - BA
José Luiz Barros Pena - MG
José Olimpio Dias Júnior - MG
Rafael Willain Lopes - SP

Scientific Committee

Coordinator
Alex dos Santos Félix - RJ

Members
Simone Cristina Soares Brandão - PE
José Aldo Ribeiro Teodoro - SP
Otávio Rizzi Coelho Filho - SP
Márcio Sommer Bittencourt - SP

Qualification Committee

Coordinator
Andrea de Andrade Vilela - SP

Adult Echo Members
Antônio Amador Calvilho Júnior - SP
Candice Machado Porto - BA
Eliza de Almeida Gripp - RJ
João Carlos Moron Saes Braga - SP
Rafael Modesto Fernandes – BA
Rudyney Eduardo Uchoa de Azevedo – SP
Sandra Nívea dos Reis Saraiva Falcão - CE

Congenital Echo Members
Carlos Henrique de Marchi - SP
Daniela Lago Kreuzig - SP
Halsted Alarcão Gomes Pereira da Silva - SP
Márcio Miranda Brito - TO

Seniors
Fábio Villaça Guimarães Filho - SP
Maria Estefânia Bosco Otto - DF
Solange Bernades Tatani - SP

Communication, Information and Internet Committee

Coordinator
José Roberto Matos Souza - SP

Members
Fabio Roston
Issam Shehadeh

Committee of Institutional Relations, Fees and Advocacy

Coordinator
Marcelo Haertel Miglioranza - RS

Members
Wagner Pires de Oliveira Júnior - DF

Committee of Education and Accreditation

Coordinator
Edgar Bezerra de Lira Filho - SP

Intersociety Committee

Coordinator
Marcelo Luiz Campos Vieira - SP

DIC Youth Committee

Coordinator
Eliza de Almeida Gripp - RJ

Positioning and Guidelines Committee

Coordinator
Marcelo Dantas Tavares de Melo - PB

Consultant
José Luiz Barros Pena - MG

Representatives

ASE
José Luiz Barros Pena - MG

EACVI
Alex dos Santos Félix - RJ

SISIAC
Ana Cristina de Almeida Camarozano - PR

Board of Former Presidents
Jorge Eduardo Assef - SP
Arnaldo Rabischoffsky - RJ
Samira Saady Morhy - SP
Marcelo Luiz Campos Vieira - SP
Carlos Eduardo Rochitte -SP

Board of Directors – Year 2022 (Brazilian Society of Cardiology)

North/Northeast
Nivaldo Menezes Filgueiras Filho (BA)
Sérgio Tavares Montenegro (PE)

East
Denilson Campos de Albuquerque (RJ)
Andréa Araujo Brandão (RJ) – Vice-presidente do Conselho Administrativo

State of São Paulo
Celso Amodeo (SP)
João Fernando Monteiro Ferreira (SP) – Presidente do Conselho Administrativo

Center
Carlos Eduardo de Souza Miranda (MG)
Weimar Kunz Sebba Barroso de Souza (GO)

South
Paulo Ricardo Avancini Caramori (RS)
Gerson Luiz Bredt Júnior (PR)

Editor of ABC Cardiol (2022-2025)
Carlos Eduardo Rochitte

Editor of IJCS (2022-2025)
Claudio Tinoco Mesquita

Presidents of State and Regional Chapters

SBC/AL – Pedro Henrique Oliveira de Albuquerque
SBC/BA – Joberto Pinheiro Sena
SBC/DF – Fausto Stauffer Junqueira de Souza
SBC/ES – Tatiane Mascarenhas Santiago Emerich
SBC/GO – Humberto Graner Moreira
SBC/MA – Francisco de Assis Amorim de Aguiar Filho
SBC/MG – Antônio Fernandino de Castro Bahia Neto
SBC/MS – Mauro Rogério de Barros Wanderley Júnior
SBC/NNE – José Albuquerque de Figueiredo Neto
SBC/PB – Guilherme Veras Mascena
SBC/PE – Carlos Japhet Da Matta Albuquerque
SBC/PI – Jônatas Melo Neto
SBC/PR – Olímpio R. França Neto
SOCERJ – Ronaldo de Souza Leão Lima
SBC/RN – Antônio Amorim de Araújo Filho
SOCERGS – Fábio Cañellas Moreira
SOCESP – Ieda Biscegli Jatene

Departments and Study Groups

SBC/DA – Marcelo Heitor Vieira Assad
SBC/DCC – Bruno Caramelli
SBC/DCC/CP – Cristiane Nunes Martins
SBC/DCM – Maria Cristina Costa de Almeida
SBC/DECAGE – José Carlos da Costa Zanon
SBC/DEIC – Mucio Tavares de Oliveira Junior
SBC/DEMCA – Álvaro Avezum Junior
SBC/DERC – Ricardo Quental Coutinho
SBC/DFCVR – Elmiro Santos Resende
SBC/DHA – Lucélia Batista Neves Cunha Magalhães
SBC/DIC – André Luiz Cerqueira de Almeida
SBCCV – João Carlos Ferreira Leal
SOBRAC – Fatima Dumas Cintra
SBHCI – Ricardo Alves da Costa
DCC/GECIP – Marcelo Luiz da Silva Bandeira
DCC/GECOP – Maria Verônica Câmara dos Santos
DCC/GEPREVIA – Isabel Cristina Britto Guimarães
DCC/GAPO – Luciana Savoy Fornari
DCC/GEAT – Carlos Vicente Serrano Junior
DCC/GECETI – João Luiz Fernandes Petriz
DCC/GEDORAC – Sandra Marques e Silva
DCC/GEECG – Nelson Samesima
DCC/GERTC – Adriano Camargo de Castro Carneiro
DEIC/GEICPED – Estela Azeka
DEIC/GEMIC – Marcus Vinicius Simões
DEIC/GETAC – Silvia Moreira Ayub Ferreira
DERC/GECESP – Marconi Gomes da Silva
DERC/GECN – Lara Cristiane Terra Ferreira Carreira
DERC/GERCPM – Pablo Marino Corrêa Nascimento

What does the navigator system in interventional procedures in the hybrid room?

O que o sistema navegador agrega aos procedimentos intervencionistas na sala híbrida?

Denisse Guzman Ramirez[1]; *Jose Maria Hernandez Hernandez*[2,3]

Hospital de Cardiología Unidad Medica de Alta Especialidad No. 34, Instituto Mexicano del Seguro Social[1], *Monterrey, México. Doctors Hospital*[2], *Monterrey, México. SISIAC*[3], *Santiago, Chile.*

What does the navigator system add to interventional procedures in the hybrid room?

The usefulness of two-dimensional fixed projection fluoroscopic imaging in the characterization of soft tissues and complex cardiac anatomy is limited. Moreover, it is currently insufficient for cardiac structural interventionism. Including recent three-dimensional cardiac ultrasound imaging techniques is necessary to improve anatomical images and spatial resolution.[1]

Fusion or hybrid imaging using two-dimensional fluoroscopy in combination with static or dynamic imaging obtained from cardiac computed tomography angiography (CCT), cardiac magnetic resonance (CMR), and transesophageal echocardiography (TEE) have been successfully used for structural cardiac interventions.[2] A fusion image is the superimposition of images acquired from different modalities within the same spatial coordinate. This image mapping process is called co-registration or image registration.

As the echocardiography/fluoroscopy fusion image arises in the catheterization laboratory, we must understand the need to obtain adequate-quality three-dimensional moving images since the use of static pre-procedural images such as CMR/CCT cannot improve the intraprocedural situation. With emerging technologies constantly improving TEE resolution, this imaging modality is considered ideal for guiding structural cardiac interventions. The first published proposal, provided by Gao et al. in 2010, merged echocardiographic and fluoroscopic images using specialized software.[3]

Concept

This method uses an image based on a two-/three-dimensional registration algorithm to locate the transesophageal probe; in this way, it is possible to follow its movement and superimpose the echocardiographic image on the fluoroscopic image when the C-arc moves. The fluoroscopic image is transferred together with the echocardiographic image; the initial clinical precision in the tissue was 1.5–4 mm. This technology was FDA approved for use in 2013 for the EchoNavigator (Philips Healthcare, Best, The Netherlands) and in 2017 for the TrueFusion (Siemens Healthineers, Erlangen, Germany).[2] The first study of the software prototype, published in 2013 in Switzerland, compared two groups of non-randomized patients who received mitral clips.[4]

Strengths

Using this technology, the TEE field of view is displayed as an outline to provide an additional point of reference by showing both fused images in motion. The TEE image provides critical perspectives on soft tissue anatomy. This fusion technology allows the use of markers placed on the echo image and automatically appears on the image fused with a fluoroscopic image. Finally, on the screen, three simultaneous viewing perspectives can be changed at the operator's convenience, which favors the intervention work's fluidity. (Table 1)

Disadvantages

Availability and cost are the most important factors influencing its routine use. Limited evidence-based information is currently available; in fact, experiences of some medical centers and publications of clinical cases are the primary data sources.

New Formats

Clinical cases have been published explaining echocardiographic fusion using CCT and fluoroscopy. Fusion with CCT allows the superimposing of images taken on previous days with fluoroscopy in real time. The information obtained from both imaging modalities is synergistic during structural cardiac interventions in which immediate feedback and precision are essential.[2,5] The preload conditions may vary between the timing of the tomographic acquisition and the timing of the intervention, causing some anatomical variability. Another limitation of CCT fusion is that the correlation with thoracic anatomy may become inconsistent after catheters and wires invade the thorax.

New TEE/fluoroscopic fusion versions have optimized this technology by adding a touch screen to the echocardiographic equipment to introduce markers and automatic reconstruction

Keywords

Echocardiography; Fluoroscopy; Cardiac Surgical Procedures.

Mailing Address: Jose Maria Hernandez •
Doctor's Hospital, Ecuador 2331, Balcones de Galerias Monterrey, Mexico.
E-mail: drchemahdez@gmail.com
Manuscript received 8/3/2022; revised 8/4/2022; accepted 8/8/2022

DOI: 10.47593/2675-312X/20223503eabc332

CC BY

plans for the aortic, mitral valve, and left atrial appendage (Figure 1). Both technologies feature these characteristics in which one-click valve modeling provides automated landmarks for live fusion.

The EchoNavigator added Truevue glass technology with Doppler color to evaluate the valvular regurgitation site in the fused image. Moreover, cavities such as the ventricle and atrium can be traced by the echocardiography equipment and the relevant images transmitted to the main screen (Figure 2).

Conclusions

Fusion echocardiography fluoroscopy is a valuable tool that can guide structural cardiovascular interventional procedures. This technology facilitates teamwork and potentially contributes to reducing the time, amount of radiation, and amount of intravenous contrast. It continues to be modernized, most recently with the advent of specific protocols for structural interventionism.

Authors' contributions

Guzman-Ramirez D and Hernandez-Hernandez JM: main ideas, selection of images; Guzman-Ramirez D: writing of the article, selection of articles; Hernandez-Hernandez JM: organization of the manuscript.

Conflict of interest

The author declares that he has no conflict of interest

Table 1 - Echocardiography/fluoroscopy fusion utility procedures.

Procedure	Radiation reduction	Contrast agent reduction	Time reduction	Catheters, guidelines, and device visualization	Landmarks during procedure	Safety and feasibility
Transeptal punction	88 p; retrospective[2]		88 p; retrospective[2]		88 p; retrospective[2]	88 p; retrospective[2]
Paravalvular leak closure				Sometimes can obscure guides and catheters[2]	Small paravalvular defects or retrograde approach[2]	
Transcatheter mitral valve repair	21 p vs 21 p; non-randomized[4]	21 p vs 21 p; non-randomized[4]	21 vs 21 p;[4] in more than one implanted clip, a clinical reduction in time was noted		Can be useful in suboptimal image quality or shadowing from the guide catheter[2]	21 p vs 21 p; non-randomized[4]
Left atrial appendage closure			Theoretically[2]	Facilitate LAA cannulation[2]	Facilitate device implantation[2]	Theoretically[2]
Transcatheter aortic valve replacement		Theoretic reduction in CKD non-suitable for CCT[2]		Theoretically better evaluation of wire and device position[2]		
Congenital heart disease in adults					51 p;[6] improved confidence	51 p[6]

CCT, cardiac computed tomography; CKD, chronic kidney disease; LAA, left atrial appendage. p: patients; Green: advantages obtained in the study; Orange: some advantages and disadvantages observed in the study; Red: no benefits observed in the study.

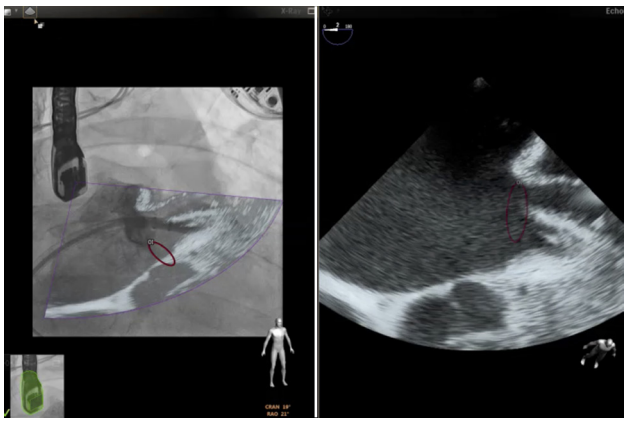

Source: Dr. Jose Maria Hernandez, Monterrey, México.

Figure 1 – *Left atrial appendage closure guidance. Note the oval mark is showing the site of the left atrial appendage ostium.*

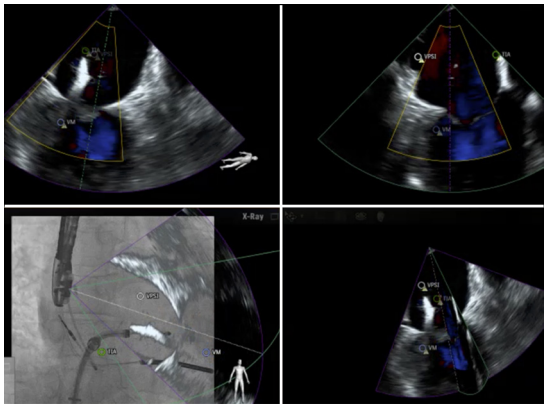

Source: Dr. Jose Maria Hernandez, Monterrey, México.

Figure 2 – *Fusion echocardiography/fluoroscopy in mitral clip guidance. Notice the three landmarks that provide safety during device implantation.*

References

1. Gao G, Penney G, Ma Y, Gogin N, Cathier P, Arujuna A, Morton G, Caulfield D, Gill J, Aldo Rinaldi C, Hancock J, Redwood S, Thomas M, Razavi R, Gijsbers G, Rhode K. Registration of 3D trans-esophageal echocardiography to X-ray fluoroscopy using image-based probe tracking. Med Image Anal. 2012 Jan;16(1):38-49. doi: 10.1016/j.media.2011.05.003.
2. Wiley BM, Eleid MF, Thaden JJ. Fusion Imaging for Procedural Guidance. Rev Esp Cardiol (Engl Ed). 2018 May;71(5):373-381. English, Spanish. doi: 10.1016/j.rec.2017.10.029.
3. Gao, G. et al. (2010). Rapid Image Registration of Three-Dimensional Transesophageal Echocardiography and X-ray Fluoroscopy for the Guidance of Cardiac Interventions. In: Navab, N., Jannin, P. (eds) Information Processing in Computer-Assisted Interventions. IPCAI 2010. Lecture Notes in Computer Science, vol 6135. Springer, Berlin, Heidelberg. https://doi.org/10.1007/978-3-642-13711-2_12
4. Sündermann SH, Biaggi P, Grünenfelder J, Gessat M, Felix C, Bettex D, Falk V, Corti R. Safety and feasibility of novel technology fusing echocardiography and fluoroscopy images during MitraClip interventions. EuroIntervention. 2014 Feb;9(10):1210-6. doi: 10.4244/EIJV9I10A203.
5. Safi LM, Jelnin V, Patel R, Oguayo K, Pasala TKR, Ruiz CE. Novel Use of Echo Fusion and Cardiac Computed Tomographic Imaging Guidance for Percutaneous Paravalvular Leak Closure. CASE (Phila). 2020 Jun 11;4(4):303-310. doi: 10.1016/j.case.2020.05.006.
6. Hadeed K, Hascoet S, Karsenty C, Chausseray G, Alacoque X, Dulac Y, et al. Echonavigator in children with congenital heart disease. Arch Cardiovasc Dis Supplements. 2019:11 (3);e307. Doi: 10.1016/j.acvdsp.2019.04.006.

Role of Echocardiography in Assessment of Patients with Suspected Ph: Beyond the Peak Tricuspid Regurgitant Velocity

Papel da Ecocardiografia na Avaliação de Pacientes com Suspeita de Hipertensão Pulmonar: Além da Velocidade de Pico do Jato de Insuficiência Tricúspide

Viviane Tiemi Hotta[1,2]

Instituto do Coração, Faculdade de Medicina, Universidade de São Paulo,[1] *(InCor/FMUSP) São Paulo, SP, Brazil. Fleury Medicina e Saúde,*[2] *São Paulo, SP, Brazil.*

Pulmonary hypertension (PH) causes great clinical and functional limitations and significantly impacts quality of life and survival.[1,2] Current pharmacological treatment options for PH include phosphodiesterase-5 inhibitors, endothelin receptor antagonists, and prostanoids. However, an early diagnosis and etiological definition are essential to improve prognosis.[3]

Transthoracic echocardiography (TTE) is the first-line test for suspected PH, as it is widely available, noninvasive, relatively low cost, does not involve radiation exposure, and carries minimal risk to patients. However, TTE can only suggest the diagnosis of PH since the definitive diagnosis requires invasive hemodynamic measurements via right heart catheterization.[4]

In addition to measuring pulmonary artery systolic pressure by analyzing the peak tricuspid regurgitant velocity, TTE evaluates diagnostic and prognostic variables.[4,5]

Brito et al. correlated parameters evaluated by TTE and invasive hemodynamic analysis, considered the diagnostic gold standard.[6] Despite the limited sample size, the study had adequate methodology and analyzed parameters such as right atrial area, mean pulmonary artery pressure, and right atrial strain in addition to conventional quantitative variables and free wall strain to analyze right ventricular systolic function.

Studies correlating right atrial deformations using invasive measurements are quite scarce in the literature, which makes the study by Brito et al. original and interesting. The analysis of atrial myocardial deformation may detect early signs of diastolic dysfunction; however, unlike left atrial strain analysis, which has an increasing role in several clinical scenarios, the value of right atrial strain analysis in clinical practice remains uncertain. The Brito et al. study presented a relevant proposal by incorporating new echocardiographic variables such as right atrial strain and right ventricular free wall strain associated with conventional measurements such as right atrial area, with a moderate correlation with invasive data. The analysis of the indexed volume of the right atrium and/or the association of variables in a study with a larger number of patients may improve the efficiency of TTE in the initial evaluation of patients with suspected PH.

Thus, although the definitive diagnosis of PH requires invasive right heart catheterization, new echocardiographic variables such as atrial and right ventricular strain analysis in addition to traditional right heart indices have a promising role in refining PH diagnosis, refining classification as well as improving prognosis.

Author contributions

Research conception and design: VTH; manuscript writing: VTH; Critical review of the manuscript for important intellectual content.

Conflict of interest

The author declares that he has no conflict of interest

References

1. Moreira EM, Gall H, Leening MJ, Lahousse L, Loth DW, Krijthe BP, et al. Prevalence of Pulmonary Hypertension in the General Population: The Rotterdam Study. PLoS One. 2015;10(6):e0130072. doi: https://doi.org/10.1371/journal.pone.0130072

2. Simonneau G, Montani D, Celermajer DS, Denton CP, Gatzoulis MA, Krowka M, et al. Haemodynamic definitions and updated clinical classification of pulmonary hypertension. Eur Respir J. 2019;53(1):1801913. doi: https://doi.org/10.1183/13993003.01913-2018.

Keywords

Pulmonary Hypretension; Echocardiography; Right Atrium; Right Ventricle.

Mailing Address: Viviane Tiemi Hotta •
Instituto do Coração HC-FMUSP, Unidade Clínica de Miocardiopatias e Doenças da Aorta. Av. Dr Enéas Carvalho de Aguiar, 55. CEP 05403-900, São Paulo, SP – Brazil.
E-mail: viviane.hotta@gmail.com
Manuscript received v8/2022; revised 7/8/2022; accepted 5/9/2022

DOI: 10.47593/2675-312X/20223503eed24

CC BY

3. Galiè N, Humbert M, Vachiery JL, Gibbs S, Lang I, Torbicki A, et al.; ESC Scientific Document Group. 2015 ESC/ERS Guidelines for the diagnosis and treatment of pulmonary hypertension: The Joint Task Force for the Diagnosis and Treatment of Pulmonary Hypertension of the European Society of Cardiology (ESC) and the European Respiratory Society (ERS): Endorsed by: Association for European Paediatric and Congenital Cardiology (AEPC), International Society for Heart and Lung Transplantation (ISHLT). Eur Heart J. 2016;37(1):67-119. doi: https://doi.org/10.1093/eurheartj/ehv317.

4. Masson-Silva JB, Silva Júnior CG. Como eu faço a avaliação ecocardiográfica na hipertensão pulmonar. Arq Bras Cardiol: Imagem cardiovasc. 2022; 35(1) ecom18. DOI: https://doi.org/10.47593/2675-312X/20223501ecom18

5. Rudski LG, Lai WW, Afilalo J, Hua L, Handschumacher MD, Chandrasekaran K, et al. Guidelines for the echocardiographic assessment of the right heart in adults: a report from the American Society of Echocardiography endorsed by the European Association of Echocardiography, a registered branch of the European Society of Cardiology, and the Canadian Society of Echocardiography. J Am Soc Echocardiogr. 2010;23(7):685-713; quiz 786-8. doi: https://doi.org/10.1016/j.echo.2010.05.010.

6. Brito AT, Silva JB, Rassi DC, Silva DG, Costa SA, Oliveira DS, et al. Correlação entre medidas ecocardiográficas e hemodinâmicas na avaliação do átrio direito e ventrículo direito em pacientes com hipertensão pulmonar. Arq Bras Cardiol: Imagem cardiovasc. 2022; DOI: 10.47593/2675-312X/20223503eabc308

My Approach to Managing Left Ventricular Diastolic Function of Children and in Congenital Heart Disease

Como eu Faço Avaliação de Função Diastólica do Ventrículo Esquerdo em Crianças e em Cardiopatias Congênitas

Laura Mercer Rosa[1,2]; *Samira Saady Morhy*[3,4]

[1]*Perelman School of Medicine, University of Pennsylvania, Pensilvânia;* [2]*Echolab Research Unity at Children's Hospital of Philadelphia, EUA;* [3]*Albert Einstein College of Health Sciences, São Paulo, SP;* [4]*Albert Einstein Israeli Benevolent Society, São Paulo, SP, Brasil.*

Echocardiography is the primary diagnostic method for assessing ventricular function in children and patients with congenital heart disease; however, it traditionally focuses on systolic function. Despite the growing interest in echocardiographic parameters for assessing diastolic function in children, diastolic dysfunction has been less investigated and, therefore, is less understood.

Some factors have limited this assessment:[1,3]

Although diastolic dysfunction is a component of pediatric heart disease, it remains rare in this population.

1. Doppler assessment parameters vary significantly with age, body surface area, and heart rate.

2. No single measurement adequately describes diastolic function like ejection fraction does for systolic function.

3. A gold standard parameter to diagnose diastolic dysfunction is lacking. Even measurements obtained during cardiac catheterization are inaccurate and provide partial information about ventricular diastole characteristics.

4. Considering these difficulties, available guidelines for assessing diastolic function apply to adults, not children.

The latest American Society of Echocardiography guidelines for echocardiographic studies in children were published 12 years ago and included diastolic function analysis parameters.[4] The recommended echocardiographic parameters for assessing diastolic function in this document include (Figure 1):

1. Mitral flow pulsed-wave Doppler: E and A wave velocities, E/A ratio, and E wave deceleration time;

2. Pulmonary venous flow pulsed-wave Doppler: S, D, and reverse A (Ar) wave velocities and Ar wave duration;

3. Left ventricular inlet/outlet flow continuous-wave Doppler: Isovolumetric relaxation time (IVRT);

4. Tissue Doppler: e' and a' wave velocities, E/e' ratio, and IVRT; and

5. Left atrial volume obtained in the apical four- and two-chamber planes.

Keywords

Child; Congenital Heart Disease; Echocardiography.

Mailing Address: Samira Saady Morh •
Avenida Albert Einstein, 627/701, Morumbi. CEP 05652-900 – São Paulo, SP, Brasil.
E-mail: samira.morhy@einstein.br
Manuscript received 4/15/2022; revised 5/30/2022; accepted 7/5/2022

DOI: 10.47593/2675-312X/20223503ecom29

CC BY

Obtaining normal values for the pediatric population is challenging. Cantinotti and Lopez[3] critically analyzed 33 studies of parameter nomograms obtained by Doppler to assess diastolic function, aiming to establish an ideal diastolic function nomogram for children and review its limitations, especially in neonates, and highlight its strengths. However, the authors reported several methodological limitations, such as a lack of standardization for obtaining parameters, normalizing the data, and presenting normal Z scores, percentiles, or mean values. Most studies adjusted for age, but few adjusted for body surface area and heart rate. The authors also reported a wide range of normal values for similar age groups.

Could the guidelines on diastolic dysfunction in adults prepared by the American and European Societies[5,6] (Figures 2 and 3) apply to children?

Dragulescu et al.[2] and Chang et al.[7] evaluated this question. Dragulescu et al.[2] evaluated children with dilated, restrictive, and hypertrophic cardiomyopathies and reported that these criteria were inadequate for diagnosing diastolic dysfunction in the study group and misdiagnosed diastolic dysfunction in the control group. They also observed that the wide range of pediatric normal reference values limited the diagnosis of diastolic dysfunction to a small number of cases. Chang et al.[7] evaluated children and adolescents with systemic lupus erythematosus and reported that all diastolic function parameters were changed in the study versus control group. However, none of the cases met the criteria for diastolic dysfunction found in the adult guidelines.

Considering this complexity, how should left ventricular diastolic function be assessed in children? We suggest the method proposed by Frommelt[1], which included a Doppler analysis of pulmonary and mitral venous flow in all children (Figure 4) followed by tissue Doppler assessment of the mitral annulus, atrial volume, and strain rate. Despite its challenges, diagnosing diastolic dysfunction in children, an echocardiographic evaluation is critical. However, new standardized studies should be conducted to determine normal parameters for different age groups.

Authors' contributions

Research conception and design: Mercer-Rosa L and Saady SM. Data collection: Mercer-Rosa and Samira Saady SM. Data analysis and interpretation: Mercer-Rosa L and Saady SM; Critical review of the manuscript for intellectual content: Mercer-Rosa L and Saady SM.

Conflict of interest

The author declares that he has no conflict of interest

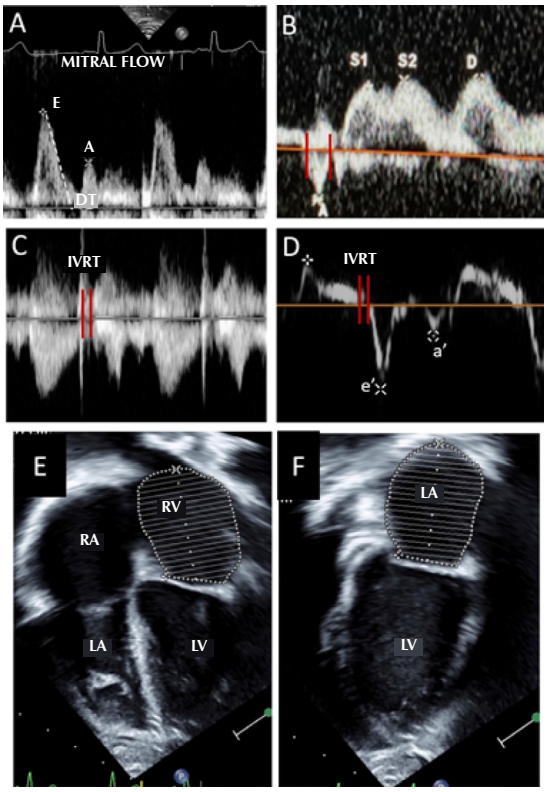

TD: tempo de desaceleração; TRIV: tempo de relaxamento isovolumétrico; AE: átrio esquerdo; VE: ventrículo esquerdo; VD: ventrículo direito; AD: átrio direito.

Figure 1 – *A: Mitral flow pulsed-wave Doppler: E and A wave velocities, E/A ratio, and deceleration time (DT). B: Pulmonary venous flow pulsed-wave Doppler: S, D, and reverse A wave velocities, and reverse A wave duration. C: Left ventricular inlet/outlet flow continuous-wave Doppler: isovolumetric relaxation time (IVRT). D: Tissue Doppler: e' and a' wave velocities, E/e' ratio, and isovolumetric relaxation time (IVRT). E: Left atrial (LA) volume obtained in the apical four- and F: two-chamber planes.*

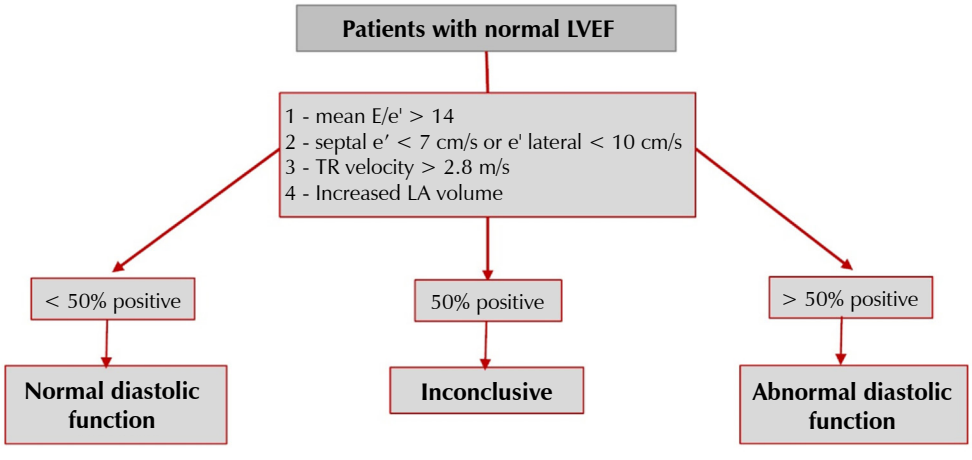

Source: Nagueh et al.[6] LA, left atrium; TR, tricuspid regurgitation.

Figure 2 – *Algorithm for diagnosing left ventricular diastolic dysfunction in adult patients with a normal left ventricular ejection fraction.*

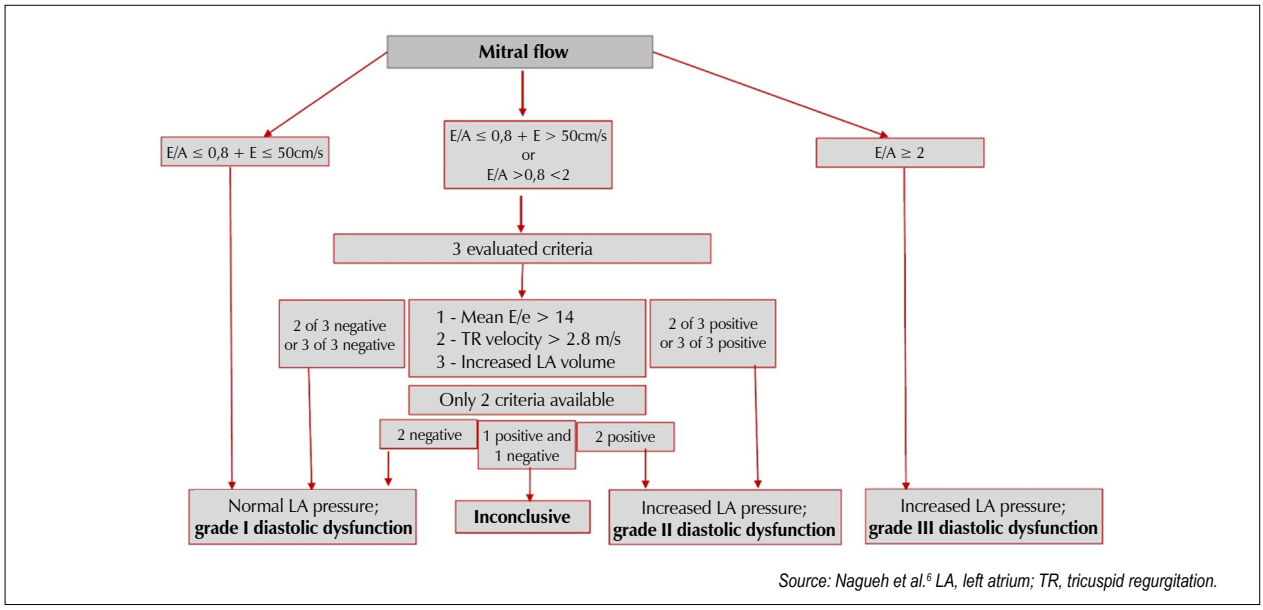

Source: Nagueh et al.[6] LA, left atrium; TR, tricuspid regurgitation.

Figure 3 – *Algorithm for left ventricular diastolic dysfunction graduation in adult patients with cardiomyopathies and a normal left ventricular ejection fraction.*

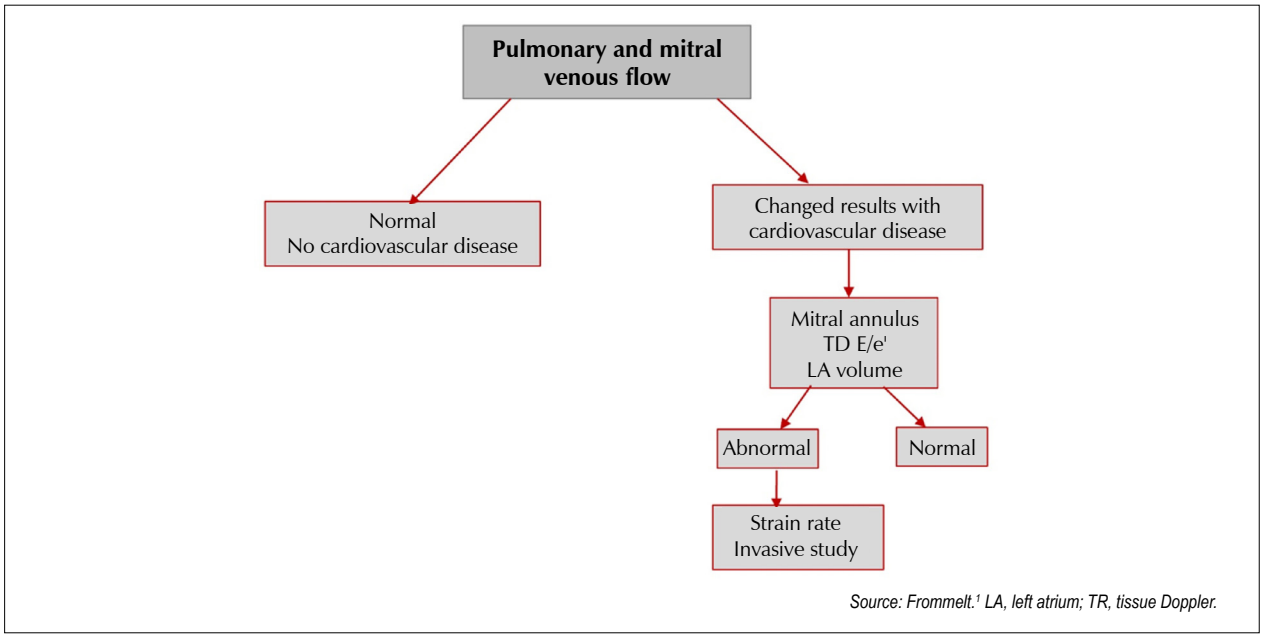

Source: Frommelt.[1] LA, left atrium; TR, tissue Doppler.

Figure 4 – *Algorithm for assessing left ventricular diastolic function in children.*

References

1. Frommelt PC. Diastolic ventricular function assessment. Lai W, Mertens M, Cohen MS, Geva T. Echocardiography in pediatric and congenital heart disease - from fetus to adult. USA: John Willey & Sons LTD.; 2009. p. 95-116.
2. Dragulescu A, Mertens L, Friedberg MK. Interpretation of left ventricular diastolic dysfunction in children with cardiomyopathy by echocardiography: problems and limitations. Circ Cardiovasc Imaging. 2013;6(2):254-61. doi: 10.1161/CIRCIMAGING.112.000175
3. Cantinotti M, Lopez L. Nomograms for blood flow and tissue Doppler velocities to evaluate diastolic function in children: a critical review. J Am Soc Echocardiogr. 2013;26(2):126-41. doi: 10.1016/j.echo.2012.11.017
4. Lopez L, Colan SD, Frommelt PC, Ensing GJ, Kendall K, Younoszai AK, et al. Recommendations for quantification methods during the performance of a pediatric echocardiogram: a report from the Pediatric Measurements Writing Group of the American Society of Echocardiography Pediatric and

Congenital Heart Disease Council. J Am Soc Echocardiogr. 2010;23(5):465-95; quiz 576-7. doi: 10.1016/j.echo.2010.03.019

5. Nagueh SF, Appleton CP, Gillebert TC, Marino PN, Oh JK, Smiseth OA, et al. Recommendations for the evaluation of left ventricular diastolic function by echocardiography. J Am Soc Echocardiogr. 2009;22(2):107-33. doi: 10.1016/j.echo.2008.11.023

6. Nagueh SF, Smiseth OA, Appleton CP, Byrd BF 3rd, Dokainish H, Edvardsen T, et al. Recommendations for the Evaluation of Left Ventricular Diastolic Function by Echocardiography: An Update from the American Society of Echocardiography and the European Association of Cardiovascular Imaging. J Am Soc Echocardiogr. 2016;29(4):277-314. doi: 10.1016/j.echo.2016.01.011

7. Chang JC, White BR, Elias MD, Xiao R, Knight AM, Weiss PF, et al. Echocardiographic Assessment of Diastolic Function in Children with Incident Systemic Lupus Erythematosus. Pediatr Cardiol. 2019;40(5):1017-25. doi: 10.1007/s00246-019-02107-1

My Approach to Lung Ultrasound to Evaluate Extravascular Lung Water

Como Eu Faço Ultrassom de Pulmão para Avaliar Congestão

[1]Cardiology and Transplant Institute of the Federal District. [2]DF Star. [3]Dante Pazzanese Cardiology Institute. [4]Samaritano Hospital.

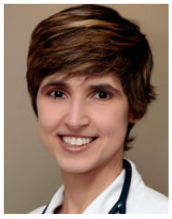

Maria Estefânia Bosco Otto[1,2]

Vanessa Andreoli Esmanhoto[3,4]

Introduction

A clinical history, physical examination, and focused ultrasound can accelerate the appropriate diagnosis and treatment of patients with progressive or acute dyspnea.[1] Extravascular lung water (EVLW) is easily detected with lung ultrasound (LUS). Pivetta et al.[2] reported excellent accuracy detecting EVLW by clinical evaluation and by the presence of "B" lines on LUS heigher than B natriuretic peptide dosage.

The usefulness of LUS for intensive care unit patients was described in the 1980s, later than that of other ultrasound modalities.[3] LUS is useful not only for diagnosing EVLW but also for risk stratification in myocardial infarction[4] and acute congestive heart failure (CHF).[5]

Echocardiologists can easily learn this technique, which requires moving the transducer only a few centimeters from the usual accustic window used in echocardiography.

My approach to the technique

Equipment and transducers

Simple and hand-held ultrasound equipment can obtain adequate LUS images. If the equipment has no lung presets, the abdominal preset is most appropriate due to its higher persistence. However, the adult cardiac preset can be used without losing information despite its reduced persistence.

Three types of transducers can be used for LUS: 5-MHz convex, 3–5-MHz sectorial, and 5–12-MHz linear, the latter specifically to better assess the pleural line and slip. The sector transducer is most commonly used by echocardiologists due to ease of use and its narrow surface, which facilitates its transverse or longitudinal placement in the intercostal spaces.[6] The transducer can be used perpendicularly to the rib cage for rib visualization above and below the intercostal space. The ribs generate acoustic shadows that form an image called the bat sign (Figure 1).

Patient positioning and LUS protocols

LUS can be performed with the patient in supine or seated position. Air-predominant structures will be positioned more apically and anteriorly (such as air trapped in a pneumothorax), while fluids will be located more inferiorly and posteriorly (as in pleural effusion). Thus, the patient should be kept at a 30–45 degree chest inclination for the assessment of pleural effusion.[7]

The Bedside Lung Ultrasound in Emergency (BLUE) protocol, schematically described in Figure 2A, enables a more systematic chest evaluation.[8] This protocol divides the anterior region of the chest into eight segments from the right and left anterior axillary line. Each segment should be evaluated for the presence of the pulmonary artifact patterns described below. In addition to these eight anterior quadrants, the right and left costophrenic space region in the posterior axillary line should be evaluated for pleural effusion (Figure 2B).

LUS findings

Normal findings

Pleural line

The pleural line is a more superficial hyperechogenic structure that is actually the only normal lung image finding that is not an artifact. This line slides (between the parietal and visceral pleura) with respiratory movements. The absence of this movement may indicate pneumothorax which is beyond the scope of this article (Figure 1).[9]

A lines

The presence of air in the lung prevents proper ultrasound imaging. Thus, aerated lungs result in no interpretable

Keywords

Ultrasonography; Lung; Dyspneia.

Mailing Address: Maria Estefânia Bosco Otto •
E-mail: mariaestefaniaotto@gmail.com
Manuscript received 5/30/2022; revised 6/13/2022; accepted 6/17/2022.

DOI: 10.47593/2675-312X/20223503ecom22

CC BY

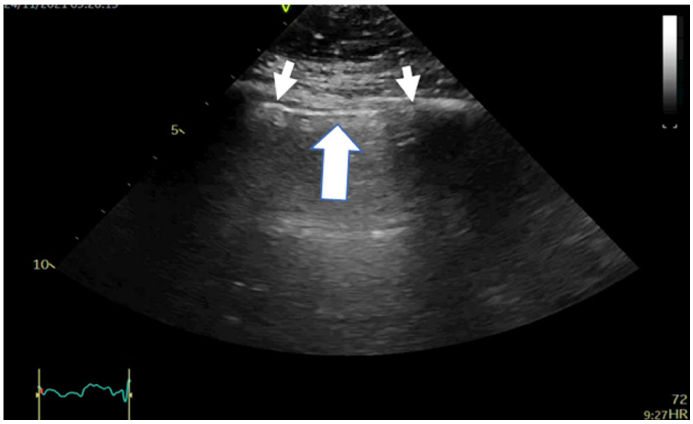

Source: Internal archive of the Echocardiography Department of Dante Pazzanese Cardiology Institute.

Figure 1 – *Lung ultrasound image with the transducer in the longitudinal position. Larger arrow, pleural line; smaller arrows, acoustic shadow of the rib called the bat sign.*

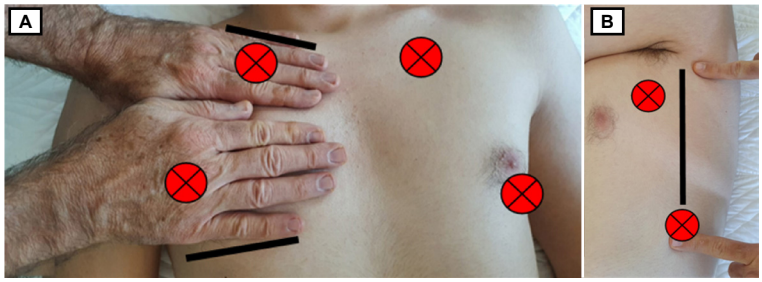

Source: Image produced by Dr. Maria Estefânia Bosco Otto based on information from several sources.[6,8–10]

Figure 2 – *Schematic representation of the Bedside Lung Ultrasound in Emergency (BLUE) protocol. A. Anterior chest analysis; B. Costophrenic sinus analysis using the posterior axillary line as a reference. A, B: Model to locate the points to be evaluated by lung ultrasound (LUS) using the BLUE protocol. Figure A: Using both hands on the patient's hemithorax with the superior little finger just below the clavicle (black line above the little finger) excluding the thumbs, and the inferior region of the other hand is positioned at the diaphragmatic line (black line). The "superior BLUE" point (red) is in the middle of the superior hand. The "inferior BLUE" point is in the middle of the inferior palm. These four points follow the anatomy of the lung and avoid the cardiac area. Figure B: The costophrenic sinus region point (red) is constructed from the horizontal line continuing the inferior BLUE point and the vertical line continuing the posterior axillary line (black). A superior point can be added between the posterior and anterior axillary line on the upper thorax floor. Thus, we will have four points in each hemithorax. This is a suggestion of a standardized location, but depending on the patient's anatomy and size of the cardiac area, adaptations can be made to obtain the pulmonary window.*

ultrasound findings. However, the hyperechogenic pleural line causes part of the ultrasound to reflect back to the transducer and another part to propagate in the aerated lung, causing a reverberation phenomenon with several equidistant "A" or pleural lines. This normal finding is called the "A" pattern and is more visible in thin patients or those with lung hyperinflation (emphysema) (Figure 3A).[9]

Abnormal findings

B lines

As the air content of the lung parenchyma is reduced, the density of the lung increases due to the increased presence of EVLW, exudate, transudate (in edema), collagen, or blood. Increased parenchymal density leads to contrast between lung structures, which now contain water in addition to air, and the ultrasound wave can be repeatedly reflected at deeper points from the pleura, creating vertical reverberation artifacts extending through the entire ultrasound accustic window depth. These artifacts are called "B" lines or comet tails. B lines move along the pleural line following its sliding with breathing. The number of B lines increases with increasing EVLW volume. A diagnosis of increased EVLW in a chest quadrant is significant in the presence of more than two B lines, being bilaterally considered significant EVLW by the BLUE protocol if four quadrants present more than two B lines (Figure 3B).[9] Sometimes B lines coalesce, forming a gray or white lung pattern that hinders A line visualization (Figure 3C).[9,10]

Consolidation

Other findings such as consolidation and air bronchograms reflect the presence of a pulmonary process with increased

extravascular fluid. These findings are common in pulmonary embolism, bacterial or viral pneumonia, and atelectasis (Figure 3D).[9]

Search for pleural effusion

LUS is a sensitive tool for detecting pleural effusion. It can detect effusion volumes of 20 ml, while a chest X-ray detects only volumes larger than 100 ml. Pleural effusion detection should include a bilateral costophrenic sinus analysis (Figures 2B, 4). Some authors recommend the use of formulas to evaluate pleural effusion volume. The most commonly used is the Balik formula, in which effusion volume (ml) = 20 × the greatest transversal distance containing the pleural effusion in millimeters.[7]

How to describe changes in a structured lung report

Figure 5 shows a sequential report model for the eight-segment BLUE protocol understanding of the findings clinician's understanding of the findings. It is essential to describe findings on the right and left sides of each segment using a table. For more extensive lung involvement, segmentation can be expanded to 12, 16, or 32 segments.[9,10] However, the eight-segment protocol is practical and adds important information for echocardiologists who use LUS as a complement to echocardiography.

Conclusion

LUS was neglected for decades, but it has recently become indispensable for outpatient follow-up[11] or for the emergency treatment[5] of patients with dyspnea. LUS is fast and simple and provides crucial information. It is also of low cost and can be performed at the bedside using portable equipment. LUS is not a substitute for clinical examinations and should be considered in the context of the patient's history.

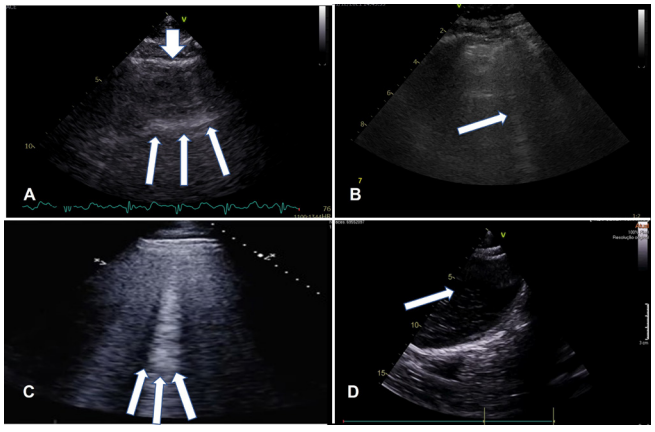

Source: Institute and the Cardiology and Transplant Institute of the Federal District.

Figure 3 – *Lung ultrasound findings in the parenchyma. Internal archive of the Echocardiography Department of Dante Pazzanese Cardiology. A. Lung ultrasound (LUS) quadrant. Thick arrow: pleural line; slin arrow: A line. B. LUS quadrant. Arrow: B line. C. LUS quadrant with coalescing B lines (arrows). It is not possible to differentiate A lines, only the pleural line. D. LUS quadrant showing consolidation and some air bronchograms (arrow).*

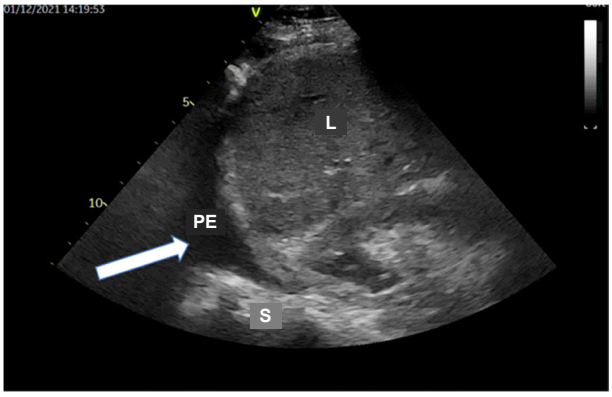

Source: Internal archive of the Echocardiography Department of Dante Pazzanese Cardiology Institute. L, liver; PE, pleural effusion (arrow); S, spine.

Figure 4 – *Costophrenic space with pleural effusion.*

Test indication:
Test technique:

Quadrant	Number of B lines	Quadrant	Number of B lines
D1		E1	
D2		E2	
D3		E3	
D4		E4	

Pleural effusion
Right costophrenic sinus:
Left costophrenic sinus:
Pleural effusion quantification by the Balik formula: _ mL

Conclusion: Uni-/bilateral presence of B lines in X quadrants

Figure 5 – *Essential report elements. Table with columns on the left with four quadrants on the right (D1–D4) and on the right with the four left quadrants (E1–E4).*

Authors' contributions

This is a review article, there was no data collection or statistical analysis. Otto MEB and Esmanhoto VA equitably reviewed the literature, provided the images, and wrote the manuscript.

Conflict of interest

The authors have declared that they have no conflict of interest.

References

1. Zanobetti M, Scorpiniti M, Gigli C, Nazerian P, Vanni S, Innocenti F, et al. Point-of-Care Ultrasonography for Evaluation of Acute Dyspnea in the ED. Chest. 2017;151(6):1295-301. doi: 10.1016/j.chest.2017.02.003.
2. Pivetta E, Goffi A, Lupia E, Tizzani M, Porrino G, Ferreri E, et al.; SIMEU Group for Lung Ultrasound in the Emergency Department in Piedmont. Lung Ultrasound-Implemented Diagnosis of Acute Decompensated Heart Failure in the ED: A SIMEU Multicenter Study. Chest. 2015;148(1):202-10. doi: 10.1378/chest.14-2608.
3. Slasky BS, Auerbach D, Skolnick ML. Value of portable real-time ultrasound in the ICU. Crit Care Med. 1983;11(3):160-4. doi: 10.1097/00003246-198303000-00002
4. Araujo GN, Silveira AD, Scolari FL, Custodio JL, Marques FP, Beltrame R, et al. Admission Bedside Lung Ultrasound Reclassifies Mortality Prediction in Patients With ST-Segment-Elevation Myocardial Infarction. Circ Cardiovasc Imaging. 2020;13(6):e010269. doi: 10.1161/CIRCIMAGING.119.010269
5. Platz E, Campbell RT, Claggett B, Lewis EF, Groarke JD, Docherty KF, et al. Lung Ultrasound in Acute Heart Failure: Prevalence of Pulmonary Congestion and Short- and Long-Term Outcomes. JACC Heart Fail. 2019;7(10):849-58. doi: 10.1016/j.jchf.2019.07.008
6. Stassen J, Bax JJ. How to do lung ultrasound. Eur Heart J Cardiovasc Imaging. 2022;23(4):447-9. doi: 10.1093/ehjci/jeab241
7. Balik M, Plasil P, Waldauf P, Pazout J, Fric M, Otahal M, et al. Ultrasound estimation of volume of pleural fluid in mechanically ventilated patients. Intensive Care Med. 2006;32(2):318. doi: 10.1007/s00134-005-0024-2
8. Lichtenstein DA. BLUE-protocol and FALLS-protocol: two applications of lung ultrasound in the critically ill. Chest. 2015;147(6):1659-70. doi: 10.1378/chest.14-1313.
9. Picano E, Scali MC, Ciampi Q, Lichtenstein D. Lung Ultrasound for the Cardiologist. JACC Cardiovasc Imaging. 2018;11(11):1692-705. doi: 10.1016/j.jcmg.2018.06.023
10. Picano E, Pellikka PA. Ultrasound of extravascular lung water: a new standard for pulmonary congestion. Eur Heart J. 2016;37(27):2097-104. doi: 10.1093/eurheartj/ehw164
11. Miglioranza MH, Gargani L, Sant'Anna RT, Rover MM, Martins VM, Mantovani A, et al. Lung ultrasound for the evaluation of pulmonary congestion in outpatients: a comparison with clinical assessment, natriuretic peptides, and echocardiography. JACC Cardiovasc Imaging. 2013;6(11):1141-51. doi: 10.1016/j.jcmg.2013.08.004

What do cardiologists expect from Echocardiography in the evaluation of non-compacted myocardium

O que o cardiologista espera do Ecocardiograma na avaliação de miocárdio não compactado

Luciano Nastari[1]

[1]*Assistant Physician - Clinical Unit Cardiomyopathies and Aortic Diseases - Instituto do Coração - HCFMUSP (InCor), São Paulo, SP, Brazil.*

Echocardiography, the first-line diagnostic screening method for non-compacted myocardium (NCM), is easy to perform and features low cost and low risk for patients. It is also widely available in clinical practice. However, it is also an operator-dependent method, with limitations including a dependent echocardiographic window, primary focus of visualizing the ventricular apex, and operator difficulty accurately distinguishing between compacted and non-compacted ventricular layers.

Another important limitation of echocardiography is the presence of greater trabeculations among healthy populations of Black people, athletes, and pregnant women, which may overestimate diagnoses. Thus, some authors determined diagnostic criteria for NCM by echocardiography. The currently most accepted criteria were proposed by Chin et al.[1], who analyzed five men with NCM by analyzing the parasternal view, short and apical axes, left ventricular (LV) free wall in maximum diastole, distance from the epicardial surface to the trabecular recess (X), and distance from the epicardial surface to the peak of the trabeculae (Y). The NCM diagnosis is made when $X/Y < 0.5$.

Other criteria were proposed by Jenni et al.[2], who studied 34 patients (25 men) with NCM and analyzed the location of the trabeculae in the apical, medial, and inferior medial LV walls and LV wall thicknesses of the compacted (C) versus non-compacted (NC) regions. Using this classification, the NCM diagnosis is made when $NC/C > 2$ in the short-axis view at the end of systole.

Stöllberger et al.[3] and Kohli et al.[4] analyzed 62 patients (49 men) with NCM and identified defined it as the presence of more than three trabeculations in the LV wall in the apical area of the papillary muscles and visible in a single apical four-chamber plane. On color Doppler, intertrabecular spaces are filled with blood from the ventricular cavity.

Paterick et al.[5] recently proposed the diagnosis of NCM as NCM/compacted myocardium > 2, with parasternal short-axis view measurements taken at end-diastole. This criterion showed a good correlation with cardiac magnetic resonance findings and, according to the authors, provided more accurate NCM and myocardium layer thickness measurements. However, this requires validation, additional confirmation, and comparison with other populations with structural heart disease before it can be accepted as a viable diagnostic option.

Another study[4] compared 199 patients, 143 of whom had an LV ejection fraction (LVEF) < 40%, referred to an accredited heart failure assessment center with 60 healthy volunteers (30 Black). The authors used the three echocardiographic definitions to identify NCM, assessed trabeculation number and size as well as the relative thickness of the non-compacted layer whenever possible. The three echocardiographic definitions showed a poor correlation, with only 29.8% of patients fulfilling all three criteria. Also, 8.3% of the normal controls met the criteria for NCM. Five subjects in the control group (four Black, one White) met at least one diagnostic criterion for NCM. This result emphasizes the limitation of echocardiographic criteria for diagnosing NCM, especially in Black individuals, leading to its overdiagnosis. In that study, if the control group included individuals with heart failure, these results could have been even more discrepant. The study findings suggest that current echocardiographic diagnostic criteria are very sensitive and result in NCM overdiagnosis in patients with LV systolic dysfunction. This seems particularly true in the Black population.

Extensive and detailed studies including normal populations of different races are necessary to determine the upper limits of normal trabecular patterns to avoid unnecessary investigations and treatments in patients and their relatives. Hypertrabeculation can also be a transient phenomenon. A study[6] of 102 primiparous pregnant women undergoing serial echocardiographic tests showed that 26 developed increased trabeculations during pregnancy (8 women met NCM criteria). These patients were followed up for a mean two years, with total trabeculation reductions occurring in 19 women and marked trabeculation reductions occurring in the remaining group. The inability to distinguish noncompaction from hypertrabeculation cardiomyopathy has significant clinical implications.

Despite the increasingly frequent diagnosis of NCM, the echocardiographic criteria are based on studies of limited numbers of patients and different methods. The point in the cardiac cycle at which NCM and compacted myocardium thickness are measured directly influences the relationship between the two evaluated layers. Myocardial thickness peaks in systole and troughs in diastole, directly affecting the relationship between NCM and compacted myocardium. In addition, we must consider the echocardiographic view in which these measurements are taken. Most criteria suggest

Keywords

Isolated Noncompaction of the Ventricular Myocardium; Echocardiography; Nuclear magnetic resonance.

Mailing Address: Luciano Nastari •
Av. Dr. Avenida Enéas de Carvalho Aguiar, 44, Cerqueira Cesar, CEP: 05403-000 – São Paulo, SP, Brazil.
E-mail: luciano-nastari@uol.com.br
Manuscript received 4/30/2022; revised 5/18/2022; accepted 5/25/2022

DOI: 10.47593/2675-312X/20223503ecard07

CC BY

that these measurements be taken in the parasternal short-axis view; however, in daily clinical practice, they are often taken in the apical two- and four-chamber views.[7] Finally, some studies showed that a considerable number of young athletes met NCM diagnostic criteria, highlighting the non-specificity of the current diagnostic criteria for highly trained athletes.[8]

Thus, consensus is lacking about which classification is the most efficient for diagnosing NCM. In this situation, patients fulfilling all three diagnostic criteria would be ideal. In current clinical practice, the Jenni et al.[2] criteria are the most widely used, but increased ventricular trabeculation (without the criteria defined above) and echocardiography findings suggestive of possible NCM are also common; thus, the clinician is expected to perform another imaging test to confirm the diagnosis.

Another important factor worth consideration is the underestimation of familial NCM disease since echocardiography is used to screen for it and has a high misdiagnosis rate. The trabeculae are better assessed with echocardiographic contrast and three-dimensional echocardiography. Some recent publications[9–11] with small sample sizes compared NCM patients with healthy and dilated cardiomyopathy subjects. Thus, subclinical myocardial impairment was identified by speckle tracking[10] in patients with a preserved LVEF and NCM versus normal subjects. Other authors identified LV longitudinal strain reductions in the mid and apical regions and normal motility in the basal region, unlike patients with dilated cardiomyopathy, who presented reduced motility in the three regions in apical sections. The authors suggested that longitudinal strain may contribute to the differentiation of cases of dilated cardiomyopathy, therefore reducing NCM overdiagnosis.[9–11]

As for the current guidelines, we have the following recommendations and evidence levels.[12]

Recommendation level IIb; evidence level B

- In individuals with suspected NCM, diagnostic criteria on echocardiography or magnetic resonance imaging may be reasonable for establishing the diagnosis when measured as an effective NC/C.
- In individuals with suspected NCM and ventricular arrhythmias, magnetic resonance imaging or other advanced cardiac imaging tests may be able to establish the diagnosis and perform the risk stratification.[12]

Conflict of interest

The author declares that he has no conflict of interest

References

1. Chin TK, Perloff JK, Williams RG, Jue K, Mohrmann R. Isolated noncompaction of left ventricular myocardium. A study of eight cases. Circulation. 1990;82(2):507-13. doi: https://doi.org/10.1161/01.cir.82.2.507
2. Jenni R, Oechslin E, Schneider J, Attenhofer Jost C, Kaufmann PA. Echocardiographic and pathoanatomical characteristics of isolated left ventricular non-compaction: a step towards classification as a distinct cardiomyopathy. Heart. 2001;86(6):666-71.
3. Stöllberger C, Gerecke B, Finsterer J, Engberding R. Refinement of echocardiographic criteria for left ventricular noncompaction. Int J Cardiol. 2013;165(3):463-7. doi: https://doi.org/10.1016/j.ijcard.2011.08.845
4. Kohli SK, Pantazis AA, Shah JS, Adeyemi B, Jackson G, McKenna WJ, et al. Diagnosis of left-ventricular non-compaction in patients with left-ventricular systolic dysfunction: time for a reappraisal of diagnostic criteria? Eur Heart J. 2008;29(1):89-95. doi: https://doi.org/10.1093/eurheartj/ehm481
5. Paterick TE, Umland MM, Jan MF, Ammar KA, Kramer C, Khandheria BK, et al. Left ventricular noncompaction: a 25-year odyssey. J Am Soc Echocardiogr. 2012;25(4):363-75. doi: https://doi.org/10.1016/j.echo.2011.12.023
6. Gati S, Papadakis M, Papamichael ND, Zaidi A, Sheikh N, Reed M, et al. Reversible de novo left ventricular trabeculations in pregnant women: implications for the diagnosis of left ventricular noncompaction in low-risk populations. Circulation. 2014;130(6):475-83. doi: https://doi.org/10.1161/CIRCULATIONAHA.114.008554
7. Hotta VT, Tendolo SC, Rodrigues AC, Fernandes F, Nastari L, Mady C. Limitations in the Diagnosis of Noncompaction Cardiomyopathy by Echocardiography. Arq Bras Cardiol. 2017;109(5):483-8. doi: https://doi.org/10.5935/abc.20170152
8. Gati S, Chandra N, Bennett RL, Reed M, Kervio G, Panoulas VF, et al. Increased left ventricular trabeculation in highly trained athletes: do we need more stringent criteria for the diagnosis of left ventricular non-compaction in athletes? Heart. 2013;99(6):401-8. doi: https://doi.org/10.1136/heartjnl-2012-303418. Erratum in: Heart. 2013;99(7):506. Wilson, Matthew [corrected to Wilson, Mathew].
9. Mullens W, Damman K, Harjola VP, Mebazaa A, Brunner-La Rocca HP, Martens P, et al. The use of diuretics in heart failure with congestion - a position statement from the Heart Failure Association of the European Society of Cardiology. Eur J Heart Fail. 2019;21(2):137-55. doi: https://doi.org/10.1002/ejhf.1369
10. Bellavia D, Michelena HI, Martinez M, Pellikka PA, Bruce CJ, Connolly HM, et al. Speckle myocardial imaging modalities for early detection of myocardial impairment in isolated left ventricular non-compaction. Heart. 2010;96(6):440-7. doi: https://doi.org/10.1136/hrt.2009.182170
11. Tarando F, Coisne D, Galli E, Rousseau C, Viera F, Bosseau C, et al. Left ventricular non-compaction and idiopathic dilated cardiomyopathy: the significant diagnostic value of longitudinal strain. Int J Cardiovasc Imaging. 2017;33(1):83-95. doi: https://doi.org/10.1007/s10554-016-0980-3
12. Towbin JA, McKenna WJ, Abrams DJ, Ackerman MJ, Calkins H, Darrieux FCC, Daubert JP, de Chillou C, DePasquale EC, Desai MY, Estes NAM 3rd, Hua W, Indik JH, Ingles J, James CA, John RM, Judge DP, Keegan R, Krahn AD, Link MS, Marcus FI, McLeod CJ, Mestroni L, Priori SG, Saffitz JE, Sanatani S, Shimizu W, van Tintelen JP, Wilde AAM, Zareba W. 2019 HRS expert consensus statement on evaluation, risk stratification, and management of arrhythmogenic cardiomyopathy: Executive summary. Heart Rhythm. 2019;16(11):e373-e407. doi: 10.1016/j.hrthm.2019.09.019.

Special Article

Pediatric Cardiac Tumors: Echocardiographic Imaging Features

Tumores Cardíacos Pediátricos: Características de Imagens Ecocardiográficas

Nathalie Jeanne Magioli Bravo-Valenzuela[1,2], Eliane Lucas[3,4], Nadinne Velloso Netto[3], Larissa Vieira da Conceição[3], Natalia Pinheiro Duque Estrada[3], Maria Respondek-Liberska[5], Edward Araujo Júnior[6]

S[1]SBC/INC/INCA, Rio de Janeiro, RJ, Brazil; [2]School of Medicine, Federal University of Rio de Janeiro (UFRJ), Rio de Janeiro, RJ, Brazil; [3]Federal Bonsucesso Hospital, Rio de Janeiro-RJ, Brazil; [4]Central Military Hospital, Brazilian Army (Hospital Central do Exército), Rio de Janeiro, RJ, Brazil; [5]Polish Mother's Memorial Hospital, Research Institute, Medical University of Lodz, Poland; [6]Federal University of São Paulo (EPM-UNIFESP), São Paulo, SP, Brazil.

Abstract

Cardiac tumors (CTs) in children are very rare, but their diagnosis is crucial for patient management. Echocardiography is the most commonly used cardiovascular imaging modality in clinical practice for the initial diagnosis of CTs in pediatric patients. Knowing the echocardiographic characteristics of CTs can enable an increasingly early diagnosis and the identification of its most likely etiology. Primary and benign CTs are the most frequent types in the pediatric population. Among benign CTs, the most frequent in fetuses and neonates are rhabdomyomas and teratomas. In children and adolescents, rhabdomyomas and fibromas are more common. Here we describe the echocardiographic characteristics of the most common CTs in pediatric patients.

Introduction

Cardiac tumors (CTs), rarely encountered in clinical practice, are classified into primary and secondary types according to their site of origin. In the pediatric age group, CTs occur in 0.001–0.03% of autopsy findings, with primary CTs (PCTs) being the most prevalent and usually benign[1,2]. The most frequent benign PCTs in fetuses and newborns are rhabdomyomas, followed by teratomas and fibromas; in older children, these are rhabdomyomas and fibromas. In adults, myxomas are the most common benign PCTs[3-5]. As for malignant PCTs, sarcomas are the most frequent in both children and adults. In adults, secondary malignant CTs (metastatic) are more frequent than primary ones, unlike in the pediatric population[5-8]. Characteristics such as CT density, number, and location aid the identification of CT type (Figure 1, Table 1). Echocardiography is an accessible non-invasive test and the most commonly used imaging method for the initial evaluation of cardiac masses in routine clinical practice. In this scenario, the analysis of CT aspects by echocardiography and its association with patient age groups and other epidemiological aspects can significantly impact the therapeutic approach and clinical evolution of these patients. Although rare, CTs should be considered a differential diagnosis with other types of cardiac masses such as thrombi and vegetations. This pictorial review aimed to describe the characteristics of echocardiographic images of the main PCT types found in the pediatric population, providing tools for its diagnosis.

Keywords

Cardiac Tumors; Echocardiography; Screening; Imaging; Pediatrics.

Mailing Address: Nathalie J M Bravo-Valenzuela •
Rua Bruno Lobo, 50, 3º andar - Rio de Janeiro-RJ, Brazil. CEP: 21941-912
E-mail: njmbravo@cardiol.br
Manuscript received 5/4/2022; revised 6/6/2022; accepted 7/1/2022

DOI: 10.47593/2675-312X/20223503eabc302

Benign CTs

Most (90%) pediatric primary CTs (primary site: heart) are benign[3]. In the pediatric population, rhabdomyomas, teratomas, and fibromas are the most prevalent PCTs[2,3,7]. Other rarer benign pediatric PCTs are hemangiomas, myxomas, and hamartomas[2,6]. Next we will describe the main echocardiographic characteristics of the most frequent benign PCTs.

Rhabdomyomas

Rhabdomyomas are the most common benign PCTs in children, constituting 45–60% of tumors in this age group[2,3,7-9]. In a review including 27,640 patients with PCTs, Beghetti *et al.* described that rhabdomyomas were diagnosed as multiple or single CTs when associated with a family history of tuberous sclerosis or the involvement of other organs (central nervous system, kidneys, and skin)[7,8]. Rhabdomyomas are homogeneous masses that vary in size. They generally present as multiple well-delimited masses (in >60% of these patients) or, less commonly, as a pedunculated mass in the cardiac cavity (Figures 2A and B; Video clip 1). They typically occur at an equal distribution in the right and left ventricular (intracavitary) cardiac chambers[9,10]. Rhabdomyomas can also occur in the interventricular septum, and they can occasionally be intramural.

Most patients are asymptomatic; however, depending on their location, rhabdomyomas can cause arrhythmias (when located in the atrioventricular region), heart failure (HF), and signs of low cardiac output (ventricular) outflow obstruction[10]. In cases of hemodynamic repercussions, pharmacological treatment (rapamycin inhibitor [Everolimus]) or surgical treatment may be indicated[7,11-13].

These tumors usually occur in the fetal period or during the first year of life, as they are hormone-dependent and can grow in the fetal period until the 32nd week of pregnancy[14]. The presence of multiple cardiac masses on obstetric ultrasonography and/or fetal echocardiography should draw

CC BY

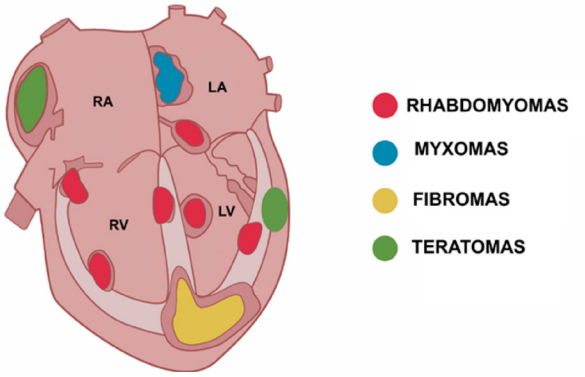

LA, left atrium; LV, left ventricle; RA, right atrium; RV, right ventricle.

Figure 1 – *Pediatric primary cardiac tumor locations. Schematic image of the heart with the most typical locations of where the more common different types of pediatric primary cardiac tumors are located.*

Table 1 - Typical characteristics of the most common pediatric primary CTs.

Cardiac Tumor Type	Location/Association	Echo Features
Rhabdomyoma	Ventricular cardiac chambers, interventricular septum Associated with tuberous sclerosis	Homogeneous and well-delimited masses, variable in size, multiple or less commonly as a pedunculated mass
Fibroma	Interventricular septum and the ventricular free wall Associated with Gorlin syndrome	Heterogeneous and well-delimited large solid mass (single tumor); calcification is an important sign
Myxoma	Atrial septum, left atrium Associated with Carney complex	Single mobile, heterogeneous (pedunculated) mass; papillary myxomas are smaller with an elongated appearance
Teratoma	Pericardium, base of Ao/PA and SVC Associated with pericardial effusion	Non-homogeneous density, (cystic and multilobulated aspect); large mass

Ao, aorta; CTs, cardiac tumors; PA, pulmonary artery; SVC, superior vena cava.

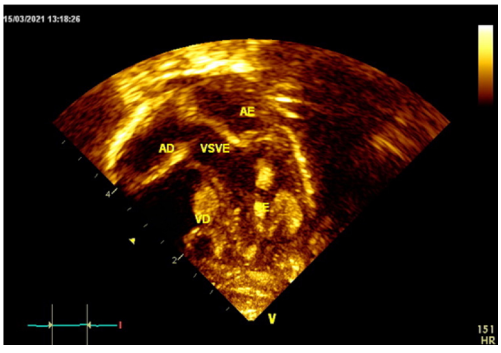

Ao, aorta; IVS, interventricular septum; LA, left atrium; LV, left ventricle; RA, right atrium; RV, right ventricle

Figure 2 – *Imaging of rhabdomyomas. Pediatric echocardiogram demonstrating multiple ventricular masses (red arrows) appearing as rhabdomyomas: (A) in the 4-chamber subcostal view (Video clip 1) and (B) in the parasternal left ventricle (LV) view by scanning the LV more apically. Note that the (increased) echogenicity of masses differs from that of the myocardium of the adjacent ventricular cavities.*

attention to the diagnosis of rhabdomyomas. In some cases, the masses can be large and obstruct the ventricular outflow and/or inlet tracts. In such cases, blood flow obstruction may occur, carrying the risk of HF and fetal death. In the postnatal period, the tumor masses may shrink or even completely regress, especially in early childhood.

There is a strong association between rhabdomyoma and tuberous sclerosis, especially in cases of multiple cardiac masses. About 60–80% of patients with rhabdomyomas have tuberous sclerosis[6,7,15], a genetic syndrome with variable clinical presentation, including cognitive deficit, seizures, multiple facial angiofibromas, skin patches (hypochromic "coffee au lait" spots), multiple retinal hamartomas, and cardiac rhabdomyomas, among other features. Rhabdomyoma-type CT is most common fetal and neonatal clinical presentation of tuberous sclerosis. Therefore, the presence of multiple

CTs in fetuses and children should draw attention to the diagnosis of rhabdomyoma and its association with tuberous sclerosis (Figure 3). The identification of mutations in the *TSC1* or *TSC2* genes is sufficient for the diagnosis of tuberous sclerosis, and genetic research should be requested in cases of rhabdomyomas[16,17].

Fibromas

Although rare, fibromas are the second most common benign PCTs in pediatric patients except fetuses and neonates[2,7]. On echocardiography, these CTs usually present as a large solid myocardial mass (single tumor mass) that is well-delimited, non-contractile, echogenic, and heterogeneous within the myocardium (Figure 4, Video clip 2). Their central portion may have calcifications that are pathognomonic, reflecting a poor blood supply to the tumor. Calcification is an important tool that enables the differentiation of fibroma from rhabdomyoma within a single tumor mass. The most common fibroma locations are the interventricular septum and the ventricular free wall, and its extension into the ventricular cavity can lead to obstruction and HF symptoms. Alternatively, myocardial location can lead to arrhythmias[3,19].

These tumors do not regress spontaneously and often require resection. Surgical excision of CTs is recommended and can be subtotal to minimize loss of the myocardial mass. In cases of the evolution to myocardial failure or the involvement of a large cardiac area with the impossibility of complete tumor resection, a heart transplant may be considered.

Patients with multiple basal cell carcinomas should be screened for Gorlin syndrome[20], an autosomal dominant disease caused by a mutation in the *PTCH1* gene. Gorlin syndrome is characterized by skeletal and developmental abnormalities with a tendency for neoplasms such as medulloblastomas, basal cell carcinomas, and cardiac fibromas. In such cases, genetic counseling is crucial and the diagnosis is made through DNA analysis, even from the prenatal period[21].

Myxomas

Cardiac myxomas, the most common PCTs in adults, usually present at age 30–60 years, most frequently in women. However, they are rare in children. Most of these PCTs (60%)

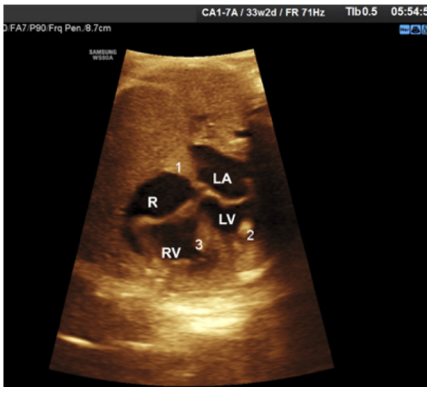

Ao, aorta; IVS, interventricular septum; LA, left atrium; LV, left ventricle; RA, right atrium; RV, right ventricle.

Figure 3 – *Fetal rhabdomyoma in a case of tuberous sclerosis. Fetal echocardiogram showing multiple masses (1, 2, 3) in ventricular cavities and interventricular septum in a case of rhabdomyoma and tuberous sclerosis.*

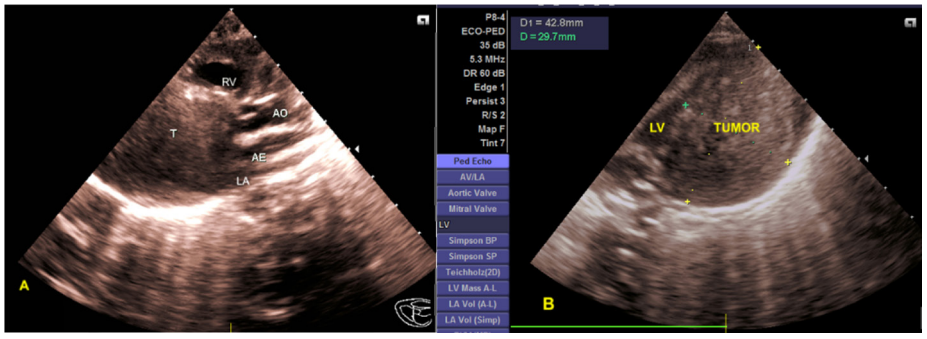

Ao, aorta; LA, left atrium; LV, left ventricle; T, tumor (fibroma).

Figure 4 – *Fibroma. Transthoracic echocardiogram showing the presence of a large (single) homogeneous mass corresponding to a fibroma. The large single mass is visible in the LV free wall from the parasternal view by scanning of the LV long (A/ Video clip 2) and short axes (B). The cardiac tumor was removed by cardiac surgery and a histopathological examination confirmed the echocardiographic diagnostic hypothesis.*

are located within the left atrium, characteristically originating from the middle portion of the atrial septum by a narrow pedicle, while 28% originate in the right atrium[22].

On echocardiography, myxomas usually present as a single mobile and heterogeneous (pedunculated) atrial mass (Figures 5A, 5B). Polypoid myxomas are larger with a smooth surface and a rough core and include cystic areas due to hemorrhage and necrosis. Papillary myxomas tend to be smaller and have an elongated appearance with multiple villi. Papillary myxomas are associated with embolic phenomena, while polypoid myxomas tend to obstruct the blood flow, with HF symptoms being the most frequent (Video clip 3). Patients with myxomas may present with systemic symptoms such as fever, weight loss, night sweats, and arthralgia and exhibit laboratory abnormalities such as anemia and elevated inflammatory markers.

Cardiac myxomas may be associated with Carney complex, a syndrome inherited in an autosomal dominant pattern[23]. Carney complex results in several neuroendocrine tumors and cardiac and cutaneous myxomas associated with changes in skin pigmentation resulting from mutations in the *PRKAR1A* gene. Myxomas in this syndrome occur at an earlier age and tend to recur more frequently[24-27].

An atrial myxoma warrants resection due to the risk of cardiovascular embolization, complications, and sudden death. Surgical resection is associated with low operative mortality rates and good outcomes. A small percentage of patients (up to 5%), typically those with a family history, show smaller tumors or ventricular locations and are at risk of recurrence or new myxomas, highlighting the importance of periodic follow-up.

Teratomas

Teratomas are PCTs of which 70% of cases occur in childhood, more frequently in fetuses and neonates[3]. The main echocardiographic characteristics of teratomas include large masses with a non-homogeneous density and a cystic and multilobulated aspect, as they contain all germinative layers[3,28]. Their most common location is the pericardium, close to the base of the great arteries (adherent to the aorta and pulmonary arteries), and the superior vena cava. In some cases, extrinsic compression of these vessels can occur[3,28]. These patients may have dyspnea and HF signs. Pericardial effusion is generally present and may progress to cardiac tamponade, especially in fetuses[6,28].

Teratomas are frequently detected on prenatal ultrasound or fetal echocardiography with a risk of fetal death of extrinsic compression or cardiac tamponade (Figure 6). These fetuses may benefit from prenatal intervention[3,28,29]. Teratomas have a good postnatal prognosis after curative surgical resection and generally show no recurrence in long-term follow-up[7,30].

Hemangiomas

Hemangiomas are rare CTs usually located in the right

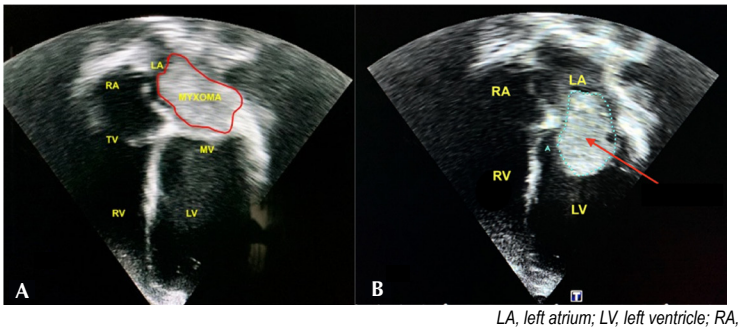

LA, left atrium; LV, left ventricle; RA, right atrium; RV, right ventricle.

Figura 5 – *Left atrial myxoma. Transthoracic echocardiogram (apical 4-chamber view) demonstrating a large mobile mass (red arrow) in the left atrium with irregular contours (A) obstructing the LV inlet tract flow (B; Video clip 3).*

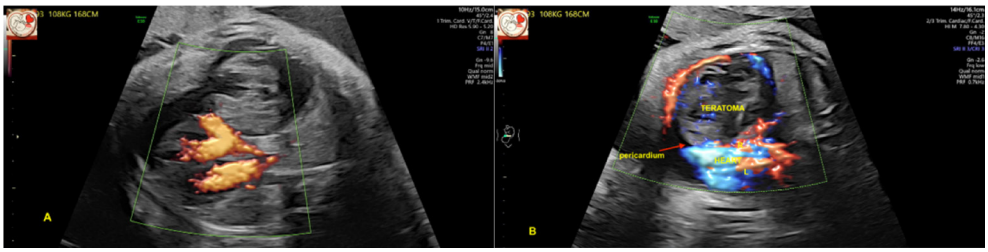

LA, left atrium; LV, left ventricle; RA, right atrium; RV, right ventricle.

Figure 6 – *Fetal teratoma. Three-dimensional fetal echocardiogram with power and color Doppler imaging demonstrating a teratoma in a fetus at 32 weeks' gestation. Note the large pericardial mass (A) and pericardial effusion (B).*

atrium and right ventricle. Depending on their location and size, they can cause systemic venous congestion, right ventricular outflow tract obstruction, elevated right ventricular end-diastolic pressure, and irreversible right ventricular dysfunction. Electrocardiography can reveal ST-segment abnormalities, signs of right ventricular hypertrophy, signs of pre-excitation, and arrhythmias. The presence of pericardial effusion is prevalent in hemangioma cases[31]. Remarkably, this type of CT has the best prognosis due to the possibility of its spontaneous regression[32].

Malignant CTs

Malignant tumors account for about 15% of CTs and are rather rare in childhood[30]. They typically show rapid growth, local invasion, hemorrhagic pericardial effusion, and precordial pain. Among them, the most prevalent are sarcomas and rhabdomyosarcomas.

a. Sarcomas

Sarcomas are the most common among malignant CTs and typically diagnosed in the mid-4th decade of life. Undifferentiated sarcomas appear as broad masses on echocardiography, typically in the left atrium (which allows differential diagnosis with myxomas), heterogeneous echogenicity, and hypoechoic areas, indicating tumor necrosis. The most common sarcoma in the heart is angiosarcoma. It is often located to the right, particularly the right atrium. Echocardiograms show a clearly heterogeneous lobulated mass with areas of necrosis and hemorrhage but without a pedicle, differentiating it from other tumors. Sarcomas tend to show direct involvement with the pericardium, resulting in hemorrhagic effusion that may or may not cause tamponade.

Angiosarcomas tend to replace the cardiac wall of the right atrium and fill the chamber. Depending on their location and hemodynamic repercussions, they can show signs and symptoms of pericardial precordial pain, obstruction, congestion, dyspnea, and fatigue. Unfortunately, metastasis to the lung is common at diagnosis and the prognosis is restricted, even after surgery, due to recurrence and metastasis[3,31].

b. Rhabdomyosarcomas

Rhabdomyosarcomas, the second most common malignant tumor type, can appear in any cardiac structure without location preference. They tend to occupy multiple areas and can cause obstructions. They grow quickly, involve the pericardium early, and carry a poor prognosis[4,31].

Leiomyosarcomas, osteosarcomas, fibrosarcomas, and undifferentiated sarcomas are other rare types that have a very poor prognosis[3,21].

c. Lymphomas

In general, due to cardiac involvement in patients with Hodgkin's and non-Hodgkin's lymphoma, however. Primary cardiac lymphomas show an increased incidence in immunocompromised patients, those after transplantation, and those infected with HIV. These tumors are most commonly diffuse large B cell lymphoma. On echocardiography, they are homogeneous and infiltrative, leading to wall thickening and hemodynamic restriction, with nodular masses occupying the cardiac chambers, mainly the right atrium (Figure 7, Video clip 4). The atrioventricular region can be affected, involving the right coronary artery and pericardial effusion.

Transesophageal echocardiography is the best imaging technique and should be performed to identify tumor type. Depending on its location, it can generate symptoms of inlet obstruction, leading to vena cava syndrome, HF, and arrhythmias such as complete atrioventricular block and embolism.

The diagnosis can be made by pericardial effusion cytology or echo-guided biopsy. Cytology is the key to lymphoma prognosis, which is usually much better than that of other primary CTs, especially if patients are candidates for adequate chemotherapy. Radiotherapy is less favorable, while surgical resection of the entire tumor is very difficult[4,31].

d. Mesothelioma

Mesotheliomas represent half of primary pericardial tumors, the other half being benign (teratomas, fibromas, and lipomas). Their symptoms include chest pain, cough, and palpitations. These tumors form bulky nodules within the pericardial cavity, circumventing the heart, mimicking

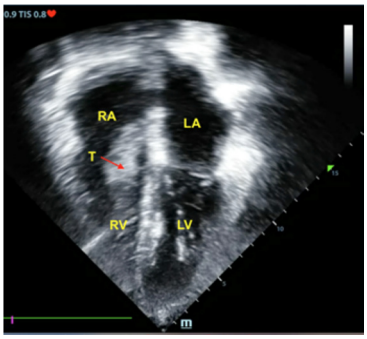

LA, left atrium; LV, left ventricle; RA, right atrium; RV, right ventricle; T, tumor (lymphoma).

Figure 7 – *Lymphoma. Two-dimensional echocardiogram showing a large nodular mass (lymphoma) in the RA cavity (red arrow). The features of this mass in an adolescent patient infected with the human immunodeficiency virus raised the suspicion of this diagnosis.*

pericarditis, and cardiac tamponade[30]. Echocardiography typically reveals pericardial effusion and a tumor involving the heart, but a mild mass may not be seen. The patient prognosis is restricted, although surgery and radiotherapy can provide palliative benefits.

e. Metastasis

Cardiac metastasis is not uncommon, with an incidence of around 0.7–3.5% in the general population that reaches 7.1% in people with known malignancies[3]. They can invade the heart by hematogenous dissemination, contiguity, or via the venous/lymphatic route. Heart metastasis is most common in primary breast and lung tumors, esophageal carcinoma, malignant lymphoma, leukemia, and malignant melanoma (Figure 8). Melanoma is more prone to cardiac metastasis due to its hematogenous spread. The pericardium is more seriously affected, with an effusion that can even be asymptomatic. However, metastasis should be considered in any patient with a known malignant disease and new cardiovascular symptoms.

Echocardiography should be performed as an initial diagnostic test for the presence of metastatic implants, and it can be complemented with other imaging tests. Unfortunately, metastatic cardiac disease occurs in patients with already disseminated disease, making its prognosis quite poor when identified[3,33].

We can currently detect CT, make the diagnosis, and treat and follow patients, but in this chain, the missing link is very first one: What causes CTs, and why? To answer this question, international cooperation is needed, as is the establishment of national databases. Is it possible that air pollution plays a role? The first such suggestion came from Poland[34].

Differential diagnosis

The main differential diagnosis of CTs is thrombi, which occur more frequently on the right side of the heart and are related to a clinical history of central venous catheter use (Figure 9A) or structural heart diseases with dilated cardiomyopathy (Figure 9B). Cardiac thrombi generally appear as mural masses or pedunculated and mobile intraluminal masses. Unlike CTs, they are avascular and do not show increased echogenicity on contrast-enhanced echocardiography[3,30,35,36].

Left ventricular diverticulum is another differential diagnosis characterized by the image of a structure connected to the ventricular cavity by a narrow pedicle presenting asynchronous contractility with the left ventricular myocardium (Figure 10)[3,37].

Other differential diagnoses are pericardial cysts and vegetations, the latter being associated with a clinical history of fever and, in general, the presence of structural heart disease (valvular disease or shunt heart disease with communication

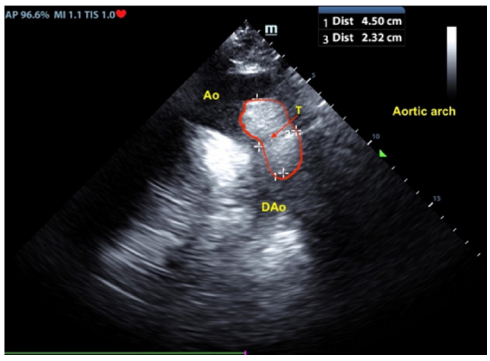

Ao, aorta; DAo, descending aorta; T, secondary cardiac tumor (red arrow).

Figure 8 – *Transthoracic echocardiogram showing a secondary cardiac tumor (metastasis) in the aorta in an adult patient. Secondary cardiac tumors are encountered more frequently in the adult population than in the pediatric population.*

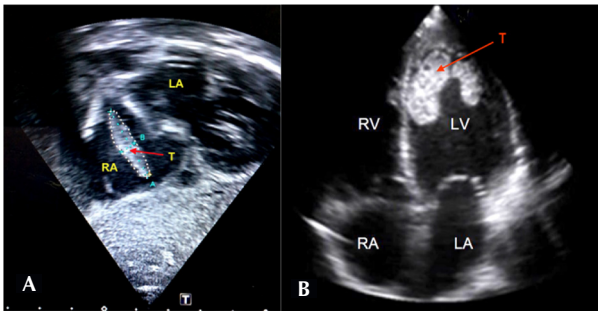

LA, left atrium; LV, left ventricle; RA, right atrium; T, thrombus (red arrow).

Figure 9 – *Cardiac thrombus. Transthoracic echocardiogram showing a thrombus (red arrow): (A) in the right atrium adherent to a catheter and (B) in the LV apical wall. The first was identified in a child with a central venous catheter and the latter was identified in an adolescent with myocardial disease.*

between the left and right sides of the heart) (Figure 11, Video clip 5)[3,30,38]. Vegetations generally appear as echogenic masses attached to the atrial side of the atrioventricular valves or the ventricular side of the semilunar valves. Indeed, important features of vegetations on echocardiography are isoechoic to the tissue, move independently, and are associated with valvular regurgitation[38-40].

Conclusions

Although CTs are rarely encountered in the pediatric age group, their early diagnosis can impact the conduct and prognosis of these patients. Primary CTs are most frequently seen in children, with a high prevalence of a benign nature. Echocardiography, the most commonly used cardiovascular diagnostic test, provides important tools for an initial diagnosis. Knowledge of the echocardiographic characteristics of pediatric CTs can enable the identification of different CT types and their differential diagnosis with other images of masses such as thrombi, contributing to treatment optimization (Table 1, Figure 12).

Authors' contributions

Conception and study design: Bravo-Valenzuela NJM, Lucas E; Data collection, data analysis and interpretation, manuscript writing: Bravo-Valenzuela NJM, Lucas E, Velloso Netto N, Conceicao LV, Estrada NPD and Respondek-Liberska M; Critical revision of the manuscript for important intellectual content: Araújo Júnior E and Bravo-Valenzuela NJM.

Acknowledgment

The authors acknowledge Liana Bravo-Valenzuela e Silva, graphic designer at Pedicor Pediatric Cardiology Center in Brazil, for editing figures to this manuscript.

Conflict of interest

The authors have declared that they have no conflict of interest.

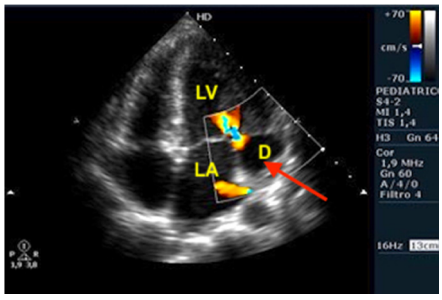

D, diverticulum (red arrow); LA, left atrium; LV, left ventricle

Figure 10 – *Ventricular diverticulum. Transthoracic echocardiogram (4-chamber view) of a child with left ventricular diverticulum. Observe the color Doppler on the narrow pedicle demonstrating that this structure is communicating with the ventricular cavity.*

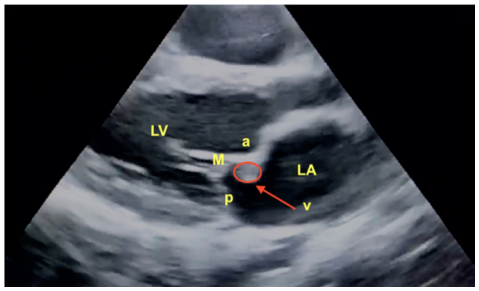

a, anterior cusp; LA, left atrium; LV, left ventricle; M, mitral valve; MR, mitral regurgitation; p, posterior cusp; V, vegetation.

Figure 11 – *Infective endocarditis in a pediatric patient affecting the anterior cusp of the mitral valve on the atrial side of the valve (Video clip 5).*

References

1. Centofanti P, Di Rosa E, Deorsola L, Dato GM, Patanè F, La Torre M, Barbato L, Verzini A, Fortunato G, di Summa M. Primary cardiac tumors: early and late results of surgical treatment in 91 patients. Ann Thorac Surg. 1999;68(4):1236-41. doi: 10.1016/s0003-4975(99)00700-6.
2. Uzun, O., Wilson, D.G., Vujanic, G.M. et al. Cardiac tumours in children. Orphanet J Rare Dis. 2007; (2) 11: 1750-72/https://doi.org/10.1186/1750-1172-2-11.
3. Tao TY, Yahyavi-Firouz-Abadi N, Singh GK, Bhalla S. Pediatric cardiac

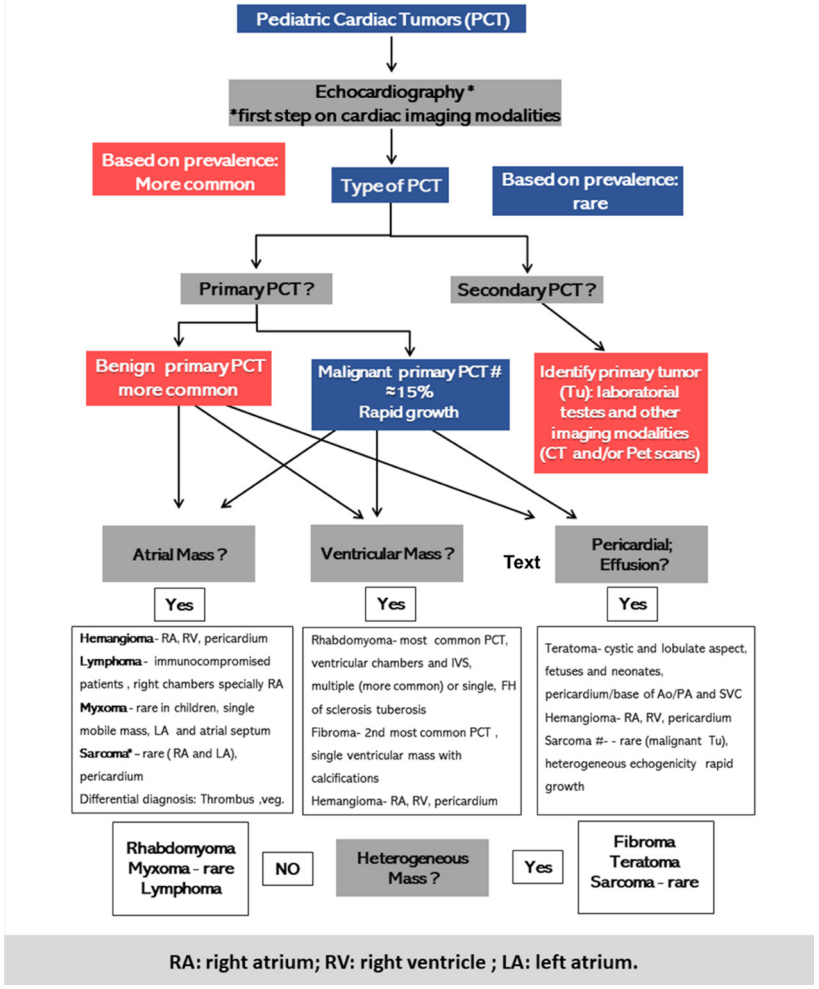

Tyebally, S. et al. J Am Coll Cardiol Cardio Onc. 2020.

Figure 12 – *Echocardiographic approach to pediatric cardiac tumors (PCT).*

tumors: clinical and imaging features. Radiographics. 2014;34(4):1031-46. doi: 10.1148/rg.344135163.

4. Pinede L, Duhaut P, Loire R. Clinical presentation of left atrial cardiac myxoma. A series of 112 consecutive cases. Medicine (Baltimore). 2001;80(3):159-72. doi: 10.1097/00005792-200105000-00002.

5. Sarjeant JM, Butany J, Cusimano RJ. Cancer of the heart: epidemiology and management of primary tumors and metastases. Am J Cardiovasc Drugs. 2003;3(6):407-21. doi: 10.2165/00129784-200303060-00004.

6. Burke A, Virmani R. Pediatric heart tumors. Cardiovasc Pathol. 2008;17(4):193-8. doi: 10.1016/j.carpath.2007.08.008. Epub 2008 Mar 4.

7. Beghetti M, Gow RM, Haney I, Mawson J, Williams WG, Freedom RM. Pediatric primary benign cardiac tumors: a 15-year review. Am Heart J. 1997;134(6):1107-14. doi: 10.1016/s0002-8703(97)70032-2.

8. Chan HS, Sonley MJ, Moës CA, Daneman A, Smith CR, Martin DJ. Primary and secondary tumors of childhood involving the heart, pericardium, and great vessels. A report of 75 cases and review of the literature. Cancer. 1985;15;56(4):825-36. doi: 10.1002/1097-0142(19850815)56:4<825:aid-cncr2820560421>3.0.co;2-7.

9. Tzani A, Doulamis IP, Mylonas KS, Avgerinos DV, Nasioudis D. Cardiac Tumors in Pediatric Patients: A Systematic Review. World J Pediatr Congenit Heart Surg. 2017;8(5):624-632. doi: 10.1177/2150135117723904.

10. Penha JG, Zorzanelli L, Barbosa-Lopes AA, Aiello VD, Carvalho VO, Caneo LF, Riso AA, et al. Tumores cardíacos em criança: análise retrospectiva Arquivos Brasileiros de Cardiologia 2013; (100) 2: 120-126.

11. Stelmaszewski EV, Parente DB, Farina A, Stein A, Gutierrez A, Raquelo-Menegassio AF, Manterola C, de Sousa CF, Victor C, Maki D, Morón EM, de Abrantes FF, Iqbal F, Camacho-Vilchez J, Jimenez-Pavón J, Polania JP, Thompson L, Bonanato L, Diebold M, Da Silva MVCP, Nashwan MWJ, Galvani MAG, Idris OEA, Danos P, Ortiz-Lopez R, Mahmoud RAA, Gresse S, Loss KL. Everolimus for cardiac rhabdomyomas in children with tuberous sclerosis. The ORACLE study protocol (everOlimus for caRdiac rhAbdomyomas in tuberous sCLErosis): a randomised, multicentre, placebo-controlled, double-blind phase II trial. Cardiol Young. 2020;30(3):337-345. doi: 10.1017/S1047951119003147. Epub 2020 Jan 27.

12. Demir HA, Ekici F, Yazal Erdem A, Emir S, Tunç B. Everolimus: a challenging drug in the treatment of multifocal inoperable cardiac rhabdomyoma. Pediatrics. 2012;130(1):e243-7. doi: 10.1542/peds.2011-3476. Epub 2012 Jun 25.

13. Ebrahimi-Fakhari D, Stires G, Hahn E, Krueger D, Franz DN. Prenatal Sirolimus Treatment for Rhabdomyomas in Tuberous Sclerosis. Pediatr Neurol. 2021;125:26-31. doi: 10.1016/j.pediatrneurol.2021.09.014. Epub 2021 Sep 25.

14. Shi L, Wu L, Fang H, Han B, Yang J, Ma X, Liu F, Zhang Y, Xiao T, Huang M, Huang M. Identification and clinical course of 166 pediatric cardiac tumors. Eur J Pediatr. 2017;176(2):253-260. doi: 10.1007/s00431-016-2833-4. Epub 2017 Jan 10.

15. Kocabaş A, Ekici F, Cetin İİ, Emir S, Demir HA, Arı ME, Değerliyurt A, Güven A. Cardiac rhabdomyomas associated with tuberous sclerosis complex in 11 children: presentation to outcome. Pediatr Hematol Oncol. 2013;30(2):71-9. doi: 10.3109/08880018.2012.734896. Epub 2012 Nov 14.

16. Hinton RB, Prakash A, Romp RL, Krueger DA, Knilans TK; International Tuberous Sclerosis Consensus Group. Cardiovascular manifestations of tuberous sclerosis complex and summary of the revised diagnostic criteria and surveillance and management recommendations from the International Tuberous Sclerosis Consensus Group. J Am Heart Assoc. 2014; 25;3(6):e001493. doi: 10.1161/JAHA.114.001493. PMID: 25424575.

17. Lee KA, Won HS, Shim JY, Lee PR, Kim A. Molecular genetic, cardiac and neurodevelopmental findings in cases of prenatally diagnosed rhabdomyoma associated with tuberous sclerosis complex. Ultrasound Obstet Gynecol. 2013;41(3):306-11. doi: 10.1002/uog.11227..

18. Tyebally S, Chen D, Bhattacharyya S, Mughrabi A, Hussain Z, Manisty C, Westwood M, Ghosh AK, Guha A. Cardiac Tumors: JACC CardioOncology State-of-the-Art Review. JACC CardioOncol. 2020; 16;2(2):293-311. doi: 10.1016/j.jaccao.2020.05.009. PMID: 34396236.

19. Atallah J, Robertson M, Rebeyka IM, Dyck J, Noga ML. Antenatal diagnosis and successful surgical removal of a large right ventricular fibroma. Pediatr Cardiol. 2006;27(4):493-6. doi: 10.1007/s00246-006-1260-0. Epub 2006 Jul 11.

20. Mankad R, Herrmann J. Cardiac tumors: echo assessment. Echo Res Pract. 2016;3(4):R65-R77. doi: 10.1530/ERP-16-0035. Epub 2016 Sep 6. PMID: 27600455.

21. Lo Muzio L. Nevoid basal cell carcinoma syndrome (Gorlin syndrome). Orphanet J Rare Dis. 2008; 25;3:32. doi: 10.1186/1750-1172-3-32. PMID: 19032739.

22. Grebenc ML, Rosado-de-Christenson ML, Green CE, Burke AP, Galvin JR. Cardiac myxoma: imaging features in 83 patients. Radiographics. 2002;22(3):673-89. doi: 10.1148/radiographics.22.3.g02ma02673.

23. Ríos JC, Chávarri F, Morales G, Vera L, Adrianzén M, Abarca A, Arboleda M, de Guzmán IN. Cardiac myxoma with prenatal diagnosis. World J Pediatr Congenit Heart Surg. 2013;4(2):210-2. doi: 10.1177/2150135112472210..

24. Pack SD, Kirschner LS, Pak E, Zhuang Z, Carney JA, Stratakis CA.Patients with the "complex of spotty skin pigmentation, myxomas, endocrine overactivity and schwannomas" (Carney complex). J Clin Endocrinol Metab. 2000; 85:3860–3865.

25. Iwata T, Tamanaha T, Koezuka R, Tochiya M, Makino H, Kishimoto I, Mizusawa N, Ono S, Inoshita N, Yamada S, Shimatsu A, Yoshimoto K. Germline deletion and a somatic mutation of the PRKAR1A gene in a Carney complex-related pituitary adenoma. Eur J Endocrinol. 2015;172(1):K5-10. doi: 10.1530/EJE-14-0685. Epub 2014 Oct 21.

26. Carney JA. Carney complex: the complex of myxomas, spotty pigmentation, endocrine overactivity, and schwannomas. Semin Dermatol. 1995;14(2):90-8. doi: 10.1016/s1085-5629(05)80003-3.

27. Borkar SS, Kamath SG, Kashyap N, et al. Carney complex: case report and review. J Cardiothorac Surg 2011;6(1):25.

28. Respondek-Liberska MR. Fetal cardiac tumors. In: Araújo Júnior E, Bravo-Valenzuela NJM, Peixoto AB, editors. Perinatal Cardiology- Part 2. 1st ed. Singapore: Bentham Science Publishers 2020;36-49.

29. Lacey SR, Donofrio MT. Fetal cardiac tumors: prenatal diagnosis and outcome. Pediatr Cardiol. 2007;28(1):61-7. doi: 10.1007/s00246-005-0876-9.

30. 30. Mankad R, Herrmann J. Cardiac tumors: echo assessment. Echo Res Pract. 2016;3(4):R65-R77. doi: 10.1530/ERP-16-0035. Epub 2016 Sep 6. PMID: 27600455..

31. Sharma J, Hirata Y, Mosca RS. Surgical repair in neonatal life of cardiac haemangiomas diagnosed prenatally. Cardiol Young. 2009;19(4):403-6. doi: 10.1017/S1047951109004168. Epub 2009 May 15.

32. Cartagena AM, Levin TL, Issenberg H, Goldman HS. Pericardial effusion and cardiac hemangioma in the neonate. Pediatr Radiol. 1993;23(5):384-5. doi: 10.1007/BF02011966.

33. Huh J, Noh CI, Kim YW, Choi JY, Yun YS, Shin HY, Ahn HS, Kim YJ. Secondary cardiac tumor in children. Pediatr Cardiol. 1999;20(6):400-3. doi: 10.1007/s002469900500..

34. Wieckowska K, Piatek K, Respondek-Liberska M. Heart tumours in 33 fetuses - review of twenty-two years of the single-centre experience. Prenatal Cardiology. 2016; 6(1):22-30.

35. Ozbek N, Alioglu B, Avci Z, Malbora B, Onay O, Ozyurek E, Atac FB. Incidence of and risk factors for childhood thrombosis: a single-center experience in Ankara, Turkey. Pediatr Hematol Oncol. 2009;26(1):11-29. doi: 10.1080/08880010802423969.

36. Choi SH, Jeong SI, Yang JH, Kang IS, Jun TG, Lee HJ, Huh J. A single-center experience with intracardiac thrombosis in children with dilated cardiomyopathy. Pediatr Cardiol. 2010;31(2):264-9. doi: 10.1007/s00246-009-9602-3.

37. Ohlow MA. Congenital left ventricular aneurysms and diverticula: definition, pathophysiology, clinical relevance and treatment. Cardiology. 2006;106(2):63-72. doi: 10.1159/000092634. Epub 2006 Apr 12.

38. Li JS, Sexton DJ, Mick N, Nettles R, Fowler VG Jr, Ryan T, Bashore T, Corey GR. Proposed modifications to the Duke criteria for the diagnosis of infective endocarditis. Clin Infect Dis. 2000;30(4):633-8. doi: 10.1086/313753. Epub 2000 Apr 3.

39. Sordelli C, Fele N, Mocerino R, Weisz SH, Ascione L, Caso P, Carrozza A, Tascini C, De Vivo S, Severino S. Infective Endocarditis: Echocardiographic Imaging and New Imaging Modalities. J Cardiovasc Echogr. 2019;29(4):149-155. doi: 10.4103/jcecho.jcecho_53_19. PMID: 32089994.

40. Li JS, Sexton DJ, Mick N, Nettles R, Fowler VG Jr, Ryan T, Bashore T, Corey GR. Proposed modifications to the Duke criteria for the diagnosis of infective endocarditis. Clin Infect Dis. 2000;30(4):633-8. doi: 10.1086/313753. Epub 2000 Apr 3.

Impairment of Right Ventricular Function in Patients with Systemic Sclerosis and Interstitial Lung Disease: Tissue Doppler Evaluation

Acometimento da Função Ventricular Direita em Pacientes com Esclerose Sistêmica e Doença Pulmonar Intersticial: Avaliação pelo Doppler Tecidual

Ana Clara Tude Rodrigues[1]; Fernando U. Kay[1]; Marina Roque[1]; Thais Emerick Henriques Gripp[1]; Derly Becker[1]; Ana Lucia Arruda[1]; Giovanni Guido Cerri[1]; Percival D. Sampaio-Barros[2]

InRad - HC- University of São Paulo[1], São Paulo, SP, Brazil. Division of Rheumatology, Hospital das Clínicas HCFMUSP, School of Medicine[2], University of São Paulo, São Paulo, SP, Brazil.

Abstract

Introduction: Systemic sclerosis (SSc) is an autoimmune tissue connective disease that courses with fibrosis and microvascular dysfunction. Involvement of the visceral organs, including the lungs and heart, is the main cause of death among patients with SSc. In this context, here we analyzed the relationship between right ventricle (RV) parameters assessed by tissue Doppler echocardiography and lung involvement in patients with SSc.

Methods: Patients fulfilling the 2013 SSc Classification Criteria underwent tissue Doppler echocardiography for the assessment of left ventricular (LV) systolic function (ejection fraction) and RV fractional area change (FAC), tissue Doppler s' (systolic) velocity, myocardial performance index, and tricuspid annular plane systolic excursion for the assessment of RV systolic function. Pulmonary systolic pressure was estimated using tricuspid regurgitation. Chest high-resolution computed tomography was used to evaluate the presence of pulmonary fibrosis. The patients were divided into two subgroups accordingly: Group I, patients with pulmonary fibrosis (n=26); and Group II, those without fibrosis (n=17).

Results: Among the 43 patients with SSc, most were female (86%), and the mean age was 51 ± 12 years. All patients had normal systolic ventricular function as evidenced by an LV ejection fraction > 55% and an RV FAC > 35%. No significant intergroup difference was noted in age or disease duration. Except for a decreased tissue Doppler s' velocity in patients with lung fibrosis, all indexes of RV performance were similar. Conclusion: In patients with SSc and pulmonary fibrosis, tissue Doppler identified early RV longitudinal myocardial involvement despite preserved RV radial systolic performance.

Keywords: Systemic Sclerosis; Tissue Doppler; Pulmonary Fibrosis.

Resumo

Introdução: *A esclerose sistêmica (ES) é uma doença autoimune do tecido conjuntivo que cursa com fibrose e disfunção microvascular. O envolvimento dos órgãos viscerais, incluindo os pulmões e o coração, é a principal causa de óbito na ES. Nesse contexto, analisamos a relação entre os parâmetros ventriculares direitos (VD) pela ecocardiografia com Doppler tecidual e o acometimento pulmonar em pacientes com ES.*

Métodos*: Os pacientes que preencheram os Critérios de Classificação da ES de 2013 foram submetidos à ecocardiografia com Doppler tecidual para avaliação da função sistólica (fração de ejeção) ventricular esquerda (VE), enquanto a função sistólica do VD foi avaliada por meio da fração de variação de área do VD (fractional area change — FAC), velocidade (sistólica) do Doppler tecidual, índice de desempenho miocárdico (IDM) e excursão sistólica do plano anular tricúspide (TAPSE). A pressão sistólica pulmonar foi estimada por insuficiência tricúspide. A tomografia computadorizada de alta resolução (TCAR) de tórax avaliou a presença de fibrose pulmonar. De acordo com os resultados da TCAR, os pacientes foram divididos em 2 subgrupos: Grupo I, incluindo pacientes com fibrose pulmonar (n=26), e Grupo II sem fibrose (n=17).*

Resultados: *Entre os 43 pacientes com ES, a maioria era do sexo feminino (86%) com idade de 51±12 anos. Todos os pacientes apresentavam função ventricular sistólica normal, avaliada pela FEVE>55% e FAC VD>35%. Não houve diferença significativa em termos de idade ou duração*

Mailing Address: Ana Clara Tude Rodrigues. •
Instituto de Radiologia (InRad). Hospital das Clínicas da Faculdade de Medicina da Universidade de São Paulo. Rua Dr. Ovídio Pires de Campos, 75. CEP 05403-010, Cerqueira César, São Paulo, SP – Brazil.
E-mail: ana.rodrigues@hc.fm.usp.br
Manuscript received 7/28/2022; revised 8/4/2022; accepted 8/8/2022

DOI: 10.47593/2675-312X/20223503eabc331

CC BY

da doença para os grupos. Exceto pela diminuição das velocidades do Doppler tecidual em pacientes com fibrose pulmonar, todos os índices de desempenho do VD foram semelhantes.

Conclusão: *Em pacientes com ES e fibrose pulmonar, o Doppler tecidual identifica acometimento miocárdico longitudinal precoce do VD, apesar do desempenho sistólico radial preservado do VD.*

Palavras-chave: *Esclerose Sistêmica; Doppler tecidual; Fibrose Pulmonar.*

Introduction

Systemic sclerosis (SSc) is an autoimmune connective tissue disease that courses with endothelial dysfunction, resulting in diffuse vascular lesions, excessive collagen production, and fibrosis of the skin and major organs, including the lungs, kidneys, and heart.[1] As the pulmonary fibrotic and vascular manifestations of SSc, including pulmonary hypertension and lung fibrosis, are the leading cause of death,[2] the early recognition of lung and heart involvement are essential for the proper management of these patients. Cardiac involvement includes right heart dysfunction due to pulmonary hypertension, myocardial fibrosis, and pericardial involvement and is usually associated with a poor prognosis.[3] It is unclear whether involvement of the right ventricle (RV) results directly from organ lesion or indirectly from lung disease (pulmonary hypertension and fibrosis). Thus, the noninvasive estimation of RV function with imaging is challenging due to the complex RV geometry. As tissue Doppler echocardiography has been adequately used to assess RV function and pulmonary pressures, here we analyzed the relationship between RV performance and lung involvement in patients with SSc.

Methods

Patients: Our population consisted of outpatients older than 18 years of both sexes who were diagnosed with SSc according to the 2013 Classification Criteria.[4] Only patients with a normal systolic left ventricular (LV) function (LV ejection fraction > 0.55) and preserved RV function (as assessed by a fractional area > 35%) were included in the study. Patients with suboptimal echocardiography windows were excluded. All patients provided written informed consent to participate. The study was approved by the local institutional ethics committee.

Echocardiography: A comprehensive echocardiography examination was performed of all patients by an experienced echocardiographer using commercially available equipment (Artida, Toshiba, Japan). LV diameters and systolic function (Teichholz formula) and mass were measured from bidimensional images obtained from the parasternal long-axis view. Left atrial volumes were obtained on two- and four-chamber views using the modified Simpson's biplane rule. Diastolic function was evaluated with transmitral Doppler, with the sample volume placed at the tips of the mitral valve on the apical four-chamber plane to obtain velocity recordings of early (E) and late (A) wave and E wave deceleration time. Tissue Doppler velocities were obtained from basal septal and lateral mitral annulus to record early (e') tissue Doppler myocardial velocities. Images were obtained at end expiration, and the average of three cycles was used in the analysis.

Assessment of RV function: RV performance was evaluated using RV fractional area change (FAC) defined as: (end-diastolic area − end-systolic area)/end-diastolic area × 100. From the apical four-chamber view, endocardial borders of the RV free wall and septum were traced to obtain end-diastolic area identified as the onset of the electrocardiography R wave from a simultaneously recorded electrocardiogram and end systole considered the smallest RV cavity size before tricuspid valve opening. Tissue Doppler myocardial systolic (s') velocity was obtained from the apical four-chamber view, with the sample volume placed at the lateral base of the tricuspid annulus. Myocardial performance index (MPI) was obtained from tissue Doppler recordings measured from the lateral RV wall and calculated as (a − b)/b, where (a) was the interval from the end of the late diastolic annular velocity to the onset of the early diastolic annular velocity and (b) was measured from the onset to the end of the systolic annular velocity. Tricuspid annular plane systolic excursion (TAPSE) was acquired by the placement of an M-mode cursor through the tricuspid annulus and the measurement of the distance of longitudinal movement of the annulus during systole. Pulmonary systolic pressure was measured from tricuspid regurgitation jet velocity and added to the right atrial pressure estimated as the inferior vena cava diameter at rest and after respiratory excursion. The diagnosis of pulmonary hypertension was considered when estimated pulmonary systolic pressure was >36 mmHg on Doppler echocardiography.

Chest high-resolution computed tomography (HRCT): Chest HRCT was performed within 1 month of the echocardiography to assess the presence of lung fibrosis. Fibrotic interstitial lung disease was considered present based on any of the following findings: reticular opacities, traction bronchiectasis, or honeycombing (isolated or in combination). According to the chest HRCT results, patients were divided into two groups: Group I, SSc patients with pulmonary fibrosis; and Group II, SSc patients without pulmonary fibrosis. Studies were reviewed to consensus by cardiothoracic radiologists with 1 (T.G.) and 6 years (F.K.) of experience with HRCT. (Figure 1)

Statistics: Continuous variables are expressed as mean ± standard deviation, while categorical variables are expressed as percentages. Continuous variables were compared using the two-sided Student's t test, whereas categorical variables were tested with the Chi squared or Fisher's exact test. Values of $p < 0.05$ were considered statistically significant.

Echocardiographic measurements of RV function (FAC, TAPSE, IPM, RV s') were repeated for 15 patients by two

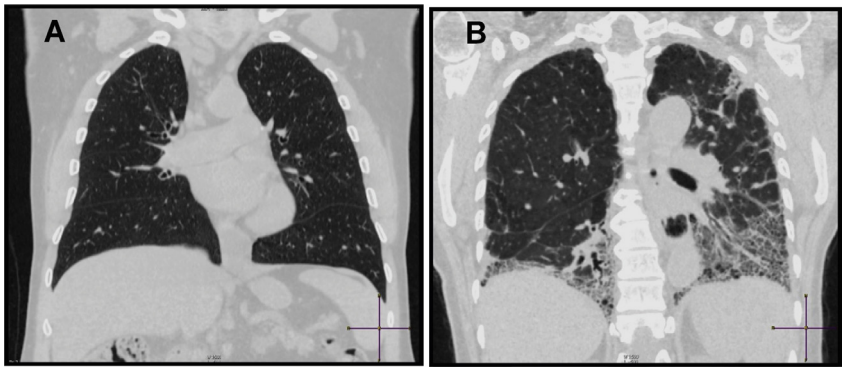

Figure 1 – *High-resolution chest computed tomography images of patients with systemic sclerosis showing (A) coronal reconstruction of a normal lung parenchyma; and (B) coronal reconstruction of fibrotic interstitial lung disease associated with systemic sclerosis showing reticular opacities, traction bronchiectasis, and honeycombing.*

readers (ACR and MR) for the assessment of intra- and interobserver variability. Variability was calculated as the difference between the two observations divided by the mean of the observations expressed as percentages.

Results

Among the 51 patients who underwent echocardiography, eight were excluded, five of them for not having undergone chest HRCT, two for having suboptimal echocardiographic images, and one for severe LV dysfunction; thus, the final group included 43 patients. Most patients were female (86%), with a mean age of 51 ± 12 years and a mean disease duration of 11.4 ± 8.7 years (median, 9.5 years). The mean LV ejection fraction was 0.63 ± 0.04, while the LV mass index was 92 ± 28 g/m^2. Regarding the RV assessment, the measurement of pulmonary artery systolic pressure from tricuspid regurgitation was feasible in 33 patients, with a mean value of 30 ± 14 mmHg. Pulmonary hypertension was uncommon in this group, with only five patients (15%) having a pulmonary systolic pressure > 36 mmHg. The other indices used to assess RV performance were normal as observed by TAPSE (22 ± 4 mm) and RV s' wave (12.7 ± 2.7 cm/s). The mean FAC was 47 ± 7%. The mean tissue Doppler RV MPI for the entire population was also within the normal range (0.47 ± 0.10).

Chest HRCT analysis: According to the HRCT results, there were 26 patients in Group I (lung fibrosis) and 17 patients in Group II (no lung fibrosis). There was no significant intergroup difference in age or sex, but disease duration was longer for patients with pulmonary fibrosis (12.9 ± 10 years vs. 8.1 ± 4.9 years, p < 0.03). LV systolic function and mass were also similar between groups. Regarding the assessment of RV function, except for the significant (p = 0.02) decrease in tissue Doppler s' velocities in patients with pulmonary fibrosis on chest CT, all indexes of RV performance were similar. (Table 1)

Discussion

As lung fibrosis and pulmonary hypertension are the leading causes of death in SSc,[5] the 2013 Classification Criteria defined visceral involvement as the lung only.[4] The early recognition of lung involvement is essential as *more than two-thirds of* patients will have interstitial abnormalities on chest HRCT,[6] which is well-established as an accurate and noninvasive tool for detecting and characterizing lung fibrosis.[7] The HRCT pattern in SSc patients is generally nonspecific interstitial pneumonia, with a greater proportion of ground-glass opacity and a lower proportion of coarse reticulation.[8] We studied two groups of patients with SSc with HRCT, one with lung fibrosis and the other without fibrosis, and showed that patients with SSc and lung fibrosis have significant lower tissue Doppler s' velocities than patients without fibrosis. A decrease in tissue Doppler velocities in patients with SSc, along with an increase in MPI, was already observed in association with a worse prognosis,[9] allowing the speculation that RV dysfunction could be related to RV fibrosis. Our findings are new because we showed the association between decreased longitudinal RV function and the presence of lung fibrosis. RV myocardial fibrosis reportedly occurred

Tabela 1 - Clinical and echocardiographic variables of patients with (Group I) and without (Group II) lung fibrosis.

	Group I (n=26)	Group II (n=17)	*p*
Age, years	53±11	51±12	NS
Female sex	23 (88%)	16 (94%)	NS
Disease duration, years	12.9±10	8.1±4.9	0,03
LV EF, %	62±2	64±4	NS
LV mass index, g/m2	92±18	89±34	NS
E/e' septal	11±4	11±3	NS
FAC, %	48±6	45±6	NS
RV s', cm/s	11.9±1.6	13.5±2.4	0,02
RV MPI	0.48±0.1	0.46±0.1	NS
TAPSE, mm	22.0±3.2	23.3±4.8	NS
PASP, mmHg	32±16	28±12	NS

EF, ejection fraction; FAC, fractional area change; LV, left ventricular; MPI, myocardial performance index; PASP, pulmonary artery systolic pressure; RV, right ventricular; s', systolic tissue Doppler wave; TAPSE, tricuspid annular plane systolic excursion. Values are shown as mean ± standard deviation or n (%).

concomitantly with lung fibrosis in pathological studies, so it is conceivable that RV dysfunction (assessed by RV s' velocity) results from RV fibrosis, particularly in this sample with a low prevalence of pulmonary hypertension (only five patients).

We acknowledge that this hypothesis is predominantly speculative, as endomyocardial biopsies were not performed to correlate histopathological findings with imaging techniques; however, these patients had no other right heart disease that would fully explain the decrease in tissue Doppler velocity. Furthermore, endomyocardial biopsy also has some disadvantages: myocardial fibrosis can be found in a patchy distribution throughout the myocardium, thus limiting biopsy accuracy, apart from being invasive and not without risk, in addition to a lack of studies with subclinical heart disease.

Histopathological studies comparing patients with SSc and idiopathic pulmonary hypertension showed a similar degree of RV myocardial fibrosis but greater inflammation in the former.[10] Tissue Doppler was able to identify incipient RV dysfunction better than other conventional parameters of RV performance. Tissue Doppler velocities are reduced in cardiomyopathies and have been used for the preclinical detection of several diseases. We also found no association with TAPSE, mainly due to pulmonary hypertension.[11]

The assessment of RV function is critical in these patients, as studies analyzing survival among patients with SSc have shown worse survival in patients with a high mean right atrial pressure and low cardiac index. A study comparing SSc patients with a control group using echocardiography with tissue Doppler observed a decrease in biventricular systolic and diastolic dysfunction; after a 3-year follow-up, the deterioration of these indices was also reported.[12]

The prevalence of PH in SSc is variable and depends on the method of detection and the population studied. Although cardiac catheterization is considered the gold standard for investigating PH, Doppler echocardiography is an important screening factor in daily rheumatologic practice.[13] Using transthoracic Doppler echocardiography, the prevalence of PAH is reportedly 13–35%.[14] This study had a low prevalence of PH, most likely due to the exclusion of patients with right and left myocardial dysfunction. Additionally, there was no significant difference in the presence of PH between subgroups.

Therefore, tissue Doppler s' velocity could be used as a potential predictor of RV dysfunction and possible pulmonary fibrosis in patients with SSc. Tissue Doppler has the advantage of being less dependent on load than usual indexes used to evaluate RV myocardial performance and could be used to serially monitor RV performance in patients with SSc. The RV s' velocity represents the integral of myocardial shortening velocity from base to apex; therefore, it provides information on global rather than regional ventricular function.

Limitations: As stated above, the presence of RV myocardial fibrosis can only be speculated since endomyocardial biopsies were not performed in this population. Moreover, delayed enhancement magnetic resonance imaging has been used to assess the presence of myocardial fibrosis in the LV,[15] so additional studies are necessary to identify the pattern and presence of RV fibrosis in association with lung fibrosis in patients with SSc.

In conclusion, this study showed that tissue Doppler systolic velocity may be an early indicator of myocardial RV involvement in patients with SSc and pulmonary fibrosis and could potentially be used to monitor RV performance in this population.

Authors' contributions

Each author contributed individually and significantly to the development of this article. Rodrigues ANT: conception and writing of the manuscript; Kay FU: CT assessment; Roque MCF and Becker D: performance of exams and measurements; Gripp TEH: tomography evaluation; Arruda AL: writing of the manuscript; Cerri GG and Sampaio-Barros PD; manuscript review.

Conflict of interest

The author declares that he has no conflict of interest

References

1. Denton CP, Khanna D. Systemic sclerosis. Lancet. 2017 Oct 7;390(10103):1685-1699. doi: 10.1016/S0140-6736(17)30933-9.

2. Sampaio-Barros PD, Bortoluzzo AB, Marangoni RG, Rocha LF, Del Rio AP, Samara AM, et al. Survival, causes of death, and prognostic factors in systemic sclerosis: analysis of 947 Brazilian patients. J Rheumatol. 2012 Oct;39(10):1971-8. doi: 10.3899/jrheum.111582.

3. Bruni C, Ross L. Cardiac involvement in systemic sclerosis: Getting to the heart of the matter. Best Pract Res Clin Rheumatol. 2021 Sep;35(3):101668. doi: 10.1016/j.berh.2021.101668.

4. van den Hoogen F, Khanna D, Fransen J, Johnson SR, Baron M, Tyndall A, *et al*. 2013 classification criteria for systemic sclerosis: an American college of rheumatology/European league against rheumatism collaborative initiative. Ann Rheum Dis. 2013 Nov;72(11):1747-55. doi: 10.1136/annrheumdis-2013-204424.

5. Elhai M, Meune C, Boubaya M, Avouac J, Hachulla E, Balbir-Gurman A, et al. Mapping and predicting mortality from systemic sclerosis. Ann Rheum Dis. 2017 Nov;76(11):1897-1905. doi: 10.1136/annrheumdis-2017-211448.

6. Hoffmann-Vold AM, Allanore Y, Alves M, Brunborg C, Airó P, Ananieva LP, et al. Progressive interstitial lung disease in patients with systemic sclerosis-associated interstitial lung disease in the EUSTAR database. Ann Rheum Dis. 2021 Feb;80(2):219-227. doi: 10.1136/annrheumdis-2020-217455.

7. Khanna SA, Nance JW, Suliman SA. Detection and Monitoring of Interstitial Lung Disease in Patients with Systemic Sclerosis. Curr Rheumatol Rep. 2022 May;24(5):166-173. doi: 10.1007/s11926-022-01067-5.

8. Perelas A, Silver RM, Arrossi AV, Highland KB. Systemic sclerosis-associated interstitial lung disease. Lancet Respir Med. 2020 Mar;8(3):304-320. doi: 10.1016/S2213-2600(19)30480-1.

9. Hsiao SH, Lee CY, Chang SM, Lin SK, Liu CP. Right heart function in scleroderma: insights from myocardial Doppler tissue imaging. J Am Soc Echocardiogr. 2006;19(5):507-14. doi: 10.1016/j.echo.2005.12.003.

10. Nagueh SF, Bachinski LL, Meyer D, Hill R, Zoghbi WA, Tam JW, et al. Tissue Doppler imaging consistently detects myocardial abnormalities in patients with hypertrophic cardiomyopathy and provides a novel means for an early diagnosis before and independently of hypertrophy. Circulation. 2001 Jul 10;104(2):128-30. doi: 10.1161/01.cir.104.2.128.

11. Forfia PR, Fisher MR, Mathai SC, Housten-Harris T, Hemnes AR, Borlaug BA, et al. Tricuspid annular displacement predicts survival in pulmonary hypertension. Am J Respir Crit Care Med. 2006 Nov 1;174(9):1034-41. doi: 10.1164/rccm.200604-547OC.

12. D'Alto M, Cuomo G, Romeo E, Argiento P, Iudici M, Vettori S, et al. Tissue Doppler imaging in systemic sclerosis: a 3-year longitudinal study. Semin Arthritis Rheum. 2014 Apr;43(5):673-80. doi: 10.1016/j.semarthrit.2013.10.004.

13. Weatherald J, Montani D, Jevnikar M, Jaïs X, Savale L, Humbert M. Screening for pulmonary arterial hypertension in systemic sclerosis. Eur Respir Rev. 2019; 28(153):190023. doi: 10.1183/16000617.0023-2019.

14. Ramirez A, Varga J. Pulmonary arterial hypertension in systemic sclerosis: clinical manifestations, pathophysiology, evaluation, and management. Treat Respir Med. 2004;3(6):339-52. doi: 10.2165/00151829-200403060-00002.

15. Tzelepis GE, Kelekis NL, Plastiras SC, Mitseas P, Economopoulos N, Kampolis C, et al. Pattern and distribution of myocardial fibrosis in systemic sclerosis: a delayed enhanced magnetic resonance imaging study. Arthritis Rheum. 2007 Nov;56(11):3827-36. doi: 10.1002/art.22971.

Correlation Between Echocardiographic and Hemodynamic Measurements in Right Atrium and Right Ventricle Assessments of Patients with Pulmonary Hypertension

Correlação entre Medidas Ecocardiográficas e Hemodinâmicas na Avaliação do Átrio Direito e Ventrículo Direito em Pacientes com Hipertensão Pulmonar

Ana Tereza Azeredo Bastos Brito[1], João Batista Masson Silva[1], Daniela do Carmo Rassi[1], Daniela Graner Schuwartz Tannus Silva[1], Sandra Araújo Costa[2], Diogo Sampaio de Oliveira[2], Flavio de Souza Veiga Jardim[2], Leandro Zacarias F. de Freitas[2], Aguinaldo F. de Freitas Júnior[1], Salvador Rassi[1]

Hospital das Clínicas, Federal University of Goiás[1], Goiânia, GO, Brazil. School of Medicine, Federal University of Goiás[2], Goiânia, GO, Brazil.

Abstract

Introduction: Pulmonary hypertension (PH), a serious clinical condition, can lead to right ventricular systolic dysfunction (RVSD) with prognostic implications. Patients with suspected PH should undergo transthoracic echocardiography (TTE) for diagnosis and evaluation as the main screening and follow-up exam.

Objective: To verify the associations of and agreement between measurements of mean pressure in the right atrium (RA) and RVSD with TTE

Method: Individuals diagnosed with PH were included. All patients underwent TTE and RCC. The following were evaluated by TTE: right atrial area (RAA), mean right atrial pressure through the diameter and collapsibility of the inferior vena cava (RMAPTTE), RA strain (RAS), tricuspid annular plane systolic excursion, fractional area change, RV free wall strain, and tricuspid s' wave. Mean RA pressure (RMAPRCC) and cardiac index (CI) were evaluated through the RCC.

Results: Of the 16 patients, 13 were female. The mean patient age was 44.4 (±14.9) years. An association was found between RMAPRCC and AAD, RMAPTTE, and RAS (r=0.845, r=0.621, and r=-0.523, respectively; p<0.05). There was an association between the mortality risk categories measured by the RAA and RMAPRCC measures (X2=10.42; p=0.003), with moderate agreement (k=0.44; p=0.012). RVSDJ was present in 10 patients. There was an association between RVSD (present or absent) and CI (r=0.522; p=0.04) with moderate agreement (k=0.43; p=0.037).

Conclusion: The TTE and RCC measurements showed an association in the assessment of mean right atrial pressure, especially between RAA and RMAPRCC. An association with RVSD and moderate agreement between methods were also noted.

Keywords: Hypertension, Pulmonary, Echocardiography, Ventricular Dysfunction, Right, Catheterization.

Resumo

Introdução: *Hipertensão Pulmonar (HP), uma condição clínica grave, pode levar à disfunção sistólica do ventrículo direto (DSVD), com implicações prognósticas. Pacientes com suspeita de HP devem ser submetidos ao ecocardiograma transtorácico (ECOTT) para diagnóstico e avaliação, colocando-o como o principal exame de triagem e acompanhamento.*

Objetivo: *Verificar a associação e a concordância das medidas referentes à pressão média no átrio direito (AD) e à disfunção sistólica do ventrículo direto (DSVD) ao (ECOTT) e ao cateterismo de câmaras direitas (CCD) em pacientes com (HP).*

Métodos: *Foram incluídos indivíduos com diagnóstico de (HP). Todos os pacientes foram submetidos ao ECOTT e CCD. Avaliou-se pelo ECOTT: área do átrio direito (AAD), pressão média do átrio direito (AD) através por meio do diâmetro e da colapsabilidade da veia cava inferior ($PMAD_{ECOTT}$), strain AD (SAD), TAPSE (excursão sistólica do plano anular tricúspide), MAF (mudança da área fracional), SPLVD (strain da parede livre do VD) e onda s´ tricuspídea. Pelo CCD avaliaram-se pressão média do ($PMAD_{CCD}$) e índice cardíaco (IC).*

Mailing Address: Ana Tereza Azeredo Bastos Brito •
Avenida Primeira Avenida, quadra 68, lote AR 1, Setor Leste Universitário. CEP 74605-020 – Goiânia, GO, Brazil.
E-mail: anaterezaa@hotmail.com
Manuscript received 5/23/2022; revised 7/18/2022; accepted 8/8/2022

DOI: 10.47593/2675-312X/20223503eabc308

CC BY

Resultados: *Dos 16 pacientes, 13 eram do sexo feminino. A idade média foi de 44,4 anos (±14,9). Constataram-se associação entre pressão média do átrio direito PMADCCD com área do átrio direito, PMADECOTT pressão média do átrio direito e SAD strain do átrio direito (r=0,845, r=0,621 e r=-0,523, respectivamente; p< 0,05). Verificou-se associação entre as categorias de risco de mortalidade, mensuradas pelas medidas AAD da área do átrio direito e pressão média do átrio direito PMADCCD (X2=10,42; p=0,003), com concordância moderada (k=0,44; p=0,012). DSVD A disfunção sistólica do ventrículo direto estava presente em dez pacientes. Houve associação entre disfunção sistólica do ventrículo direto DSVD (presente ou ausente) e índice cardíaco IC (r=0,522; p=0,04), com concordância moderada (k=0,43; p=0,037).*

Conclusão: *As medidas do ecocardiograma transtorácico (ECOTT) e cateterismo de câmara direita (CCD) demostraram associação na avaliação da pressão média do átrio direito com melhor associação entre área do átrio direito AAD e pressão média do átrio direito ($PMAD_{CCD}$). Houve associação com concordância moderada quanto à disfunção sistólica do ventrículo direto (DSVD) entre métodos.*

Palavras-chave: *Hipertensão pulmonar, Ecocardiografia, Disfunção Ventricular Direita, Cateterismo.*

Introduction

Pulmonary hypertension (PH) is a potentially severe clinical condition characterized by hemodynamic changes resulting from several pathophysiological mechanisms that can lead to progressive right ventricular (RV) failure and even death.[1]

The early detection and accurate disease severity classification are essential for diagnosing PH and ensuring that patients receive the best treatment.[2]

All patients with suspected PH should undergo transthoracic echocardiography (TTE) to diagnose and evaluate PH repercussions as the main screening test.[3,4] RV systolic pressure and right atrial (RA) mean pressure are estimated by TTE. Additionally, right chamber characteristics are evaluated, especially regarding PH-related structural and functional disorders.[2,3,5] TTE measurements have prognostic importance in PH patients. Those referring to RV systolic function assessment, which can be determined by quantifying the tricuspid annular plane systolic excursion (TAPSE), RV fractional area changes (FAC), tricuspid annular systolic velocity (tricuspid s□), and RV free wall strain (RVFWS) stand out.[6] Adequate RA assessments are highly relevant in the context of PH, as mean RA pressure and its dimensional increase are prognostic factors for patients with PH,[7–9] but the reliability and accuracy of noninvasive assessments are limited. RA strain (RAS) analysis also has prognostic importance for patients with PH.[6]

PH treatment is linked to an adequate diagnosis, which starts after clinical suspicion and echocardiogram compatible with the disease, followed by the PH group identification. After concluding the diagnosis of pulmonary arterial hypertension (group 1), a differential diagnosis is made between several causes with a subsequent risk stratification (1-year mortality). This stratification considers clinical, imaging, and hemodynamic parameters, including RA area (RAA) and mean pressure obtained by right chamber catheterization (RCC). This assessment is recommended every 3–6 months to achieve/maintain a low-risk profile with treatment associated with good exercise capacity, good quality of life, good RV function, and a low risk of mortality.[4]

Most patients with PH are referred for RCC to confirm the diagnosis and assess its severity, prognosis, and response to specific therapies during the disease course. This test is considered the gold standard for these assessments.[10] Although safe, RCC is invasive and its generalized use is not recommended, as its acquisition and interpretation require special attention and expertise.[11,12]

Thus, this study aimed to verify the accuracy and precision of mean pressure parameters in RA and RV dysfunction on TTE versus the corresponding measurements obtained by RCC in patients with PH.

Methods

The study was developed in accordance with the Regulatory Guidelines and Norms for Human Research (resolution 466/2012 of the National Health Council and Declaration of Helsinki) and approved by the local institutional ethics committee. All participants signed an informed consent form.

Participants

This study population consisted of patients referred for RCC for PH assessment in 2019–2021. The inclusion criteria were age over 14 years, being of either sex, and diagnosis of PH in groups 1 (pulmonary arterial hypertension, including idiopathic disease) and 4 (chronic thromboembolic pulmonary hypertension) according to clinical PH classification.[13] The exclusion criteria were significant arrhythmia, severe heart failure, inadequate TTE echocardiographic window, and incomplete invasive measurements.

Instruments and procedures

The patients initially attended pre-scheduled appointments at cardiology outpatient clinics for inclusion criteria screening. The included patients were evaluated for demographic data collection (age, sex, body mass index [BMI]) and clinical and physical examination findings (functional class, group, medication use) after signing the informed consent form. Subsequently, all patients underwent TEE in the echocardiography laboratory and, after 3–4 h, underwent RCC in the hemodynamics laboratory.

Transthoracic echocardiography

All patients underwent TEE performed by a single experienced echocardiographer using a Philips CX 50 device

with a 2.5–3.5 MHz multifrequency transducer. Cardiac chamber echocardiographic measurements were performed according to the transthoracic echocardiographic examination guidelines of the American Society of Echocardiography[14] and the consensus document of the European Society of Cardiovascular Imaging and the American Society of Echocardiography for left atrial, RV, and RA deformity imaging on echocardiography.[15]

The following hemodynamic measurements were obtained and/or calculated by TTE: RV systolic pressure (RVSP; in mmHg) calculated by the formula 4 × peak tricuspid regurgitation velocity^2 + estimated mean RA pressure ($MRAP_{TTE}$); and mean pulmonary artery pressure (MPAP; in mmHg) calculated by the formula 0.6 × pulmonary artery systolic pressure (PASP).

The RAA (in cm^2) was measured in the four-chamber apical plane at the end of ventricular systole (frame before tricuspid valve opening). The RAS and RVFWS were analyzed through optimized images obtained in the apical four-chamber plane focused on the RV, with a frame rate > 50 Hz with the QRS as the reference point. QLAB 13 (Philips) software version 13.0 (2019) was used for these analyses. The RVFWS was calculated as the mean peak systolic deformity of each of the three long free wall segments expressed as an absolute value. The mean RAS of each atrial wall segment (reservoir function) was calculated through the positive peak wave at the end of ventricular systole.

The parameters used to analyze RV systolic function obtained in the apical four-chamber plane were TAPSE obtained by positioning the unidimensional mode cursor (M) in the basal region of the lateral tricuspid annulus (VN > 16 mm); FAC obtained in two-dimensional mode by tracing the RV endocardial borders and area in systole and diastole and using the formula: FAC=100 (RV area in diastole – RV area in systole)/RV area in diastole (VN>34%); tricuspid s-wave velocity with the positioning of the tissue Doppler volume sample in the basal region of the lateral tricuspid ring (VN>9.4 cm/s), and RVFWS previously described (absolute VN>19%). When one of the four parameters was changed on echocardiography, the diagnosis of RV systolic dysfunction (RVSD) was confirmed.

$MRAP_{TEE}$ evaluated through the inferior vena cava was estimated by images acquired in the subcostal window. The diameter was measured 1–2 cm distant from the junction of the inferior vena cava (IVC), with the RA and the diameter evaluated at the end of expiration. An IVC diameter < 2.1 cm that collapsed > 50% with inspiration received a MRAP value of 3 mmHg, while an IVC diameter > 2.1 cm that collapsed to < 50% received a value of 15 mmHg. In scenarios in which the IVC diameter and collapse did not fit this parameter, an intermediate value of 8 mmHg was used.[4]

Right chamber catheterization

RCC was performed according to the American Heart Association guidelines[4] using a Philips FD10 fluoroscopy device and a TEB SP12 polygraph machine. A JR catheter was introduced through the right cubital or right femoral vein and advanced under radioscopic guidance through the superior vena cava, RA, and tricuspid valve to the pulmonary artery (PA).

Systolic pressure, diastolic pressure, and MPAP were measured in this position in addition to pulmonary capillary pressure, cardiac output (CO), and cardiac index (CI). CO was calculated using the indirect Fick method.

As for RCC, the following measurements were extracted from the pulmonary systolic pressure (systolic PP, in mmHg) and mean systolic pressure (mean PP, in mmHg). RA pressure (RAP; in mmHg) and CI (in L/min/m^2) were also measured to identify patients with ventricular dysfunction (<2.8 L/min/m^2) and no dysfunction (>2.8 L/min/m^2).

Statistical analysis

SPSS software version 25.0 was used for all statistical analyses.

Initially, normality and homogeneity were verified using the Shapiro-Wilk and Levene tests, respectively.

Categorical variables are presented as absolute (n) and relative (%) frequency, while parametric continuous variables are presented as mean and standard deviation (SD) or median and interquartile range.

Linear regression and the Pearson chi-square test were performed for continuous and categorical variables, respectively, to verify the association between the TTE and RCC measurements. The magnitudes of the correlations were analyzed based on Munro's classification: low (0.26–0.49), moderate (0.50–0.69), high (0.70–0.89), and very high (0.90–1.00).[16] A significance level of 5% was used here.

Bland-Altman and intraclass correlation coefficient (ICC–k) analyses were performed after identifying the associations. The Bland-Altman analysis brings two important pieces of information: (1) the bias, which consists of the difference between the measurements and whether this is constant between the range of measurements; and (2) the limit of agreement, which represents the range of possible errors. Therefore, the bias informs the accuracy and the limit of agreement (precision).[17] A significance level of 5% was considered for all analyses.

Results

Participants

The study included 19 participants referred for RCC, with three being excluded due to the unavailability of TEE or RCC data.

Of the 16 participants, 13 (81.3%) were women. Patient ages were 14–69 years, and only three participants were older than 60 years (18.8%). Patient BMI was 13.9–42.30 kg/m^2, with most participants being within the normal range (n=10 [62.5%]). Regarding New York Heart Association functional classification, 37.5% of the patients were class III and 31.2% were class II. Group 1 was predominant (n=13 [81.2%]) with the most common etiology being congenital heart disease (n=7 [53.8%]), followed by idiopathic (n=4 [30.8%]).

Another finding was that half of the patients took specific medications for PH treatment, with 4 (25%) taking

two medications, including riociguat, bosentan, sildenafil, and ambrisentan.

RV systolic pressure was estimated using the peak velocity of tricuspid regurgitation in all patients.

Table 1 presents the participants' demographic, clinical, and physical examination data.

Table 2 presents the echocardiographic measurements of the participants' cardiac chambers and ventricular function.

Table 3 presents the TEE and RCC hemodynamic measurement values.

Right atrium

In the linear regression analysis, a positive strong association was found between $MRAP_{RCC}$ and RAA; a positive moderate association between $MRAP_{RCC}$ and $MRAP_{TEE}$; and a negative moderate association between RAP and RAS (Table 4 and Figure 1). However, no agreement was observed between measurements (Figure 2).

An association was found between risk categories (1-year mortality from PH) measured by $MRAP_{RCC}$ and $MRAP_{TTE}$ (X^2=10.42; p=0.003), with moderate agreement (k=0.44; p=0.012;). (Table 5)

Table 1 - Patients' demographic, clinical, and physical examination data (N=16).

Data	Values
Sex	
Women	13 (81.2)
Men	3 (18.8)
Age, years	44.4 (14.9)
BMI, kg/m2	26.5 (7.5)
BMI category	
Low weight	1 (6.2)
Normal weight	10 (62.6)
Overweight	1 (6.2)
Grade I obesity	1 (6.2)
Grade II obesity	1 (6.2)
Grade III obesity	2 (12.5)
NYHA functional classification	
I	3 (18.8)
II	5 (31.2)
III	6 (37.5)
IV	2 (12.5)
PH group	
1	13 (81.2)
Congenic cardiopathy	7 (53.8)
Idiopathic	4 (30.8)
Rheumatologic disease	2 (15.4)
4	3 (18.8)
Chronic PTE	3 (18.8)
Medication use	
Yes	8 (50.0)
No	8 (50.0)

BMI, body mass index; NYHA, New York Heart Association; PH, pulmonary hypertension; PTE, pulmonary thromboembolism. Data on age and BMI are presented as mean and SD; data on sex, BMI category, functional class, etiology, and medication use are presented as absolute (n) and relative (%) values.

Ventricular dysfunction and cardiac index

RVSD was present in 10 participants (62.5%). A moderate association was observed between ventricular dysfunction categories (present and absent) measured by TTE and RCC (r=0.522; p=0.04), with moderate agreement (k=0.43; p=0.037; Table 6). However, no associations were observed between categories (with and without dysfunction) identified through the CI variable (RCC) for each of the echocardiographic criteria analyzed alone (TAPSE, tricuspid annulus s', FAC, RAS, and RVFWS;). (Table 7)

Discussion

The study verified the association between TEE and RCC RA and RV morphofunctional assessment values in a group of participants with PH.

Table 2 – Echocardiographic measurements.

Variable	Values
LA, mm	35.19 (±3.67)
RVOT, mm	35.13 (±7.56)
Basal RV, mm	48.13 (±11.18)
Medium RV, mm	36.81 (±10.34)
Longitudinal RV, mm	78.25 (±8.09)
RV thickness, mm	6.08 (±1.94)
RAA, cm²	23.71 (±9.34)
RVDD, mm	45.38 (±7.03)
RVSD, mm	29.31 (±5.06)
LVEF, %	64.50 (4.50)
TAPSE, mm	1919 (±5.83)
Tricuspid s', cm/s	10.61 (±2.79)
FAC, %	34.56 (±15.03)
RVFWS, %	19.68 (±8.50)
RAS, %	24.57 (±11.27)

Data are presented as mean ± standard deviation except for LVEF and RVFWS, which are presented as median (interquartile range). FAC, fractional area change; LA, left atrium; LVDD, left ventricular diastolic diameter; LVEF, left ventricular ejection fraction; LVSD, left ventricular systolic diameter; RAA, right atrial area; RAS, right atrial strain; RV, right ventricle; RVOT, RV outflow tract; RVFWS, right ventricle free wall strain; TAPSE, tricuspid annular plane systolic excursion; tricuspid s', tricuspid annulus s' wave.

Table 3 - Hemodynamic TEE and RCC measurements.

Measurement	TTE
RVSP, mmHg	59.44 (24.10)
Mean PAP, mmHg	44.21 (20.37)
Measurement	**RCC**
SPAP, mmHg	68.50 (28.71)
MPAP	37.37 (15.37)
MRAPRCC, mmHg	12.69 (8.14)
CI, L/min/m²	3.43 (1.57)

Data are presented as mean (standard deviation). CI, cardiac index; MPAP, mean pulmonary artery pressure; MRAPRCC, mean right atrial pressure by right chamber catheterization; PAP, pulmonary arterial pressure; RCC, right chamber catheterization; RVSP, right ventricular systolic pressure; SPAP, systolic pulmonary artery pressure; TTE, transthoracic echocardiography.

The mean RAP measured by RCC ($MRAP_{RCC}$) was associated with RA measurements taken on TEE (RAA, $MRAP_{TTE}$, and RAS). These data corroborate the study findings of Yuko Fukuda et al. including a moderate correlation with the sum of the three RAS components (reservoir, content, and pump) and $MRAP_{RCC}$ (r=0.56, p=0.005). The sum of RAS also demonstrated prognostic value in that study.[9] However, in our study, despite the association, no agreement was noted between measurements, probably due to the sample size.

RAA is accurately assessed through two-dimensional planimetry only in the apical four-chamber plane, which has implications since RA performance is a three-dimensional phenomenon. However, when RA measurements were evaluated in our study, the RA showed a strong association with $MRAP_{RCC}$. Greater software availability in the future that can examine cardiac resonance will provide relevant information about this framework in the context of PH.[9]

$MRAP_{TTE}$ is performed through the respiratory variability of the IVC, which has limited accuracy due to being relatively subjective. In addition, a certain degree of an RA pressure increase may be required before IVC dilation. As this measurement is used to calculate pulmonary pressures (PASP and MPAP), an inappropriate sum of values may occur. This influence depends on PH level, being less important in more severe than borderline cases.[18] Venkateshvaran et al. showed that RA pressure estimated by TEE was falsely increased in more than 1/3 of cases, which led to overestimated RVSP and MPAP values.[20] Thus, the use of the absolute tricuspid

Tabela 4 – Associação entre $PMAD_{CCD}$ e AAD, $PMAD_{ECOTT}$ e SAD.

Variable	R value	P value
RAA	0.845	<0.001
RAP	0.621	0.010
RAS	-0.523	0.038

MRAPRCC, mean right atrial pressure by right chamber catheterization; RAA, right atrial area; MRAPTTE, mean right atrial pressure on transthoracic echocardiography; RAP, right atrial pressure; RAS, right atrial strain.

Table 5 – Association between categories determined by RAA and $MRAP_{RCC}$.

$MRAP_{RCC}$ risk category	RAA risk category		
	Low	Moderate	High
Low	3 (18.75)	2 (12.50)	0 (0.00)
Moderate	1 (6.25)	3 (18.75)	1 (6.25)
High	0 (0.00)	2 (12.50)	4 (25.0)

Data are presented as absolute and relative frequency. MRAPRCC, mean right atrial pressure by right chamber catheterization; RAA, right atrial area.

Table 6 – Association between ventricular dysfunction categories by TEE and RCC measurements.

RCC: presence of CI	TTE: presence of CI	
	Absent	Present
Absent	6 (37.5)	5 (31.2)
Present	0 (0.00)	5 (31.2)

Data are presented as absolute and relative frequency. CI, cardiac index; RCC, right chamber catheterization; TTE, transthoracic echocardiography.

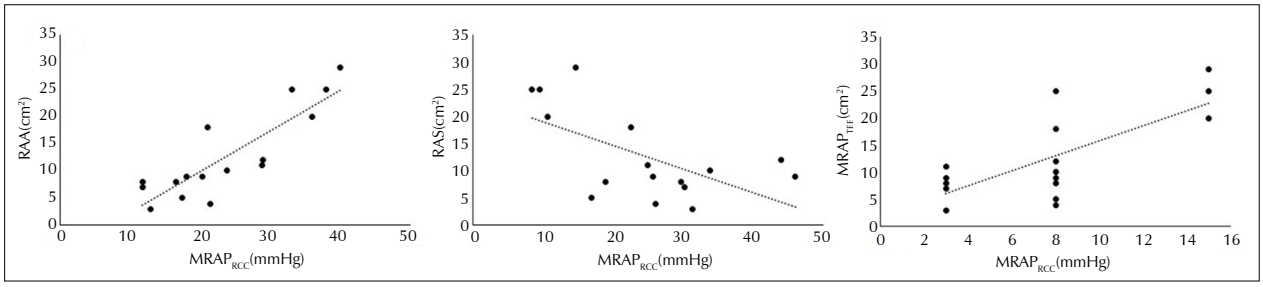

Figure 1 – *Association between MRAPRCC, RAA, MRAPTEE, and RAS.*

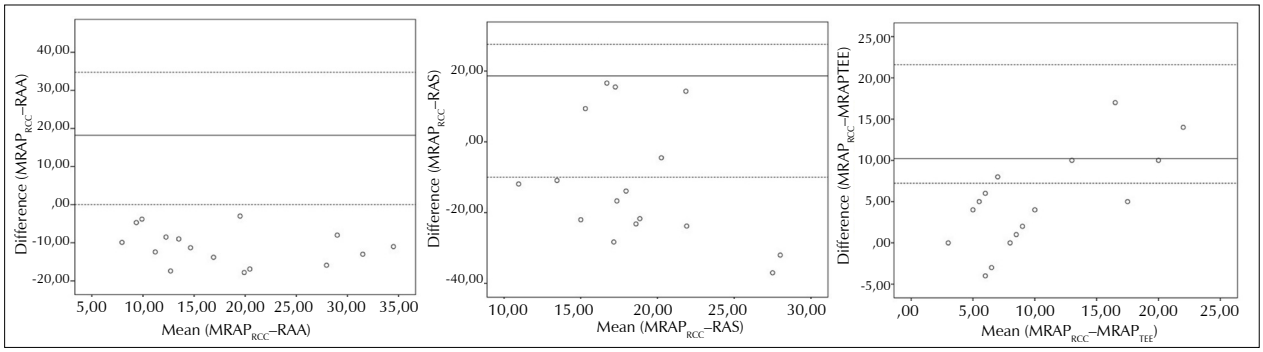

Figure 2 – *Bland-Altman plots of MRAPRCC, RAA, MRAPTEE, and RAS values.*

Table 7- Association between ventricular dysfunction variables by TTE and RCC.

Variable	Presence of dysfunction	CI: Presence of dysfunction		p value
		No	Yes	
TAPSE	No	9 (56.2)	2 (12.5)	0.107
	Yes	2 (12.5)	3 (18.8)	
Tricuspid s'	No	9 (56.2)	2 (12.5)	0.107
	Yes	2 (12.5)	3 (18.8)	
FAC	No	7 (43.8)	1 (6.2)	0.120
	Yes	4 (25.0)	4 (25.0)	
RAS	No	7 (43.8)	1 (6.2)	0.120
	Yes	4 (25.0)	4 (25.0)	
RVFWS	No	5 (31.2)	1 (6.2)	0.363
	Yes	6 (37.5)	4 (25.0)	

Data presented as absolute and relative frequency. CI, cardiac index. Other abbreviations are as shown in Table 2.

regurgitation velocity is recommended in PH assessment as recommended by international guidelines.[4,19]

PH can be classified as carrying a low, intermediate, or high risk of clinical worsening or death. Patients judged at low, intermediate, or high risk have an estimated 1-year mortality of <5%, 5–10%, and >10%, respectively.[4] $MRAP_{RCC}$ and TEE RAA are used to determine PH prognostic scores.[4] This study showed a strong association with moderate agreement between these measurements at each risk level, showing good accuracy.

Due to its anatomical complexity, the RV is the most difficult cardiac chamber to analyze functionally. Cardiac resonance, the gold standard for RV morphofunctional analysis, has no technical limitations in image acquisition, but its lower availability, greater complexity, and higher cost make it unfeasible as a method of choice. On the other hand, TEE has low cost and high feasibility, making it the most attractive method for the initial assessment of global RV function and leaving cardiac resonance for selected cases.[21,22]

RV systolic function can be identified by reduced CI values on RCC and RVSD measurements on TEE. We found an association between LVSD measurements on TEE and CI on RCC with moderate agreement. In this study, CO was calculated using the indirect Fick method, which is less accurate than the direct Fick method and thermodilution with the Swang Ganz, which may explain this result. In addition, RV measurements by TEE change early, before an effective CO change on RCC occurs, which could corroborate this finding.[17,23]

No associations were observed between categories (with and without dysfunction) assessed through the CI variable (RCC) for each of the echocardiographic criteria analyzed alone. This result is probably due to the small number of patients in our sample.

Study limitations

This study has limitations such as its small sample size. However, we consider this a pilot study from which we will expand our sample to obtain more robust results. Cardiac resonance imaging is not available in our service to correlate echocardiographic measurements with the gold standard method, but the tests were performed by an experienced echocardiographer and patients with inadequate windows were excluded. Another limitation was the lack of echocardiographic intra- and interobserver variation assessments, but the tests were performed by an examiner with extensive experience testing patients with PH. Use of the indirect Fick method to perform the RCC hemodynamic measurements may be another limiting factor, but since the high cost of the Swan Ganz catheter limits its routine use, the thermodilution method was not used in this study.

Conclusions

TEE and RCC measurements showed an association in the assessment of MRAP, especially between RAA and $MRAP_{RCC}$. An association with RVSD and moderate agreement between methods were also noted.

Authors' contributions

Each author contributed individually and significantly to the development of this article. Jardim FV, Zacarias L, Masson JB, Zeredo AT: Writing and Performing Surgeries; Azeredo AT, Rassi D, Rassi S: Data Analysis and Writing; Azeredo AT, Graner D, Rassi S, Figueiredo A, Costa S, Sampaio D: Review of the Article and Intellectual Concept of the Article.

Conflict of interest

The author declares that he has no conflict of interest

References

1. Alves JL Jr, Oleas FG, Souza R. Pulmonary Hypertension: Definition, Classification, and Diagnosis. Semin Respir Crit Care Med. 2017;38(5):561-70. doi: https://doi.org/10.1055/s-0037-1606577

2. Hoeper MM, Ghofrani HA, Grünig E, Klose H, Olschewski H, Rosenkranz S. Pulmonary Hypertension. Dtsch Arztebl Int. 2017;114(5):73-84. doi: https://doi.org/10.3238/arztebl.2017.0073

3. Fisher MR, Forfia PR, Chamera E, Housten-Harris T, Champion HC, Girgis RE, et al. Accuracy of Doppler echocardiography in the hemodynamic assessment of pulmonary hypertension. Am J Respir Crit Care Med. 2009;179(7):615-21. doi: https://doi.org/10.1164/rccm.200811-1691OC

4. Foale R, Nihoyannopoulos P, McKenna W, Kleinebenne A, Nadazdin A, Rowland E, et al. Echocardiographic measurement of the normal adult right ventricle. Br Heart J. 1986;56(1):33-44. doi: https://doi.org/10.1136/hrt.56.1.33. Erratum in: Br Heart J 1986;56(3):298298. Klienebenne A [corrected to Kleinebenne A]. Erratum in: Br Heart J 1987 Apr;57(4):396. Klienebenne A [corrected to Kleinebenne A].

5. Galiè N, Humbert M, Vachiery JL, Gibbs S, Lang I, Torbicki A, et al. 2015 ESC/ERS Guidelines for the diagnosis and treatment of pulmonary hypertension: The Joint Task Force for the Diagnosis and Treatment of Pulmonary Hypertension of the European Society of Cardiology (ESC) and the European Respiratory Society (ERS): Endorsed by: Association for European Paediatric and Congenital Cardiology (AEPC), International Society for Heart and Lung Transplantation (ISHLT). Eur Respir J. 2015;46(4):903-75. doi: https://doi.org/10.1183/13993003.01032-2015. Epub 2015 Aug 29. Erratum in: Eur Respir J. 2015;46(6):1855-6.

6. Hambly N, Alawfi F, Mehta S. Pulmonary hypertension: diagnostic approach and optimal management. CMAJ. 2016;188(11):804-12. doi: https://doi.org/10.1503/cmaj.151075

7. Sato T, Tsujino I, Ohira H, Oyama-Manabe N, Ito YM, Yamada A, et al. Right atrial volume and reservoir function are novel independent predictors of clinical worsening in patients with pulmonary hypertension. J Heart Lung Transplant. 2015;34(3):414-23. doi: https://doi.org/10.1016/j.healun.2015.01.984

8. Benza RL, Miller DP, Gomberg-Maitland M, Frantz RP, Foreman AJ, Coffey CS, et al. Predicting survival in pulmonary arterial hypertension: insights from the Registry to Evaluate Early and Long-Term Pulmonary Arterial Hypertension Disease Management (REVEAL). Circulation. 2010;122(2):164-72. doi: https://doi.org/10.1161/CIRCULATIONAHA.109.898122

9. Raymond RJ, Hinderliter AL, Willis PW, Ralph D, Caldwell EJ, Williams W, et al. Echocardiographic predictors of adverse outcomes in primary pulmonary hypertension. J Am Coll Cardiol. 2002;39(7):1214-9. doi: https://doi.org/10.1016/s0735-1097(02)01744-8

10. Fukuda Y, Tanaka H, Ryo-Koriyama K, Motoji Y, Sano H, Shimoura H, et al. Comprehensive Functional Assessment of Right-Sided Heart Using Speckle Tracking Strain for Patients with Pulmonary Hypertension. Echocardiography. 2016;33(7):1001-8. doi: https://doi.org/10.1111/echo.13205

11. Dunlap B, Weyer G. Pulmonary Hypertension: Diagnosis and Treatment. Am Fam Physician. 2016;94(6):463-9. PMID: 27637122.

12. D'Alto M, Romeo E, Argiento P, D'Andrea A, Vanderpool R, Correra A, et al. Accuracy and precision of echocardiography versus right heart catheterization for the assessment of pulmonary hypertension. Int J Cardiol. 2013;168(4):4058-62. doi: https://doi.org/10.1016/j.ijcard.2013.07.005

13. Hemnes AR, Forfia PR, Champion HC. Assessment of pulmonary vasculature and right heart by invasive haemodynamics and echocardiography. Int J Clin Pract Suppl. 2009;(162):4-19. doi: https://doi.org/10.1111/j.1742-1241.2009.02110.x

14. Simonneau G, Gatzoulis MA, Adatia I, Celermajer D, Denton C, Ghofrani A, et al. Updated clinical classification of pulmonary hypertension. J Am Coll Cardiol. 2013;62(25 Suppl):D34-41. doi: https://doi.org/10.1016/j.jacc.2013.10.029. Erratum in: J Am Coll Cardiol. 2014;63(7):746. Erratum in: J Am Coll Cardiol. 2014;63(7):746

15. Mitchell C, Rahko PS, Blauwet LA, Canaday B, Finstuen JA, Foster MC, et al. Guidelines for Performing a Comprehensive Transthoracic Echocardiographic Examination in Adults: Recommendations from the American Society of Echocardiography. J Am Soc Echocardiogr. 2019;32(1):1-64. doi: https://doi.org/10.1016/j.echo.2018.06.004

16. Badano LP, Kolias TJ, Muraru D, Abraham TP, Aurigemma G, Edvardsen T, et al.; Industry representatives; Reviewers: This document was reviewed by members of the 2016–2018 EACVI Scientific Documents Committee. Standardization of left atrial, right ventricular, and right atrial deformation imaging using two-dimensional speckle tracking echocardiography: a consensus document of the EACVI/ASE/Industry Task Force to standardize deformation imaging. Eur Heart J Cardiovasc Imaging. 2018;19(6):591-600. doi: https://doi.org/10.1093/ehjci/jey042. Erratum in: Eur Heart J Cardiovasc Imaging. 2018;19(7):830-3.

17. Munro BH. Statistical methods for health care research. 5th ed. Philadelphia: Lippincott Williams & Wilkins; 2005.

18. D'Alto M, Romeo E, Argiento P, D'Andrea A, Vanderpool R, Correra A, et al. Accuracy and precision of echocardiography versus right heart catheterization for the assessment of pulmonary hypertension. Int J Cardiol. 2013;168(4):4058-62. doi: https://doi.org/10.1016/j.ijcard.2013.07.005

19. Hoeper MM, Bogaard HJ, Condliffe R, Frantz R, Khanna D, Kurzyna M, et al. Definitions and diagnosis of pulmonary hypertension. J Am Coll Cardiol. 2013;62(25 Suppl):D42-50. doi: https://doi.org/10.1016/j.jacc.2013.10.032

20. Masson-Silva JB, Silva Júnior CG. Como eu faço a avaliação ecocardiográfica na hipertensão pulmonar. Arq Bras Cardiol: Imagem Cardiovasc. 2022;35(1): ecom18.

21. Venkateshvaran A, Seidova N, Tureli HO, Kjellström B, Lund LH, Tossavainen E, Lindquist P. Accuracy of echocardiographic estimates of pulmonary artery pressures in pulmonary hypertension: insights from the KARUM hemodynamic database. Int J Cardiovasc Imaging. 2021;37(9):2637-45. doi: https://doi.org/10.1007/s10554-021-02315-y

22. Vijiiac A, Onciul S, Guzu C, Scarlatescu A, Petre I, Zamfir D, et al. Forgotten No More-The Role of Right Ventricular Dysfunction in Heart Failure with Reduced Ejection Fraction: An Echocardiographic Perspective. Diagnostics (Basel). 2021;11(3):548. doi: https://doi.org/10.3390/diagnostics11030548

23. Evaldsson AW, Lindholm A, Jumatate R, Ingvarsson A, Smith GJ, Waktare J, et al. Right ventricular function parameters in pulmonary hypertension: echocardiography vs. cardiac magnetic resonance. BMC Cardiovasc Disord. 2020;20(1):259. doi: https://doi.org/10.1186/s12872-020-01548-4

24. Hemnes AR, Forfia PR, Champion HC. Assessment of pulmonary vasculature and right heart by invasive haemodynamics and echocardiography. Int J Clin Pract Suppl. 2009;(162):4-19. doi: https://doi.org/10.1111/j.1742-1241.2009.02110.x

Review Article

Mitral Annulus Disjunction: Diagnostic Modalities, Clinical Implications, and Prognostic Progression

Disjunção do Anel Mitral: Modalidades Diagnósticas, Implicações Clínicas e Evolução Prognóstica

Alexandre Costa Souza[1], Marcus Vinicius Silva Freire de Carvalho[1], Marco André Sales[1], Suellen Lacerda Bezerra[2], Jorge Adinon Torreão[1], Carolina Thé Macêdo[1]

[1]Hospital São Rafael, Salvador, BA; [2]Fundação Bahiana de Cardiologia, Salvador, BA, Brazil.

Abstract

Mitral annulus disjunction (MAD) is an abnormal insertion of the flexion line of the mitral annulus into the atrial wall. The annulus presents a separation (disjunction) between the posterior leaflet–atrial wall junction and the left ventricular myocardial crest.[1] MAD was first described more than 30 years ago in an autopsy study and is reportedly related to mitral valve prolapse (MVP) in 92% of cases.[2] Since then, several studies have been conducted, and reports on the prevalence of MAD in patients with MVP have varied. Ultimately, it may or may not be associated with mitral regurgitation.

Transthoracic echocardiography is part of initial MVP assessment, allowing its diagnosis and the assessment of related complications. As new diagnostic methods emerged, cardiac magnetic resonance imaging and transesophageal echocardiography improved the assessment of this pathology in terms of its diagnosis, extension, and location.

However, the phenotypic characteristics of MVP that are more closely associated with MAD remain uncertain mainly due to the limited number of patients in classic studies on the subject.

Patients with MAD may develop symptoms related to ventricular arrhythmias, configuring the MAD arrhythmic syndrome, which may progress to sudden death.

The literature presents conflicting prognostic data among several studies on the subject from clear diagnostic criteria and best imaging method to be used to treatment and prognosis. This review describes MAD characteristics associated (or not) with valve prolapse to improve the diagnosis and management of this important pathology.

Mitral annulus disjunction and diagnostic imaging modalities

Mitral annulus disjunction (MAD) has been suggested as a structural abnormality often associated with mitral valve prolapse (MVP) and malignant arrhythmias. To date, transthoracic echocardiography (TTE), transesophageal echocardiography (TEE), and cardiac magnetic resonance imaging (CMRI) have been used to assess MAD. However, none of these modalities has been adopted as a standard reference for the diagnosis of this entity.[3]

Mitral annulus disjunction analysis by transthoracic echocardiography and transthoracic echocardiography

MAD can be diagnosed by TTE in the parasternal longitudinal view and, less commonly, in the apical four- and two-chamber views. MAD distance is usually measured on TTE from the junction of the mitral valve and the left atrial wall to the base of the left ventricular wall during end-systole and in the parasternal long-axis view defined as the longitudinal distance of the MAD inferolateral wall. Equivalent CMRI projections can also detect MAD presence, extent, and location in the systolic phase.[4]

Although the two-chamber view is rarely analyzed in MAD assessments, it seems plausible that it can be clinically identified by echocardiographic imaging along the lower left ventricular (LV) wall similarly to the way it is identified in the inferolateral wall since pathological studies describe MAD at any point around the mitral valve annulus. These observations further reinforce the importance of a routine assessment of the MAD that includes the entire circumference of the valve annulus.

Another important aspect that must be analyzed on TTE is the presence of the Pickelhaube sign (Figure 1). This is an S wave with a high-velocity systolic peak on mitral annulus tissue Doppler (annular systolic velocity > 16 cm/s) that may be useful for detecting significant mitral valve annulus hypermobility. Although consistent data are still lacking in the literature, some studies label it as a risk marker for the arrhythmogenic syndrome associated with MAD.[5]

The study by Tan et al. (2018) analyzed TTE results of 185 patients with severe mitral regurgitation (MR) due to MVP. In this analysis, the researchers classified patients into four subtypes based on valve annulus mobility: type 0, no MAD; type I, hypermobile basal left ventricular segment without MAD; type II, MAD < 5 mm; and type III, MAD > 5 mm. In this scenario, 66.5% of patients were classified as type I, 25.4% as type II, 7.6% as type 0, and only 0.5% as type III.[6] However, these findings may be underestimated due to the greater accuracy of CMRI at detecting MAD, especially when close to 2 mm.[4]

LV ejection fraction (LVEF) should be cautiously measured during TTE using the Simpson method as the disjunction region does not include myocardium and should be excluded from the analysis. Thus, although some case series demonstrate

Keywords

Mitral Valve Insufficiency; Diagnosis; Mitral Valve Prolapse.

Mailing Address: Alexandre Costa Souza •
E-mail: alexandrecostahsr@gmail.com
Manuscript received 4/30/2022; revised 5/18/2022; accepted 5/25/2022

DOI: 10.47593/2675-312X/20223503eabc300

CC BY

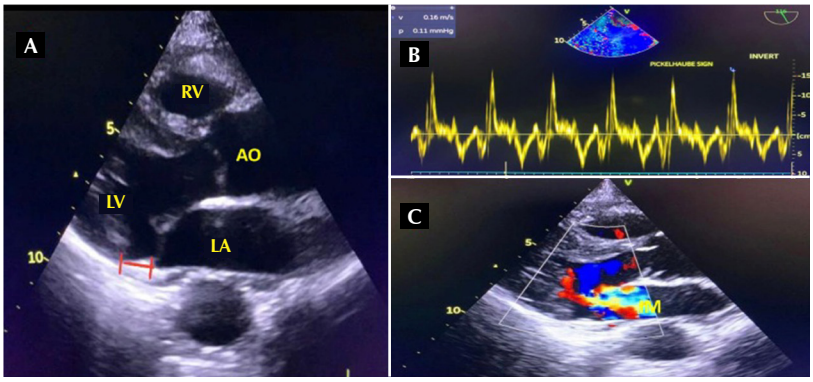

AO, aorta; LA, left atrium; LV, left ventricle; MR, mitral regurgitation; RV, right ventricle. Images cordially provided by Hospital São Rafael - BA.

Figure 1 – *Images A and C demonstrate the presence of MAD associated with mitral regurgitation. B. Pickelhaube sign.*

a decreased LVEF in these patients, this may actually be due to miscalculation. In these cases, it is also important to consider that a decreased LVEF may be more closely related to concomitant MR.[3]

In clinical practice, TEE is requested mainly in patients with inconclusive or technically difficult TTE to better define mitral valve anatomy before surgery. However, it is not routinely used to assess MAD due to its semi-invasive nature.[7]

Mitral annulus disjunction analysis by cardiac magnetic resonance imaging

The ability to visualize the valve annulus and its disjunction varies between different imaging techniques. CMRI can distinguish adjacent structures and characterize myocardial tissue, detecting a minimal disjunction of up to 01 mm from the posterior mitral valve annulus of the left ventricle (LV) wall (Figure 2). In addition, it can accurately identify the presence of myocardial fibrosis in the posterior region of the papillary muscle and in the inferior basal segment of the LV by late gadolinium enhancement.[4]

Dejgaard et al. studied patients with MAD by CMRI and found that gadolinium enhancement in the papillary muscle and the longitudinal MAD distance in the inferolateral wall were predictive of the presence of ventricular arrhythmia. Furthermore, the study reported that late gadolinium enhancement in the anterolateral papillary muscle was strongly associated with a severe arrhythmic event.[3]

Comparison of echocardiography and resonance analysis of Mitral annulus disjunction

Mantegazza et al. studied 130 patients with MVP and MAD to analyze the agreement between the findings documented by the three imaging modalities (TTE, TEE, and CMRI). Their study established a disjunction ≥ 2 mm detected by CMRI as MAD. In this scenario, 88.7% of patients diagnosed with MAD by CMRI were also diagnosed by TTE and 94.7% were also diagnosed by TEE. TTE and TEE accuracy improved to 97.0% and 96.5%% assuming a cutoff value for MAD length by CMRI ≥ 6 mm and ≥ 4 mm, respectively.[4]

The lower MAD detection rate by TTE can be justified by different mechanisms such as inadequate acoustic window, shading or reverberations caused by posterior calcification of the mitral valve annulus, and lower spatial resolution compared to CMRI.[7]

Large-scale studies showed that small disjunctions (< 4 mm) can cause malignant ventricular events; thus, CMRI may be a desirable test that can better identify the presence of MAD and MVP with high arrhythmogenic risk.[8]

MAD myocardial deformation analysis via different methods

MAD may be associated with different left ventricular myocardial deformation due to reduced cardiac muscle in the disjunction segment, such as in the inferolateral basal segment (Figure 3). Accordingly, Wang et al. (2021) analyzed global, radial, and circumferential longitudinal strain using TTE and CMRI in 63 patients divided into three groups of equal numbers of participants (group I, patients with MAD and MVP; group II, patients with MVP only; and group III, patients with no structural cardiac changes).[8]

A strain analysis by CMRI showed that patients with MAD and MVP have statistically lower values in the basal segments, especially in the inferolateral segment in circumferential and radial strain analyses. Although not statistically significant, there was a similar trend of a lower magnitude in the basal segments by longitudinal strain in the group of patients with MAD and MVP compared to the other groups (Figure 4). The CMRI global circumferential strain cutoff point was -18.0%, with a sensitivity of 76% and specificity of 76% for identifying MAD (area under the curve, 0.75). These observations on myocardial deformation by CMRI in patients with MVP and MAD can be explained by the disjunction segments being dragged in the longitudinal and apical direction by the rest of the myocardium during systole, although with less vigorous deformation and contraction in the circumferential or radial direction.[9]

Literature findings show that patients with MAD present unique strain patterns compared to those with MVP but without MAD, especially in the basal segments.[8] In addition, CMRI may be better able than TTE to assess LV characteristics associated with MAD.[9] Longitudinal, circumferential, and radial strain values by TTE were lower in patients with MAD in both studies; however, the differences were not statistically

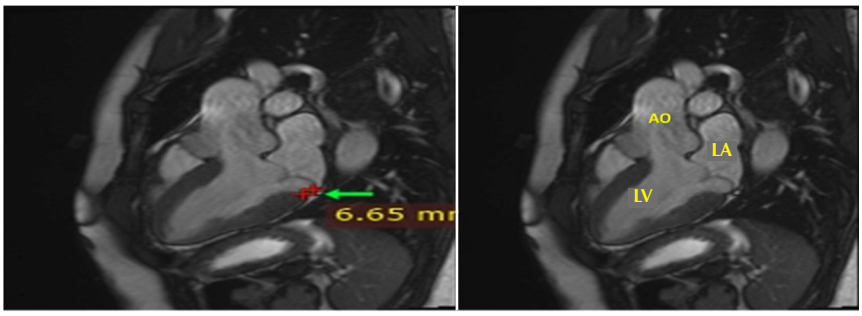

AO, aorta; LA, left atrium; LV, left ventricle.

Figure 2 – *CMRI image showing a MAD measuring 6.65 mm during ventricular systole (red marks).*

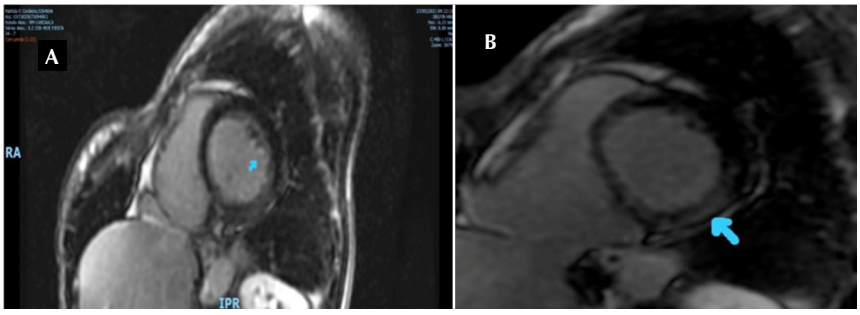

Figure 3 – *Cardiac magnetic resonance image of a patient with mitral annulus disjunction. A. Late enhancement showing fibrosis in the anterolateral papillary muscle. B. Late enhancement showing fibrosis in the inferolateral wall.*

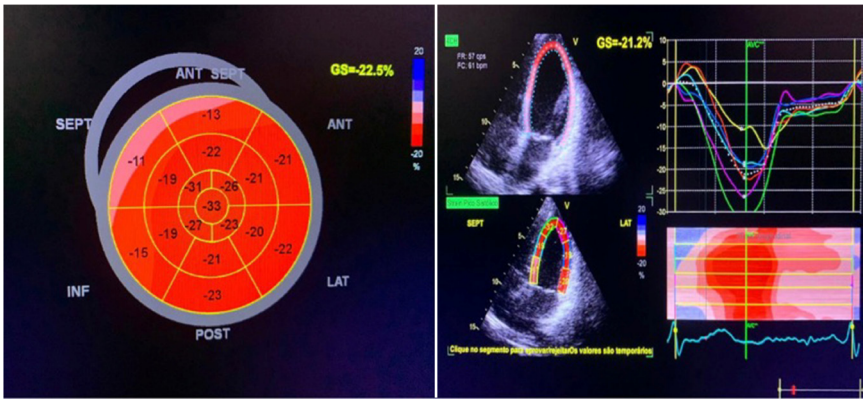

Images cordially provided by Hospital São Rafael – BA.

Figure 4 – *Global longitudinal strain (GLS) in a patient with mitral annulus disjunction. This example shows regional impairment (basal septum) with a preserved GLS.*

significant. Future prospective imaging studies with larger cohorts are necessary to confirm these findings and further assess the usefulness of the strain technique by TTE and CMRI in patients with MAD.

MAD in the normal heart

MAD anatomical findings have received increasing focus in recent studies. Complementary imaging methods play a fundamental role in better characterizing the mitral annulus in the diagnosis of MAD.[10] However, controversy persists about the prevalence of MAD in healthy people, as it remains unclear whether the anatomical diagnosis alone has a prognostic relationship regardless of MVP and associated valve regurgitation. Further prospective studies are necessary to better understand the role of MAD in normal hearts.

Tricuspid annulus disjunction

Tricuspid annulus disjunction (TAD) involves separation between the tricuspid valve annulus and the basal myocardium of the right ventricle (RV) at the end of systole. It can be associated with tricuspid valve prolapse (TVP) and MVP and has a high correlation with MAD, being present in 50% of cases. This strong correlation can be explained by the presence of fibrous annulus disease in this group of patients.[11,12]

Aebal et al. evaluated the right side of the heart in 84 patients previously diagnosed with MAD and reported the presence of TAD in 42 of them. In that study, TAD was defined by CMRI as a longitudinal distance greater than 1 mm between the tricuspid leaflet and the basal segment of the free wall of the RV both in the lateral (four-chamber window) and in the inferior region of the free wall of the RV (inlet and outlet).

There was a strong association between the presence of bi-annulus disjunction and older age, greater MAD distance, circumferential mitral disjunction, and MVP. However, there was no association with cardiac arrhythmias, which may be a selection bias, showing the need for more studies to evaluate TVP and TAD.[11]

Clinical implications

The clinical course of MAD remains a controversial topic that has generated more studies due to its association with arrhythmias and sudden death in the presence or absence of MVP, which is called MAD arrhythmic syndrome and includes the signs and symptoms of arrhythmias present in patients with MAD. Palpitations is the most common clinical presentation, but pre-syncope, syncope, and documented ventricular arrhythmias are also included.[3]

MAD can be detected both in patients with MVP and in those without structural changes on echocardiography. However, MAD is more frequently encountered in patients with TVP. Retrospective studies reported a MAD prevalence of 16–71% in patients with MVP.[13]

Several factors may be associated with a higher MAD frequency in patients with MVP. Putnam et al. retrospectively investigated 90 patients with severe MVP and MR who underwent preoperative computed tomography. MAD was detected in 20% of these patients, being most often associated with female sex, smaller mitral annulus size, and greater posterior leaflet length.[14]

The presence of MAD in patients with MVP is also related to an increased risk of arrhythmias and sudden death. One of the mechanisms studied is that greater leaflet mobility leads to mechanical stress in the inferolateral wall and papillary muscles of the LV, resulting in hypertrophy and subsequent myocardial fibrosis.[2]

A previous study by Perazollo et al. reported a significant correlation between longer MAD and the presence of late enhancement on CMRI in patients with MVP ($R = 0.61$, $p < 0.001$). An anatomopathological analysis of sudden death cases showed a longer MAD in 50 cases with MVP and myocardial fibrosis and in 20 cases without MVP.[15]

MAD extension is significantly related to the presence of non-sustained ventricular tachycardia, with an extension greater than 8.5 mm being a predictor.[5]

Dejgaard et al.[3] studied 116 patients with MAD diagnosed by echocardiography and CMRI. Palpitations were the most common symptom (71% of cases), and severe ventricular arrhythmias were detected in 12% of cases. Cases of arrhythmias were more common in younger patients with a lower LVEF and higher frequency of papillary muscle fibrosis. Greater MAD extension in the inferolateral wall by CMRI was an independent risk factor for ventricular arrhythmias. MVP was detected in 78% of these patients, but there was no association with ventricular arrhythmias, suggesting that MAD is related to symptoms and arrhythmias regardless of MVP status.[3]

The presence of MR and MVP should increase the degree of suspicion of the possibility of associated MAD. However, it can also be present alone, especially in the young population with unexplained ventricular extrasystole.

CMRI may be useful in risk stratification for detecting papillary muscle fibrosis and measuring longitudinal MAD distance in the inferolateral wall.[16,17] However, the clinical course of MAD remains a controversial topic still in the knowledge construction phase.

Predictive factors in surgical repair

Surgical repair in patients with MVP and MR is already a well-established procedure in clinical practice with proven safety and efficacy. However, the increasing ability to diagnose MAD has raised questions about its surgical prognosis and immediate and late results. The real effects of changed lateral mitral annulus dynamics on the subvalvular apparatus in these situations and its influence on final mitral repair result remains uncertain. Thus, better understanding is important to enable surgical planning.

MAD is usually related to MVP with the phenotypic expression of severe diffuse myxomatous disease, profound annular dynamics changes, and excessive annulus dilation at the end of systole, which may reduce the coaptation of its leaflets and be associated with severe MR. However, MAD does not impair valve repair viability and quality, requiring careful suturing of the annulus to the LV so that residual MAD does not persist after repair. Thus, MAD must be diagnosed in the preoperative evaluation and the condition shared with the surgeon and heart team of patients with MVP and severe MR.[18]

A recent study analyzed patients with MVP associated with severe MR eligible for mitral valve repair. The surgical outcome was studied in patients with MAD associated or not with MVP, and the groups were compared for surgical success. MAD was observed in approximately 40% of patients with MVP, with involvement of the two cusps being the most frequent type and invariable involvement of the P2 segment. Mitral repair was performed in 60 patients (98%), and leaflet resection was required more frequently in patients with versus without MAD. There was no intergroup difference in cord implantation, presence or absence of residual MR, or time of aortic clamping. The factors with statistically significant differences that influenced the surgical outcomes of patients with or without MAD were intercommissural diameter, leaflet area, and prolapse volume.[18]

After almost two decades of studies and debates, the annulus in MR correction is used at the surgeon's discretion. However, large series in centers of excellence demonstrated the effectiveness of the annulus in preventing late MR recurrence. DiBardino et al. and Gillinov et al. confirmed the significant advantage of ring annuloplasty over ringless mitral repair in terms of reconstruction durability.[19,20]

A rigid saddle-shaped mitral annulus ring has been widely recognized as able to prevent MR recurrence in cases of MVP.[21] In fact ringless repair is an independent risk factor for postoperative MR recurrence.[22]

Jensen et al. showed that saddle-shaped rigid ring annuloplasty can uniformly distribute tension forces compared to flexible rings and can maintain the medial alignment of the papillary muscles, improving leaflet coaptation and presenting greater repair durability.[23–25]

To date, consensus is lacking on the effectiveness of surgical repair in the presence of MAD, only reports that the use of rigid saddle-shaped rings by experienced surgeons would theoretically increase life expectancy.[9]

Final considerations

MAD is frequently associated with MVP, and its diagnosis is based on multimodal cardiovascular imaging. Echocardiography and CMRI play a complementary role in diagnostic assessments and prognostic characterization. Although the clinical course can vary, part of the growing importance of this diagnosis stems from the possible association with ventricular arrhythmias and sudden death.

Authors' contributions

Souza AC: article conception and final review; Carvalho MVSF: diagnostic modalities in mitral annulus disjunction; Sales MA: surgical treatment; Bezerra SL: organization and collection of images provided by the São Rafael Hospital, Salvador, BA, Brazil. Torreão JA: discussion of cardiac resonance and its diagnostic and prognostic contribution; Macedo CT: discussion of prognostic progression.

Conflict of interest

The authors have declared that they have no conflict of interest.

References

1. Faletra FF, Leo LA, Paiocchi VL, Schlossbauer SA, Pavon AG, Ho SY, et al. Morphology of mitral annular disjunction in mitral valve prolapse. J Am Soc Echocardiogr. 2022;35(2):176-86. doi: https://doi.org/10.1016/j.echo.2021.09.002
2. Hutchins GM, Moore GW, Skoog DK. The Association of Floppy Mitral Valve with Disjunction of the Mitral Annulus Fibrosus. N Engl J Med [Internet]. 1986;314(9):535-40. doi: https://doi.org/10.1056/NEJM198602273140902
3. Dejgaard LA, Skjølsvik ET, Lie ØH, Ribe M, Stokke MK, Hegbom F, et al. The mitral annulus disjunction arrhythmic syndrome. J Am Coll Cardiol. 2018;72(14):1600-9. doi: https://doi.org/10.1016/j.jacc.2018.07.070
4. Mantegazza V, Volpato V, Gripari P, Ghulam Ali S, Fusini L, Italiano G, et al. Multimodality imaging assessment of mitral annular disjunction in mitral valve prolapse. Heart. 2021;107(1):25-32. doi: https://doi.org/10.1136/heartjnl-2020-317330.
5. Carmo P, Andrade MJ, Aguiar C, Rodrigues R, Gouveia R, Silva JA. Mitral annular disjunction in myxomatous mitral valve disease: a relevant abnormality recognizable by transthoracic echocardiography. Cardiovasc Ultrasound. 2010;8:53. doi: https://doi.org/10.1186/1476-7120-8-53.
6. Konda T, Tani T, Furukawa Y. Mitral annular disjunction in consecutive cases: echocardiographic detection. J Am Coll Cardiol. 2013;61(10):E1046. doi: https://doi.org/10.1016/j.ejro.2021.100335
7. Bennett S, Thamman R, Griffiths T, Oxley C, Khan JN, Phan T, et al. Mitral annular disjunction: A systematic review of the literature. Echocardiography. 2019;36(8):1549-58. doi: https://doi.org/10.1111/echo.14437
8. Wang TKM, Kwon DH, Abou-Hassan O, Chetrit M, Harb SC, Patel D, et al. Strain evaluation for mitral annular disjunction by echocardiography and magnetic resonance imaging: A case-control study. Int J Cardiol. 2021;334:154-6. doi: https://doi.org/10.1016/j.ijcard.2021.04.052
9. Essayagh B, Sabbag A, Antoine C, Benfari G, Batista R, Yang LT, et al. The mitral annular disjunction of mitral valve prolapse: presentation and outcome. JACC Cardiovasc Imaging. 2021;14(11):2073-87. doi: https://doi.org/10.1016/j.jcmg.2021.04.029.
10. Toh H, Mori S, Izawa Y, Fujita H, Miwa K, Suzuki M, et al. Prevalence and extent of mitral annular disjunction in structurally normal hearts: comprehensive 3D analysis using cardiac computed tomography. Eur Heart J Cardiovasc Imaging. 2021;22(6):614-22. doi: https://doi.org/10.1093/ehjci/jeab022.
11. Aabel EW, Chivulescu M, Dejgaard LA, Ribe M, Gjertsen E, Hopp E, et al. Tricuspid annulus disjunction: novel findings by cardiac magnetic resonance in patients with mitral annulus disjunction. JACC Cardiovasc Imaging. 2021;14(8):1535-43. doi: https://doi.org/10.1016/j.jcmg.2021.01.028
12. Muraru D, Figliozzi S. Unlocking the mysteries of arrhythmic mitral valve prolapse by CMR imaging: is there a tricuspid annulus disjunction? JACC Cardiovasc Imaging. 2021;14(8):1544-7. doi: 10.1016/j.jcmg.2021.02.030.
13. Tani T, Konda T, Kitai T, Ota M, Furukawa Y. Mitral annular disjunction-a new disease spectrum. Cardiol Clin. 2021;39(2):289-94. doi: https://doi.org/10.1016/j.ccl.2021.01.011
14. Putnam AJ, Kebed K, Mor-Avi V, Rashedi N, Sun D, Patel B, et al. Prevalence of mitral annular disjunction in patients with mitral valve prolapse and severe regurgitation. Int J Cardiovasc Imaging. 2020;36(7):1363-70. doi: https://doi.org/10.1007/s10554-020-01818-4
15. Perazzolo Marra M, Basso C, De Lazzari M, Rizzo S, Cipriani A, et al. Morphofunctional abnormalities of mitral annulus and arrhythmic mitral valve prolapse. Circ Cardiovasc Imaging. 2016;9(8):e005030. doi: https://doi.org/10.1161/CIRCIMAGING.116.005030.
16. Basso C, Perazzolo Marra M, Rizzo S, De Lazzari M, Giorgi B, et al. Arrhythmic mitral valve prolapse and sudden cardiac death. Circulation. 2015;132(7):556-66. doi: https://doi.org/10.1161/CIRCULATIONAHA.115.016291
17. Wunderlich NC, Ho SY, Flint N, Siegel RJ. Myxomatous mitral valve disease with mitral valve prolapse and mitral annular disjunction: clinical and functional significance of the coincidence. J Cardiovasc Dev Dis. 2021;8(2):9. doi: https://doi.org/10.3390/jcdd8020009
18. Essayagh B, Sabbag A, Antoine C, Benfari G, Yang LT, Maalouf J, et al. Presentation and outcome of arrhythmic mitral valve prolapse. J Am Coll Cardiol. 2020;76(6):637-49. doi: https://doi.org/10.1016/j.jacc.2020.06.029.
19. DiBardino DJ, ElBardissi AW, McClure RS, Razo-Vasquez OA, Kelly NE,

Cohn LH. Four decades of experience with mitral valve repair: analysis of differential indications, technical evolution, and long-term outcome. J Thorac Cardiovasc Surg. 2010;139(1):76-83; discussion 83-4. doi: https://doi.org/10.1016/j.jtcvs.2009.08.058.

20. Gillinov AM, Cosgrove DM, Blackstone EH, Diaz R, Arnold JH, Lytle BW, et al. Durability of mitral valve repair for degenerative disease. J Thorac Cardiovasc Surg. 1998;116(5):734-43. doi: https://doi.org/10.1016/S0022-5223(98)00450-4

21. Levine RA, Hagége AA, Judge DP, Padala M, Dal-Bianco JP, Aikawa E, et al.; Leducq Mitral Transatlantic Network. Mitral valve disease--morphology and mechanisms. Nat Rev Cardiol. 2015;12(12):689-710. doi: https://doi.org/10.1038/nrcardio.2015.161

22. Johnston DR, Gillinov AM, Blackstone EH, Griffin B, Stewart W, Sabik JF 3rd, et al. Surgical repair of posterior mitral valve prolapse: implications for guidelines and percutaneous repair. Ann Thorac Surg. 2010;89(5):1385-94. doi: https://doi.org/10.1016/j.athoracsur.2009.12.070.

23. Jensen MO, Jensen H, Smerup M, Levine RA, Yoganathan AP, Nygaard H, et al. Saddle-shaped mitral valve annuloplasty rings experience lower forces compared with flat rings. Circulation. 2008;118(14 Suppl):S250-5. doi: https://doi.org/10.1161/CIRCULATIONAHA.107.746776

24. Jensen MO, Jensen H, Levine RA, Yoganathan AP, Andersen NT, Nygaard H, et al. Saddle-shaped mitral valve annuloplasty rings improve leaflet coaptation geometry. J Thorac Cardiovasc Surg. 2011;142(3):697-703. doi: https://doi.org/10.1016/j.jtcvs.2011.01.022.

25. Askov JB, Honge JL, Jensen MO, Nygaard H, Hasenkam JM, Nielsen SL. Significance of force transfer in mitral valve-left ventricular interaction: in vivo assessment. J Thorac Cardiovasc Surg. 2013;145(6):1635-41, 1641.e1. doi: https://doi.org/10.1016/j.jtcvs.2012.07.062.

Review Article

Stress Echocardiography Using Real-Time 3D Imaging

Ecocardiografia sob Estresse Usando Imagem Tridimensional em Tempo Real

José Roberto Matos-Souza[1], *Guilherme De Rossi*[1]
Universidade Estadual de Campinas,[1] Campinas, SP, Brasil.

Abstract

The need to examine the heart using a three-dimensional (3D) tool is not new. This complex and dynamic organ has always required 3D and real-time understanding. Without this feature, the examiner has to transform two-dimensional images to understand its volume, which requires complex knowledge and approximation interactions. Echocardiography was invented three decades ago, and its improvements resulted in commercial products at the beginning of the century. Some studies demonstrate 3D equivalence with gains in handling the necessary time. We use triplane modalities in our routine, with time gain and less stress on the examiner's upper limb. Thus, 3D examinations can answer more complex questions and provide a more geometric approach to contraction, with thickening being analyzed in the background.

Three-dimensional imaging needs

The first machine capable of presenting three-dimensional (3D) ultrasound images was described[1] in the 1990s. With the technology available at that time, it produced low-definition images, but it was able to provide valuable volumetric information. A long path has been traced toward image enhancement, evolving with transducers with numerous crystals and a high processing capacity. However, the greatest difficulty remained, the need to penetrate between the ribs and reduce the possibility of transducer lens expansion. According to specialists,[2] after nearly 20 years of development, the technology was ready for use. However, the high cost of 3D cardiac examination machines remains an obstacle to the expansion of their use in small- and medium-sized services. A complete device with a 3D heart probe can cost up to four times that of a machine without 3D capabilities but with all current technologies embedded.

A relevant aspect in Brazil is the lack of reimbursement for 3D echocardiography, making the acquisition of the machine a complex step to justifying the investment. In our opinion, the use of 3D stress echocardiography may justify the higher outlay with increased productivity.

Keywords

Echocardiography, Three-Dimensional; Echocardiography, Stress; Imaging, Three-Dimensional.

Mailing Address: José Roberto Matos Souza •
E-mail: E-mail: betojrms@unicamp.br
Manuscript received 3/24/2022; revised 4/15/2022; accepted 5/23/2022

DOI: 10.47593/2675-312X/20223503erer_07

CC BY

Stress echocardiography: A proven and widespread methodology

The most recent stress echocardiography guidelines show a safe and sensitive method of diagnosing several pathologies that can be observed in addition to the rest test.[3] The main mode indicated for investigating induced myocardial ischemia is the one with an exercise bicycle or treadmill, which is justified for use in valve and structural pathologies as well as in diastolic dysfunction analyses. The use of stress medication is limited to patients who cannot exercise and specific aortic stenosis and feasibility research cases despite the possibility of also evaluating exercise feasibility.[4]

We recommend a complete rest test first. However, the stress test should focus on changes in parameters relevant to its completion.

In our services, we use a horizontal exercise bicycle to produce effort with access to all exercise images and phases, following the Balke protocol for increasing loads (Table 1).

We have used the above mode to examine a wide range of pathologies[5] far beyond coronary artery disease[6] and based on extensive literature, mostly on the use of two-dimensional (2D) images and Doppler.

3D echocardiography in stress echocardiography

The use of real-time 3D images in stress echocardiography seems natural and can greatly expand our understanding of ischemic phenomena and ventricular geometry changes.

Peteiro was one of the first echocardiographers to compare 3D and 2D imaging for exercise-induced ischemia[7], as was Yang[8], who used the dobutamine protocol. Sensitivity and specificity were comparable during effort, with 3D being slightly worse for ease of execution. Dobutamine had a significantly reduced image acquisition time with comparable sensitivity and specificity.

The advantages of 3D imaging include a sequence of better ventricular apex visualization, rapid peak image acquisition before heart rate decline, and evaluation of multiple segments from a single position in the apical view.[9]

Table 1 - Exercise images and phases.

Rest	4-chamber	2-chamber	Apical long
Low load	4-chamber	2 chambers	Apical long
Peak	4-chamber	2-chamber	Apical long
Recovery	4-chamber	2-chamber	Apical long

These advantages are more evident when using new devices with higher frame rates and quick access buttons for programmable functions.[10] Learning and understanding 3D imaging requires targeted training and is unnatural for echocardiographers trained only in 2D imaging.

Badano et al.[11] analyzed 44 patients undergoing angiography and reported that 3D had sensitivity and specificity comparable to 2D in devices with higher frame rates and was better to analyze apical changes in the anterior descending territory. The group considers 3D echocardiography equivalent to 2D with advantages in some relevant aspects, making 3D echocardiography appropriate for different applications.

Routine use

We have been using 3D devices in stress echocardiography for just over 2 years, initially in a public university hospital and later in a supplementary medicine laboratory. The first advantage of this is the triplane method with three simultaneous planes, which provides apical long-axis and apical four- and two-chamber views. When we obtain a good four-chamber window, this setting automatically shows the other windows with a good frame rate, normally above 30 frames per second and commonly reaching 60 frames per second. Acquiring just one window to look at all windows reduces the time to acquire the clip by one-third. Performing the tests during the Balke protocol allows image capture at any time during exercise or after interruption, with repeated effort for the left upper limb, which is spared by performing only the four-chamber sections without rotation to obtain the two following sections (Figure 1).

A test routine that could involve up to 12 tests per period uses limb tension equivalent to four tests with 2D and the necessary transducer rotations.

The high frame rate and speed to obtain the complete frame have made this approach the favorite in our stress echocardiography service, where we have already performed more than 3,000 tests since arrival of the 3D machine. All tests start with the triplane mode and all images used in the analysis were in triplane format.

This mode is also easier for beginners, as rotating the transducer to obtain the three necessary planes can be challenging. We noticed the superior performance of the residents when using the triplane method, especially for obtaining the long-axis view, which requires greater transducer rotation and loss of the ideal spot for fast imaging that the test requires.

Real-time 3D use

The triplane mode has some advantages, but it remains a 2D demonstration of the cardiac chambers and does not replace the volumetric view. After decades of technological evolution, 3D images offer a reasonable frame rate with good image resolution. This frame rate can be significantly improved using device settings, ranging from 12 to 24 volumes per second with common settings such as depth and width but also decreasing or removing multi-beat analysis and gaining control and volume (Figure 2).

Adaptation to 3D analysis was facilitated in our stress echocardiography service, which maintains a geometric assessment of contraction and placing geometry variation as the first stress analysis. Thickening is in the second plane and mostly used when geometric variations are found. Using this protocol, the dependence on a high frame rate is much lower, being similar to other imaging methods that also work with low frame rates such as cardiac resonance.

The analysis of the entire heart is facilitated with 3D and provides, even for professionals non-initiated in the method, the understanding that ventricular deformation occurred in the stress condition. The disadvantage is the need to acquire apical long-axis and four- and two-chamber images as each slice presents a volume range.

We performed a volume analysis faithful to the ventricle's geometry that ignored the fast frame rate of the triplane mode.

We should make choices during the test, always starting with the triplane mode. Normal ventricles at rest are completely evaluated using this method. Abnormal ventricles may require 3D technology to ensure more accurate diagnosis.

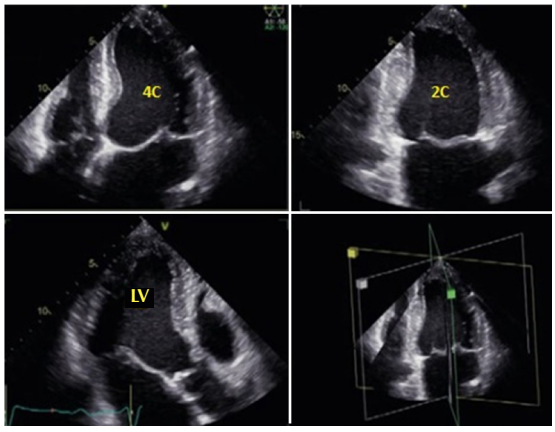

4C: four chambers; 2C: two chambers; LV: apical long axis view.

Figure 1 – *Three simultaneous planes obtained only in the apical four-chamber view.*

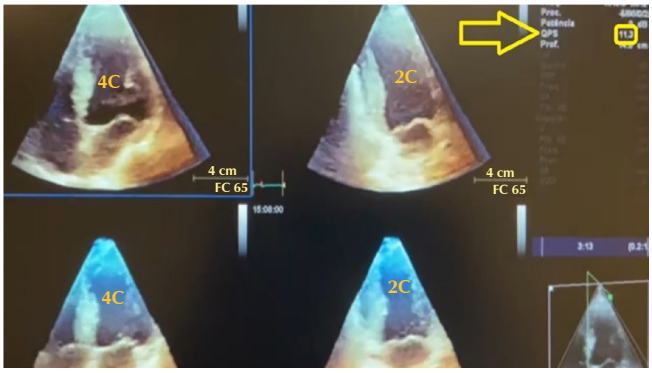

4C: four chambers; 2C: two chambers.

Figure 2 – *Comparable ventricular volumes in the dynamic examination.*

The analysis alternates between the two modalities, takes only seconds, and can be performed during exercise without difficulty. We also capture 3D for training purposes and to enable more complete interpretation of the images, but we use the triplane mode for the indispensable test basis.

Conclusion

Our extensive experience recommends the use of a 3D device to perform stress echocardiography using the triplane mode and real-time 3D.

Reimbursement difficulties are overcome by greater productivity and examiner comfort. However, this scenario is favorable for high-volume services performing above 200 tests monthly.

We believe that technological improvements will still reduce the cost of the machine to the point of being accessible to stress echocardiography services of any size.

Authors' contributions

Research conception and design: Souza JRM, Rossi G; data collection: Souza JRM, Rossi G; data analysis and interpretation: Souza JRM, Rossi G; statistical analysis: Souza JRM, Rossi G; funding: Souza JRM, Rossi G; manuscript writing: Souza JRM, Rossi G; critical review of the manuscript for important intellectual content: Souza JRM, Rossi G.

Conflict of interest

The authors have declared that they have no conflict of interest.

References

1. von Ramm OT, Smith SW. Real time volumetric ultrasound imaging system. J Digit Imaging. 1990;3(4):261-6. doi: https://doi.org/10.1007/BF03168124
2. Lang RM, Mor-Avi V, Dent JM, Kramer CM. Three-dimensional echocardiography: is it ready for everyday clinical use? JACC Cardiovasc Imaging. 2009;2(1):114-7. doi: https://doi.org/10.1016/j.jcmg.2008.10.006
3. Pellikka PA, Arruda-Olson A, Chaudhry FA, Chen MH, Marshall JE, Porter TR, et al. Guidelines for Performance, Interpretation, and Application of Stress Echocardiography in Ischemic Heart Disease: From the American Society of Echocardiography. J Am Soc Echocardiogr. 2020;33(1):1-41.e8. doi: https://doi.org/10.1016/j.echo.2019.07.001
4. Hoffer EP, Dewé W, Celentano C, Piérard LA. Low-level exercise echocardiography detects contractile reserve and predicts reversible dysfunction after acute myocardial infarction: comparison with low-dose dobutamine echocardiography. J Am Coll Cardiol. 1999;34(4):989-97. doi: https://doi.org/10.1016/s0735-1097(99)00340-x
5. Picano E, Pellikka PA. Stress echo applications beyond coronary artery disease. Eur Heart J. 2014;35(16):1033-40. doi: https://doi.org/10.1093/eurheartj/eht350
6. Lancellotti P, Pellikka PA, Budts W, Chaudhry FA, Donal E, Dulgheru R, et al. The Clinical Use of Stress Echocardiography in Non-Ischaemic Heart Disease: Recommendations from the European Association of Cardiovascular Imaging and the American Society of Echocardiography. J Am Soc Echocardiogr. 2017;30(2):101-38. doi: https://doi.org/10.1016/j.echo.2016.10.016
7. Peteiro J, Piñon P, Perez R, Monserrat L, Perez D, Castro-Beiras A. Comparison of 2- and 3-dimensional exercise echocardiography for the detection of coronary artery disease. J Am Soc Echocardiogr. 2007;20(8):959-67. doi: https://doi.org/10.1016/j.echo.2007.01.034
8. Yang HS, Pellikka PA, McCully RB, Oh JK, Kukuzke JA, Khandheria BK, et al. Role of biplane and biplane echocardiographically guided 3-dimensional echocardiography during dobutamine stress echocardiography. J Am Soc Echocardiogr. 2006;19(9):1136-43. doi: https://doi.org/10.1016/j.echo.2006.04.016.
9. Lang RM, Badano LP, Tsang W, Adams DH, Agricola E, Buck T, et al.; American Society of Echocardiography; European Association of Echocardiography. EAE/ASE recommendations for image acquisition and display using three-dimensional echocardiography. J Am Soc Echocardiogr. 2012;25(1):3-46. doi: https://doi.org/10.1016/j.echo.2011.11.010

10. Berbarie RF, Dib E, Ahmad M. Stress echocardiography using real-time three-dimensional imaging. Echocardiography. 2018;35(8):1196-203. doi: https://doi.org/10.1111/echo.14050

11. Badano LP, Muraru D, Rigo F, Del Mestre L, Ermacora D, Gianfagna P, et al. High volume-rate three-dimensional stress echocardiography to assess inducible myocardial ischemia: a feasibility study. J Am Soc Echocardiogr. 2010;23(6):628-35. doi: https://doi.org/10.1016/j.echo.2010.03.020

Long-Term Follow-Up of an Asymptomatic Man with a Cardiac Fibroma

Acompanhamento a Longo Prazo de Paciente do Sexo Masculino com Fibroma Cardíaco Assintomático

Marina Costa Jonas,[1] Maria Fernanda Braggion-Santos,[2] Marcel Koenigkam-Santos,[3] Paulo Henrique Manso,[1] Luiza Frison Dias, André Schmidt,[2] Fernando Amaral[4]

Pediatric1 and Adult4 Congenital Heart Disease Unit, Division of Cardiology2 Imaging Center3 – University Hospital, Ribeirão Preto Medical School, USP, Brazil.

Abstract

Here we describe a case of a 19-year-old asymptomatic man with a left ventricular fibroma on follow-up for 15 years with no treatment required.

Introduction

Cardiac fibroma, first described in 1855, is a benign tumor mainly affecting the left ventricular (LV) free wall that occasionally extends to the interventricular septum. Affected children may be afflicted by significant arrhythmias, creating a sudden death risk requiring prompt surgical treatment.[1] An asymptomatic presentation as well as first manifestation in adults is unusual and follow-up has not been well reported. Here we present the case of an untreated asymptomatic adult who was followed up for 15 years.

Case report

An enlarged heart was incidentally detected on the chest radiograph of a 4-year-old child with respiratory complaints (Figure 1A). Cardiac examination findings were normal. A 12-lead electrocardiogram (EKG) disclosed LV hypertrophy and inverted T waves in the anterior leads (Figure 1B). A 4.1 × 3.7 cm round mass was documented by two-dimensional echocardiography in the apical-lateral LV wall with unobstructed flow (Figure 2A). Twenty-four-hour Holter monitoring revealed one 7-beat episode of non-sustained ventricular tachycardia. On cardiac magnetic resonance (CMR), a 4.7 × 4.2 cm well demarcated mass was found in the lateral-inferior LV wall with late gadolinium enhancement consistent with cardiac fibroma (Figures 2B, 2C). Despite the brief tachycardia episode, surgery was not recommended. For 14 years, the uneventful follow-up was marked by irregular hospital visits every 1–2 years due to personal reasons including long distance to travel, but telephone consultations were frequently performed. Currently, as an asymptomatic 19-year-old with normal cardiac examination findings, he leads a normal life including moderate physical exercise and is taking no medication.

Recent chest radiography (Figure 1C), EKG (Figure 1D), and echocardiography (Figure 2D) findings were similar to those obtained 15 years prior. Holter monitoring findings were normal and arrhythmias were not triggered by a recent exercise test. Sequential CMR showed small growth of the lesion (dimensions: 5.0 × 4.3 cm), which remained stable for the last 9 years (Figures 2E, 2F). Steady-state free precession (SSFP) cine images in systolic (Figures 3A, 3C) and diastolic (Figures 3B, 3D) phases on CMR showed no significant repercussions in left ventricular function at 5 and 19 years of age. The case has been recently discussed and no consensus was reached regarding surgery. According to patient and family desire, regular 6-month follow-ups were offered after a detailed explanation about the risks and benefits of such an approach.

Discussion

Cardiac fibroma, an unencapsulated tumor composed of fibroblasts and connective tissue, is rarely found in adults and usually diagnosed by echocardiography. After the detection of such a mass on echocardiography, the differential diagnosis includes other benign cardiac tumors (especially lipoma and hemangioma).[2] Computed tomography and CMR may define lesion extension and tissue characteristics, thereby improving diagnostic accuracy and treatment planning as in other tumors.[3] In this scenario, CMR has an important role due to its unique capability to provide an advanced myocardial tissue characterization mainly through late gadolinium enhancement sequences, which allows the detection of fibrotic tissue, the main component of cardiac fibroma.[4] Its clinical presentation in children may include syncope, dyspnea, chest pain, episodes of ventricular tachycardia, and, more rarely, cardiac arrest. In this setting, agreement exists regarding complete surgical resection, which, whenever accomplished, is curative with excellent early and late results.[5] However, opinions diverge in cases of the asymptomatic child in whom the risk of sudden death is used to justify a preventable surgical policy, although fatal arrhythmia appears to occur more frequently in the first few years of life.

In 29 recently reported cases, eight patients experienced cardiac arrest in the first three years of life, seven within the first year.[6] In this remarkable retrospective investigation, an interdigitating and entrapped myocardium was uniformly

Keywords

Adult, Fibroma, Cardiac Neoplasms, Sudden Death.

Mailing Address: Fernando Amaral •
Adult Congenital Heart Disease Unit, University Hospital, Ribeirão Preto Medical School USP. Rua Ten. Catão Roxo 3900, Vila Monte Alegre, 14015-010 Ribeirão Preto SP, Brazil.
E-mail: ftamaral@cardiol.br
Manuscript received 4/18/2022; revised 4/20/2022; accepted 5/9/2022

DOI: 10.47593/2675-312X/20223503eabc287

CC BY

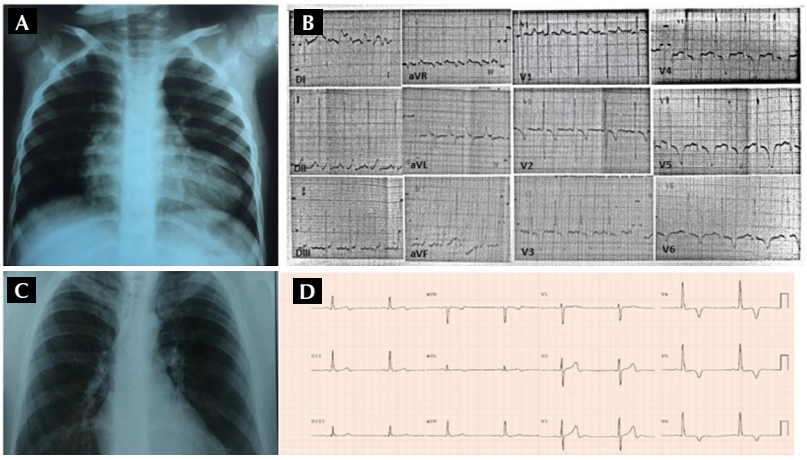

Figure 1 – *Chest radiographs taken at 4 (A) and 19 (C) years of age. Electrocardiogram taken at 4 (B) and 19 (D) years of age.*

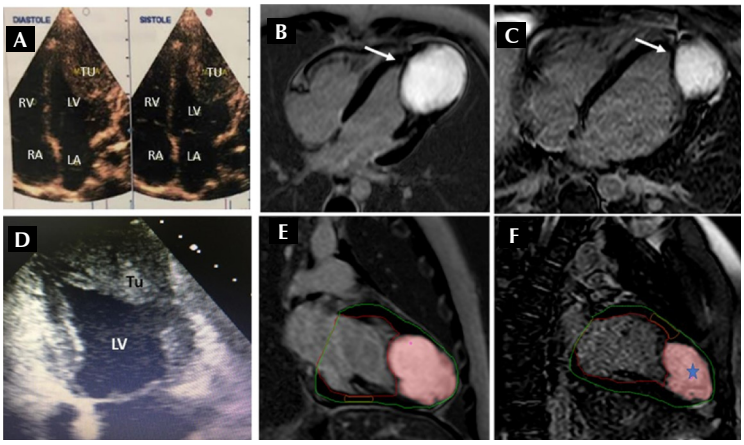

Figure 2 – *Echocardiogram at 4 (A) and 19 (D) years of age (LV, left ventricle; Tu, tumor). Cardiac magnetic resonance imaging late gadolinium enhancement at 4 (B) and (E) and 19 (C) and (F) years of age. (B) and (C) Four-chamber view characteristic hyperintense signal (arrow); (E) and (F) Two-chamber view quantitative analysis of myocardial fibrosis using the full-width half-maximum method showing the hyper-enhanced tumor (star) without areas of fibrosis mixed with normal myocardium (gray zone).*

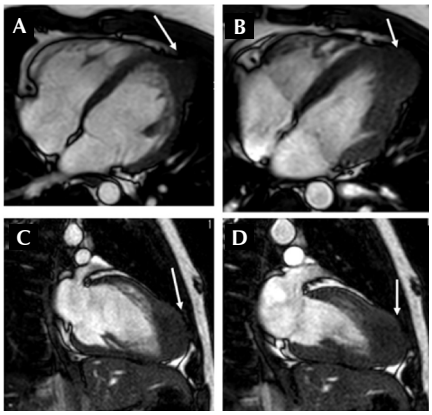

Figure 3 – *Relationship of cardiac fibroma with left ventricular contractility. Steady-state free precession cine magnetic resonance images in systolic (A and C) and diastolic (B and D) phases. (A) and (B) Four-chamber view. (C) and (D) Two-chamber view. White arrows: cardiac fibroma – note the isotense signal of the tumor related to myocardium in these sequences.*

present to various extents within the tumor in at least 80% of cases and presented three interesting features: they were more extensive at a younger age at the time of surgery, were of moderate or marked extension in the majority of patients with cardiac arrest, and tended to gradually disappear with age. This peculiar histologic aspect is similar to the one found in peri-infarct zones and is very likely the arrhythmia substrate since complete surgical resection eliminated the arrhythmia in these cases.

Management of the adult with a cardiac fibroma is debatable. Although surgery is not without risk and ventricular reconstruction might be difficult, 38 patients over 16 years of age were reported by 2011; surgery was performed in 34 of them, including four who were asymptomatic.[7] The case presented here, as well as other non-operated patients without[8] or with routine[9] follow-up, should not be used to recommend a conservative approach for the asymptomatic adult. The consensually obtained recommendation against surgery when the patient was 4 years old was not uniform when he was 19 years old, including a detailed debate in an international panel. The possible risks and benefits of the clinical or surgical management that emerged from these discussions were presented to the patient and his family, who opted for clinical management considering the patient's well-being and strong religious belief. It is interesting to note that the recently described myocardial tongues/entrapment characteristics[6], which tend to disappear with age, suggest that the asymptomatic adult probably has a low risk of arrhythmia; thus, surgery can be avoided. The CMR tumor signal homogeneity demonstrated here, suggestive of a low mixture of normal and pathological tissue, is very likely responsible for the electrical stability noted in our patient. Could this gray zone[10] absence be considered an expression of scarce interdigitating/entrapped myocardium and be used to decide its appropriate management? Which degree of this myocardium abnormality would identify a high-risk patient? There are currently no answers for these questions which could eventually be achieved using a specific registry of a good number of patients adequately followed up, however difficult. In the meantime, common sense and shared decision-making with the patient and family seems the best policy.

Author's statement: Permission was granted by the patient for the publication of this case report.

Authors' Contributions

Research conception and design: Jonas MC, Amaral FA; data collection: Jonas MC, Dias LF; data analysis and interpretation: Jonas MC, Braggion-Santos MF, Koenigkam-Santos M; manuscript writing: all authors; critical review of the manuscript: Manso PH, Schmidt A, Amaral F.

Conflict of interest

The authors have declared that they have no conflict of interest.

References

1. Miyake CY, Del Nido PJ, Alexander ME, Cecchin F, Berul CI, Triedman JK et al. Cardiac tumors and associated arrhythmias in pediatric patients, with observations on surgical therapy for ventricular tachycardia. J Am Coll Cardiol. 2011;58(18):1903-9. doi: 10.1016/j.jacc.2011.08.005.

2. Kimura A, Kanzaki H, Izumi C. A case report of primary cardiac fibroma: an effective approach for diagnosis and therapy of a pathologically benign tumour with an unfavourable prognosis. Eur Heart J Case Rep. 2020;4(4):1-5. doi: 10.1093/ehjcr/ytaa186.

3. Braggion-Santos MF, Koenigkam-Santos M, Teixeira SR, Volpe GJ, Trad HS, Schmidt A. Magnetic resonance imaging evaluation of cardiac masses. Arq Bras Cardiol. 2013;101(3):263-72. doi: 10.5935/abc.20130150.

4. Sara L, Szarf G, Tachibana A, Shiozaki AA, Villa AV, de Oliveira AC et al; Sociedade Brasileira de Cardiologia; Colégio Brasileiro de Radiologia. II Diretriz de Ressonância Magnética e Tomografia Computadorizada Cardiovascular da Sociedade Brasileira de Cardiologia e do Colégio Brasileiro de Radiologia [II Guidelines on Cardiovascular Magnetic Resonance and Computed Tomography of the Brazilian Society of Cardiology and the Brazilian College of Radiology]. Arq Bras Cardiol. 2014;103(6 Suppl 3):1-86. Portuguese. doi: 10.5935/abc.2014S006.

5. Cho JM, Danielson GK, Puga FJ, Dearani JA, McGregor CG, Tazelaar HD et al. Surgical resection of ventricular cardiac fibromas: early and late results. Ann Thorac Surg. 2003;76(6):1929-34. doi: 10.1016/s0003-4975(03)01196-2.

6. Carreon CK, Sanders SP, Perez-Atayde AR, Del Nido PJ, Walsh EP, Geva T et al. Interdigitating Myocardial Tongues in Pediatric Cardiac Fibromas: Plausible Substrate for Ventricular Tachycardia and Cardiac Arrest. JACC Clin Electrophysiol. 2019;5(5):563-575. doi: 10.1016/j.jacep.2019.01.022.

7. Nwachukwu H, Li A, Nair V, Nguyen E, David TE, Butany J. Cardiac fibroma in adults. Cardiovasc Pathol. 2011;20(4):e146-52. doi: 10.1016/j.carpath.2010.08.006.

8. Pozzi M, Deux JF, Kirsch M. Conservative management of left ventricle cardiac fibroma in an adult asymptomatic patient. Int J Cardiol. 2012;161(3):e61-2. doi: 10.1016/j.ijcard.2012.04.125.

9. Lee YJ, Kramer CM. Fourteen-Year Follow-Up Cardiac Magnetic Resonance Imaging of a Large Septal Cardiac Fibroma. Circ Cardiovasc Imaging. 2019;12(7):e009118. doi: 10.1161/CIRCIMAGING.119.009118.

10. Schmidt A, Azevedo CF, Cheng A, Gupta SN, Bluemke DA, Foo TK et al. Infarct tissue heterogeneity by magnetic resonance imaging identifies enhanced cardiac arrhythmia susceptibility in patients with left ventricular dysfunction. Circulation. 2007;115(15):2006-14. doi: 10.1161/CIRCULATIONAHA.106.653568.

Case Report

Three-Dimensional Transesophageal Echocardiography in Native Valve Endocarditis: A Case Report and Similarities Between Echocardiography and Surgical Findings

Ecocardiografia Tridimensional na Avaliação de Endocardite de Válvula Nativa: Um Relato de Caso e Semelhança entre Achados Ecocardiográficos e Cirúrgicos

Giulia Bevilacqua Schmitz[1,2], Amadeu Antonio Bertuol Filho[1,2], Solano Vinicius Berger[1], Rodrigo Petersen Saadi[2,3], Álvaro Albrecht[3], Angela Barreto Santiago Santos[1,2]

[1]Cardiology Division, Hospital de Clínicas de Porto Alegre, RS, Brasil. [2]Post-graduate program in Cardiology and Cardiovascular Sciences. UFRGS, RS, Brasil. [3]Cardiovascular Surgery Division. Hospital de Clínicas de Porto Alegre, RS, Brasil.

Abstract

Native valve bacterial endocarditis is an uncommon, complex, and highly morbid disease that requires prolonged clinical treatment and challenging surgical interventions. Transthoracic and transesophageal echocardiography are paramount assessment tools whose findings are included in the diagnostic criteria. Three-dimensional echocardiography shows further realistic imaging details.

Here we present a case demonstrating the role of echocardiography in the diagnosis of endocarditis and the identification of its complications to show how advanced imaging techniques may have a remarkable resemblance with *in vivo* surgical findings.

Introduction

A 60-year-old woman presented to the emergency department with important lumbar pain, malaise, loss of appetite, and nausea. She reported a progressive weight loss of more than 20 kg over the previous couple of months. She was an obese and fully functional woman. The patient had a Guillain-Barré syndrome episode complicated by deep venous thrombosis some years prior with no clinically relevant sequelae. She was undergoing testing for normocytic and normochromic anemia on an ambulatory basis. She had no previous cardiovascular conditions and no specific family history.

Her vital signs were unremarkable. A physical examination showed normal neurologic status with pale and hydrated mucosae. The cardiac findings were a 3/6 rough systolic murmur in the aortic and mitral areas and a 3/6 aspiration diastolic murmur in the aortic area. This finding led to careful examination of the skin and extremities: her peripheral pulses were of increased amplitude and duration (Corrigan's sign), the fingertips had papular ecchymosis compatible with Janeway's lesions, and the nail beds had a pulsatile "ebb and flow" capillary filling (Quincke's sign). Crackles were detected at the bases of both lungs.

The differential diagnosis implied systemic inflammatory diseases. She presented with insidious symptoms of lumbar pain and malaise. Deep muscle or bone infections should be considered. Inflammatory myopathies, connective tissue diseases, or neoplasm could also explain those findings.

The specific physical examination signs pointed to valvular heart disease. The systolic murmur could be secondary to a benign preexistant condition as simple as mild mitral regurgitation or aortic sclerosis. However, the diastolic murmur should indicate a pathology, especially when it has intense character.

It was unclear if the patient had a previously unknown chronic heart condition that presented as another inflammatory disease or if there was a unique clinical entity responsible for all of the findings.

Considering the peripheral pulse and skin findings, a possible diagnosis was sought and complementary exams were ordered.

Investigations

The blood cell count showed anemia (hemoglobin, 8 g/dL) with normocytic normochromic features, a leftward shift of the white blood count, and an increased serum C reactive protein level. The electrolytes and urinary panel findings were unremarkable.

Abdominal computed tomography (CT) showed inflammation and bone erosion on lumbar vertebral bodies of L2–3 compatible with spondylodiscitis. A bilateral pleural effusion was noted, as were contrast perfusion deficits compatible with renal and spleen infarction.

A transthoracic echocardiogram showed normal LV systolic function. The mitral valve demonstrated a central regurgitation jet compatible with severe mitral insufficiency. There was irregular thickening on both leaflets and nodular vegetation on the atrial face of the anterior leaflet. The aortic valve had thickened cuspids and a central regurgitation jet of severe intensity. Transesophageal echocardiography further detailed the aortic and mitral valves, showing a vegetation on the anterior

Keywords

Endocarditis, echocardiography, Echocardiography, Three-Dimensional , Mitral Valve.

Mailing Address: Amadeu Antonio Bertuol Filho •
Hospital de Clínicas de Porto Alegre, Serviço de Cardiologia. Rua Ramiro Barcelos 2350, sala 2061, CEP: 90035-903. Porto Alegre, RS, Brasil.
E-mail: amadeubertuol@gmail.com
Manuscript received 12/21/2021; revised 4/15/2022; accepted 5/9/2022

DOI: 10.47593/2675-312X/20223503eabc279

CC BY

mitral leaflet with a central perforation. The aortic valve leaflets had increased motion and at least two prolongations (8 mm each) were depicted.

Blood cultures drawn at admission tested positive for *Enterococcus faecalis*.

Management

The broad-spectrum antibiotics vancomycin and cefepime were initiated. The therapy was modified to ampicillin plus gentamicin after the bacteria was cultured and the endocarditis diagnosis was made.

The patient remained stable for the next few days despite her malaise being cumbersome and feeling fatigued after trivial efforts such as bathing. Considering the complicated endocarditis (mitral and aortic severe regurgitation), surgery was indicated.

A large vegetation was found on the atrial aspect of the anterior mitral leaflet with a round perforation. The aortic leaflets were friable, were clad in inflammatory pannus, and had three vegetations.

The transoperative findings (Figure 1) were remarkably similar with the pre-procedure echo images (Figure 2, 3, and 4).

Severe bleeding occurred during the operation that required major volumes of blood products. Although the replacement of both affected valves was technically successful, the patient developed progressive multiorgan failure and died of refractory shock within a few days despite intensive medical support.

Discussion

Native valve infective endocarditis is currently an uncommon disease. Its clinical presentation varies from a very severe onset of sepsis to an insidious and progressing condition diagnosed weeks later.

The possibility of this indolent course implies the need for a high grade of suspicion and adequate workup before

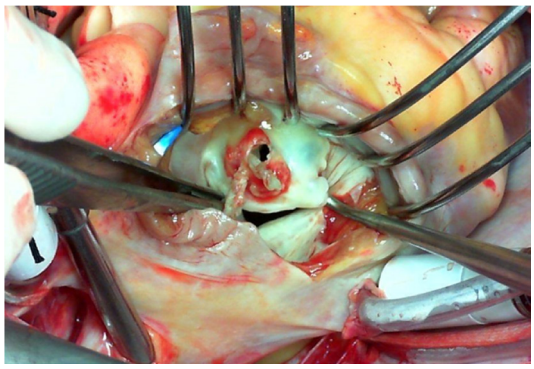

Figure 1 – *Mitral valve with anterior leaflet perforation and vegetations (transoperative view).*

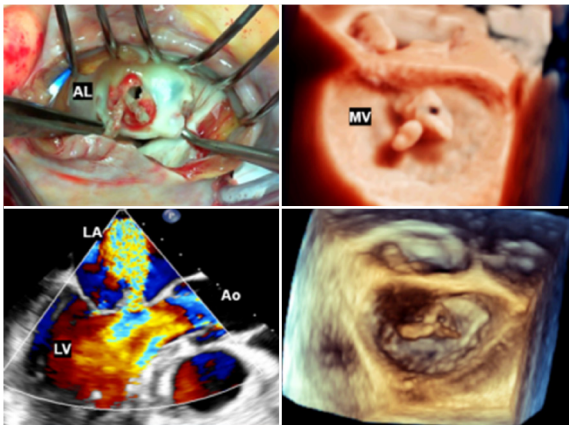

Ao, aorta; LA, left atrium; LV, left ventricle.

Figurw 2 – *Top left: Surgeon's view perspective of a central vegetation and perforation on mitral valve anterior leaflet (AL). Top right: Three-dimensional transesophageal echocardiogram (3D-TEE) showing the same view on True-View filter. Bottom left: Central regurgitation through the perforated leaflet and severe mitral insufficiency. Bottom right: 3D-TEE on a traditional filter.*

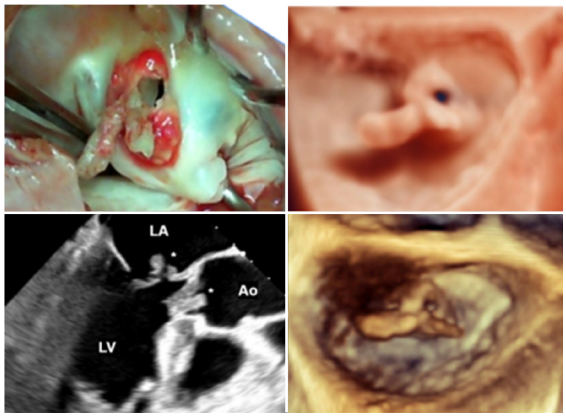

Ao, aorta; LA, left atrium; LV, left ventricle.

Figure 3 – *Top left: Zoomed-in view of the structure and prolongations array of the mitral valve anterior leaflet vegetation. Top right: three-dimensional transesophageal echocardiogram (3D-TEE) True-View image showing remarkable similarity with the surgical findings. Bottom left: Vegetations (*) on both sides of the anterior mitral leaflet and aortic cuspids. Bottom right: Traditional 3D-TEE of the vegetation and mitral valve.*

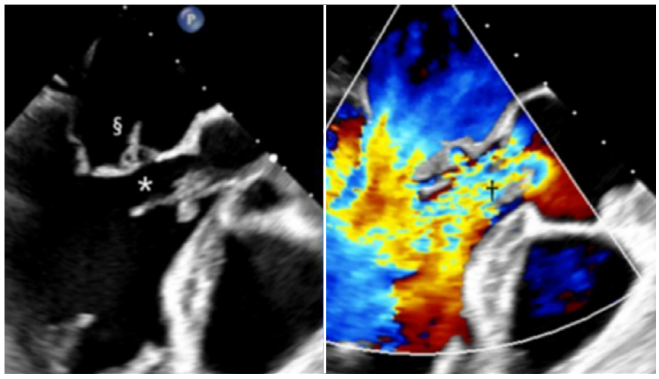

Figure 4 – *Left: Longitudinal transesophageal echocardiogram (TEE) view in end systole. Irregular thickening of the aortic cuspid and an elongated vegetation (*) are evident. The anterior mitral leaflet with the reported vegetation. Right: Longitudinal TEE view in diastole and color Doppler. An aortic regurgitation jet is occupying almost the entire outflow tract (†).*

complications ensue.[1] The most important risk associated factors are implanted prosthetic heart valves or devices, hemodialysis, indwelling catheters, immunosuppression, and the use of injectable recreational drugs.[2] Emboligenic complications can seed virtually any vascularized tissue, culminating in visceral and neurologic sequelae, sepsis, and death.

This patient presented with lumbar pain and was diagnosed with spondylodiscitis, a serious infection of the deep bone tissue of possible emboligenic origin. Thus, the diagnosis of endocarditis was made due to the embolization seen in multiple territories (renal and spleen infarctions). The patient had plenty auscultatory findings; however, these are not always present and a normal cardiac examination alone does not rule out the diagnosis, especially in cases with an earlier clinical presentation.

In addition to a careful history-taking and physical examination, echocardiography is the first-choice exam when suspicion of endocarditis occurs.[3,4] The transthoracic examination is the initial evaluation exam, with sensitivity as high as 80% in more recent clinical series. As it cannot rule out the diagnosis, transesophageal echocardiography can accurately detail the valves, with a sensitivity of 90–100% and a specificity of 90%.[1,2] One must also exclude complications such as perforation, annular abscess, and fistula. The testing should be repeated within the treatment course if the initial imaging exams are negative and clinical suspicion persists, as it increases the sensitivity to near 98%.[5]

The three-dimensional transesophageal echocardiography is becoming more familiar to cardiologists. It has a realistic approximation and can show additional morphological details of lesion mechanisms and refine surgical planning. This modality requires newer ultrasonography machines and software, although it is not cumbersome to learn and perform.[6]

Conclusion

Native valve infective endocarditis is a serious disease whose clinical presentation ranges from subtle to dramatic. It requires

detailed imaging attention with transthoracic and transesophageal studies. Its three-dimensional echocardiographic findings show notable resemblance to operative findings.

Authors' contributions

Manuscript writing: Schmitz GB, Bertuol Filho AA; 2D and 3D image acquisition: Berger SV; surgery and imaging: Saadi RP, Albrecht A; review and general guidance: Santos ABS.

Conflict of interest

The authors have declared that they have no conflict of interest.

Referências

1. Sordelli C, Fele N, Mocerino R, Weisz SH, Ascione L, Caso P, Carrozza A, Tascini C, De Vivo S, Severino S. Endocardite infecciosa: imagem ecocardiográfica e novas modalidades de imagem. J Cardiovasc Echography. 2019;29:149-55.https://doi.org/10.4103/jcecho.jcecho_53_19
2. Cahill TJ, Prendergast BD. Infective endocarditis. Lancet. 2016;387(10021):882-93. doi: 10.1016/S0140-6736(15)00067-7.
3. Baddour LM, Wilson WR, Bayer AS, Fowler VG Jr, Tleyjeh IM, Rybak MJ et al.; American Heart Association Committee on Rheumatic Fever, Endocarditis, and Kawasaki Disease of the Council on Cardiovascular Disease in the Young, Council on Clinical Cardiology, Council on Cardiovascular Surgery and Anesthesia, and Stroke Council. Infective Endocarditis in Adults: Diagnosis, Antimicrobial Therapy, and Management of Complications: A Scientific Statement for Healthcare Professionals From the American Heart Association. Circulation. 2015;132(15):1435-86. doi: 10.1161/CIR.0000000000000296. Erratum in: Circulation. 2015;132(17):e215. Erratum in: Circulation. 2016;134(8):e113. Erratum in: Circulation. 2018;138(5):e78-e79.
4. Schwalm SA, Sugeng L, Raman J, Jeevanandum V, Lang RM. Assessment of mitral valve leaflet perforation as a result of infective endocarditis by 3-dimensional real-time echocardiography. J Am Soc Echocardiogr. 2004;17(8):919-22. doi: 10.1016/j.echo.2004.04.013.
5. Vicent L, Saldivar HG, Bouza E, Muñoz P, Cuerpo G, de Alarcón A et al. GAMES investigators (Appendix 1). Prognostic implications of a negative echocardiography in patients with infective endocarditis. Eur J Intern Med. 2018;52:40-48. doi: 10.1016/j.ejim.2018.01.033..
6. Baldea SM, Velcea AE, Rimbas RC, Andronic A, Matei L, Calin SI et al. D. 3-D Echocardiography Is Feasible and More Reproducible than 2-D Echocardiography for In-Training Echocardiographers in Follow-up of Patients with Heart Failure with Reduced Ejection Fraction. Ultrasound Med Biol. 2021;47(3):499-510. doi: 10.1016/j.ultrasmedbio.2020.10.022.

Acquired Pulmonary Stenosis in an Adolescent with Lymphoma

Estenose Pulmonar Adquirida em Adolescente com Linfoma

Themissa Helena Voss[1], *Flávia Bittar Britto Arantes*[1]
[1]*Federal University of Uberlândia, Uberlândia, Minas Gerais, Brazil.*

Case report

A previously healthy 14-year-old male patient sought emergency care complaining of dyspnea. He was New York Heart Association (NYHA) functional class III and had a 1-month history of orthopnea and night sweats. Auscultation abolished in the left hemithorax, while a chest X-ray revealed extensive opacity in that region. Chest computed tomography (CT) showed a large mediastinal mass with concomitant involvement of the left pleura and retroperitoneal lymph nodes. No other palpable lymph nodes were present on physical examination.

The patient underwent pleuroscopy for pleural biopsy, which identified lymphoid cell proliferation in a "starry sky" pattern compatible with lymphoma and a histochemical pattern compatible with precursor T-cell lymphoblastic non-Hodgkin lymphoma (NHL) (pan-T and TdT, CD4 and CD4 co-expression, and high cell proliferation rate with positive Ki67 test results in 90%). Blast tests in the medulla and cerebrospinal fluid were negative.

Transthoracic echocardiography (TTE) was part of the workup to assess dyspnea and a potentially cardiotoxic pre-chemotherapy protocol. A mediastinal 12 × 5.5 cm mass with an isoechoic and heterogeneous pattern adjacent to the great vessels and causing extrinsic compression with reduced pulmonary artery trunk diameter was visualized (Figure 1). Pulmonary artery flow was turbulent, with a high peak gradient measuring 44 mmHg. The pulmonary valves seemed normal (Figure 2 and Video 1).

He also had a mild anechoic pericardial effusion of 10 mm without hemodynamic repercussions. The longitudinal function was preserved with mitral annular plane systolic excursion of 12 mm and mitral S' wave of 9.9 cm/s. No other changes were identified, with an anatomically normal heart and acquired extrinsic valve disease related to the volume and site of the mediastinal mass. Chemotherapy was promptly initiated with a regimen consisting of cyclophosphamide, vincristine, and prednisone as well as daunorubicin.

Imaging tests (chest CT and TTE) were repeated after the treatment started, and the patient reported complete symptom improvement. CT showed complete mediastinal mass and pulmonary involvement remission in addition to a reduced number and volume of mesenteric and retroperitoneal lymph nodes (Figura 1). TTE showed preserved left ventricular longitudinal function (GLS, -21%) and normal pulmonary artery flow without turbulence or systolic gradients. The patient was discharged on prophylactic Bactrim® and scheduled to return for chemotherapy maintenance.

From an oncological point of view, NHL is the fourth most common neoplasm in children and adolescents. Survival rates with current treatment exceed 80%, with T-cell or follicular lymphomas representing less than 5% of cases in this population. The Ann Arbor classification, widely used in the adult population, was not adapted for the pediatric population, with a preference for staging using the modified St. Jude classification, which considers the primary site of involvement, extranodal sites, and lymph node chain involvement above or below the diaphragm. Lymphoblastic lymphomas most commonly have a T-lineage (90%) and are diagnosed at more advanced stages (stage III–IV > 90%) with bone marrow (30%) and central nervous system (CNS) (5%) involvement. Treatment protocols include several potentially cardiotoxic drugs, such as anthracyclines and vincristine, in addition to corticosteroids and specific protocols for preventing CNS involvement (considered a "sanctuary" for lymphoma).

Mediastinal lymphomas commonly involve the great vessels with hemodynamically significant obstructions capable of generating murmurs or symptoms since they tend to grow laterally and not anteroposteriorly. In case of cardiac involvement, the most common symptoms are chest pain and dyspnea, with an audible murmur noted in 81% of patients. The prognostic implication of the presence of acquired pulmonary stenosis in NHL cases is unknown.

Acquired pulmonary stenosis is rare, with the congenital form being the most common and affecting up to 10% of the pediatric population in varying degrees of importance. Cases of extrinsic compression with supravalvular pulmonary stenosis or right ventricular outflow tract obstruction are even more uncommon, being reported only in case reports or series. Obstruction is usually caused by mediastinal tumors, the most frequent being lymphoma. Other possible causes include aortic aneurysm, mediastinal cysts, extra-mediastinal tumors, and fibrosing mediastinitis. Fixed pulmonary artery obstruction may contribute to symptoms of exertional dyspnea and orthopnea.

Long-term persistent obstruction can increase right chamber pressure, causing tricuspid insufficiency and, in the presence of patent foramen ovale, a right-to-left shunt with cyanosis, and an increased risk of paradoxical embolism. TTE has paramount importance in defining the etiology of pulmonary stenosis — in the case reported here, the mediastinal mass and its compressive effect are clearly visible in the parasternal short-axis window as well as the pulmonary valves with normal morphology, suggesting an external cause of the flow turbulence.

According to Tesoro-Tess et al., basal vessel involvement is more frequent in NHL (42%) than in Hodgkin's lymphoma

Mailing Address: Themissa Helena Voss •
E-mail: themissa@hotmail.com
Manuscript received 3/14/2022; revised 5/9/2022; accepted 5/15/2022

DOI: 10.47593/2675-312X/20223503eabc294

CC BY

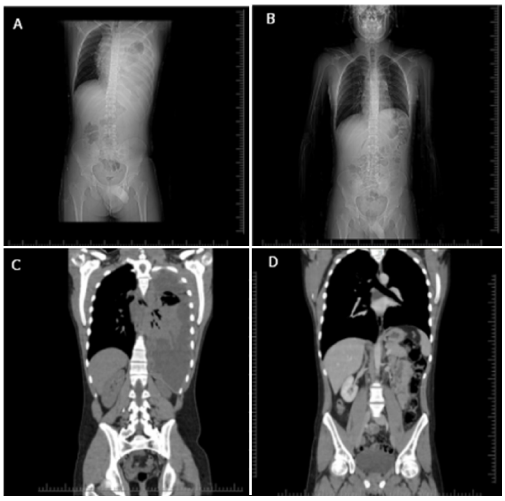

Figure 1 – *Comparison of diagnostic (left images – A and C) and post-chemotherapy (right images – B and D) chest tomography images showing complete regression of the mediastinal mass. The images below (C and D) show the extrinsic pulmonary artery compression and its subsequent relief in the post-treatment period.*

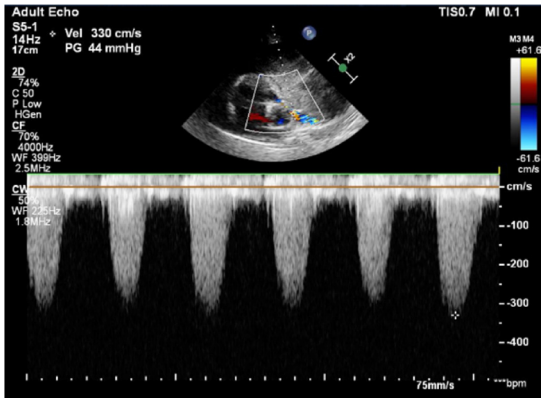

Figure 2 – *Transthoracic echocardiogram in the parasternal short-axis window with continuous Doppler of the pulmonary artery showing a maximum velocity of 3.3 m/s and peak gradient of 44 mmHg due to extrinsic compression by the mediastinal mass.*

(23%). Treatment is based on the underlying cause, consisting of chemotherapy, radiotherapy, or surgery depending on the type of mass identified. When the mass is successfully reduced, the pulmonary circulation flow is restored to normal and symptoms are expected to be resolved. With intensive treatment, refractory or recurrent disease occurs in 10–20% of patients, mainly with local recurrence in cases of T lymphoblastic lymphoma. In these cases, the cure rate decreases to 30%, so patients must maintain regular follow-up and closely monitor their symptoms.

Authors' contributions

Research conception and design: Voss TH; data collection: Voss TH; funding obtention: Voss TH; manuscript writing: Arantes FBB.

Conflict of interest

The authors have declared that they have no conflict of interest.

References

1. Tesoro-Tess JD, Biasi S, Balzarini L, Ceglia E, Matarazzo C, Piotti P, et al. Heart involvement in lymphomas. The value of magnetic resonance imaging and two-dimensional echocardiography at disease presentation. Cancer. 1993;72(8):2484-90. doi: https://

doi.org/10.1002/1097-0142(19931015)72:8<2484::aid-cncr2820720828>3.0.co;2-w

2. WALDHAUSEN JA, LOMBARDO CR, MORROW AG. Pulmonic stenosis due to compression of the pulmonary artery by an intrapericardial tumor. J Thorac Surg. 1959;37(5):679-86. PMID: 13655327.

3. Minard-Colin V, Brugières L, Reiter A, Cairo MS, Gross TG, Woessmann W, et al. Non-Hodgkin Lymphoma in Children and Adolescents: Progress Through Effective Collaboration, Current Knowledge, and Challenges Ahead. J Clin Oncol. 2015;33(27):2963-74. doi: https://doi.org/10.1200/JCO.2014.59.5827

4. Lee HH, Wu XM, Chen YH, Lin LC, External compression of the main pulmonary artery by a diffuse large B-cell lymphoma, Acta Cardiol Sin. 2008;24:109-12.

5. Ozer N, Deveci OS, Kaya EB, Demircin M. Mediastinal lymphoma causing extrinsic pulmonary stenosis. Turk Kardiyol Dern Ars. 2009;37(6):421-4. PMID: 20019459.

6. Pugliatti P, Donato R, Grimaldi P, Nunnari F, de Gregorio C, Zito C, et al. Extrinsic pulmonary stenosis in primary mediastinal B-cellular lymphoma. J Clin Ultrasound. 2015;43(1):68-70. doi: https://doi.org/10.1002/jcu.22133

7. Robinson T, Lynch J, Grech E. Non-Hodgkin's lymphoma causing extrinsic pulmonary artery compression. Eur J Echocardiogr. 2008;9(4):577-8. doi: https://doi.org/10.1093/ejechocard/jen069.

Cor Triatriatum Sinistrum in an Asymptomatic Adult: A Case Report

Triatriatum Sinistrum em Adulto Assintomático: Relato de Caso

Mauro Alves[1], Fernando Antonio de Portugal Morcerf[2], Cynara Silvia Sousa do Amaral[1]
Samig Saúde[1]; ECOR[2], Rio de Janeiro, RJ, Brazil.

Abstract

Cor triatriatum is a rare congenital heart anomaly often diagnosed in early childhood. This case study features an adult with an incidental finding of cor triatriatum sinistrum. Based on the clinical presentation, the patient was treated conservatively. Cor triatriatum sinistrum echocardiographic image findings of this patient are presented along with a narrative review of the literature about this disease.

Introduction

Cor triatriatum sinistrum (CTS) is a rare congenital heart disease that consists of a fibromuscular membrane obliquely dividing the left atrium into two chambers, one proximal, which receives the pulmonary veins, and the other distal, which contains the left atrial appendage and is continuous with the mitral valve. CTS was first observed in 1868[1] by Andral and Church; in 1905, Borst called it "cor triatriatum." It occurs in 0.1% of clinically diagnosed cases of congenital heart disease (CHD) and in 0.4% of autopsy cases of CHD. The prevalence of CTS in the general population is likely less than 0.004%. The embryological origin is controversial; some theories have been created to explain it, the most commonly accepted being the poor incorporation of the common pulmonary vein into the left atrium creating two chambers separated by a septum. Several congenital anomalies may be associated, primarily the ostium secundum atrial septal defect (ASD) and anomalous pulmonary venous drainage.[2]

CTS can be classified by the pulmonary venous drainage and the presence of ASD using Lam classification (Table 1).[3]

The clinical presentation of CTS depends on the total area of the orifice(s) and the presence and severity of any associated defects. Most patients are symptomatic since early childhood with findings similar to severe mitral stenosis (dyspnea and pulmonary congestion).[3] In the natural history of the disease, 75% of untreated affected patients die during childhood[4] due to congestive heart failure and pulmonary edema. Patients with relatively large orifices may remain asymptomatic for life and their condition be incidentally discovered,[5] or they may develop symptoms secondary to stenosis by fibrosis and calcification or mitral regurgitation (MR) after the second and third decades of life.[2]

Keywords

Cor Triatriatum sinistrum, Heart Defects, Congenital, echocardiogram.

Mailing Address: Mauro Alves •
E-mail: mauroalves0308@gmail.com
Manuscript received 12/26/2021; revised 4/15/2022; accepted 5/15/2022

DOI: 10.47593/2675-312X/20223503eabc280

CC BY

Table 1 – Lam classification.

Type	Description
A	The proximal chamber receives the pulmonary veins, while the distal chamber contains the left atrial appendage and the mitral valve. There is no defect in the interatrial septum.
A1	Interatrial communication between the right atrium and the proximal chamber.
A2	Interatrial communication between the right atrium and the distal chamber.
B	The pulmonary veins drain into the coronary sinus.
C	No anatomical connection between the pulmonary veins and the proximal chamber.

Source: Lam CR, Green E, Drake E. Diagnosis and surgical correction of 2 types of triatrial heart. Surgery 1962; 51:127–37. Saxena P, Burkhart HM, Schaff HV, Daly R, Joyce LD, Dearani JA. Surgical repair of cor triatriatum sinister: the Mayo Clinic 50-year experience. Ann Thorac Surg. 2014;97(5):1659-63.

In adults, dyspnea, hemoptysis, and orthopnea are more common[2] due to pulmonary venous drainage obstruction, pulmonary venous/arterial hypertension, and heart failure. Palpitations may also occur due to the presence of cardiac arrhythmias (extrasystole or atrial fibrillation)[6] and systemic thromboembolism due to intra-atrial thrombus formation.[7]

Physical examination findings will vary depending on the associated anomalies. Electrocardiogram (ECG) and chest X-ray findings also depend on the anatomical changes consequent to the severity of these concomitant pathologies.

Echocardiography (ECHO), whether two-dimensional, three-dimensional, or transesophageal, is an important tool in the diagnosis of this congenital condition.[8]

CTS management depends on the hemodynamic effects of the atrial membrane. Patients with restrictive and symptomatic orifices should undergo surgical membrane resection at any age.

This report describes the case of a patient with CTS evaluated with two- and three-dimensional transthoracic Doppler ECHO, transesophageal ECHO, and cardiac magnetic resonance imaging (CMRI) and the management adopted for the case.

Case report and discussion

An asymptomatic 52-year-old man attended a scheduled medical check-up. He was a car driver born in the state of MG, Brazil. He was not using any medications. Pathological history: He reported being hospitalized several times as a child with shortness of breath. His mother said it was asthma. He had a normal childhood and played like other boys his age. He denied having diabetes mellitus, rheumatic fever, alcoholism, or smoking. Family history: His brother and mother died of acute myocardial infarction (AMI), but he id not remember exactly at what age. Physical examination: Normal color. Medium height. Blood pressure: 140/110 mmHg, Heart rate: 72 bpm. An irregular heart rhythm with 2 sound and a B1 split on inspiration was noted. The patient

presented systolic regurgitation murmur ++/(6) in mitral focus. The lungs were clinically clean. The pulse was irregular but universally palpable and of good amplitude. ECG: Sinus rhythm with several ventricular extrasystole and S/V, left atrial enlargement, right atrial enlargement, and an incomplete right bundle branch block. Although the chest X-ray findings were normal, we observed a posterior left atrial increase in the posteroanterior view (Figure 1). Two-dimensional ECHO (2D ECHO) with Doppler showed thoracic aortic ectasia (3.7 cm/2.3 cm/m^2 in the sinuses of Valsalva and 3.25 cm/2.0 cm/m^2 in the ascending proximal segment). Bi-atrial augmentation and mild to moderate MR were also noted. The interatrial septum was intact. The ejection fraction calculated using Simpson's method was 78%. Pulmonary arterial systolic pressure (PASP) was estimated at 33 mmHg. Imaging findings were suggestive of CTS (Figure 2). Abdominal ultrasound (11/24/20) revealed hepatic steatosis and a renal cyst.

A three-dimensional ECHO (Figure 3) showed a clear left intra-atrial membrane (cor triatriatum). MR was moderate to severe due to mitral annular displacement and mitral valve prolapse (MVP). The leaflet was inserted in the posterior part of the left atrium but not in the muscular mitral annulus crest. This type of prolapse is often associated with cardiac arrhythmia.

Transesophageal ECHO showed (Figure 4) enlarged left cavities and slightly decreased global LV systolic function (45.95% ejection fraction using the Teichholz method) with diffuse wall hypokinesia. LV wall hypertrophy was evident. Cor triatriatum was noted in the LA with a maximum gradient of 11 mmHg (mean, 4 mmHg). He also presented MVP with signs of myxomatous degeneration and high posterior leaflet insertion into the LA. Doppler showed moderate MR. Tricuspid valve prolapse with signs of myxomatous degeneration were evident. Mild tricuspid regurgitation was noted with an estimated PASP of 21 mmHg.

CMRI confirmed the CT findings, ruling out other possible associated myocardial structural anomalies (Figure 5).

The patient also underwent a stress test on a treadmill and remained asymptomatic, reaching 9 metabolic equivalents at the end of the test, when he reached 100% of the maximum predicted frequency.

Discussion

CTS is a rare congenital heart malformation with an estimated incidence of 0.1–0.4% among CHDs. In cor triatriatum, the atrium is divided into two parts by a tissue fold, membrane, or a

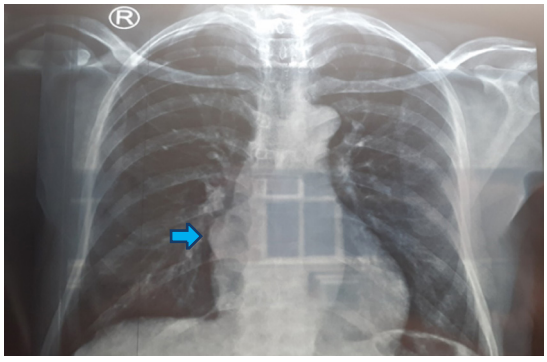

Figure 1 – *Chest X-ray in posteroanterior position. The arrow indicates posterior left atrial enlargement.*

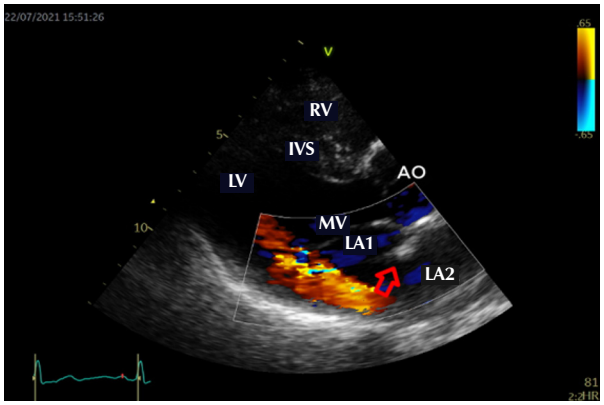

AO, aorta; IVS, interventricular septum; LV: left ventricle chamber LA1, left atrium chamber; LV2, left atrium chamber 2; MV, mitral valve; RV, right ventricle.

Figure 2 – *Transthoracic color Doppler echocardiogram in parasternal section and longitudinal axis. The red arrow indicates the membrane dividing the LA into two chambers (LA1 and LA2).*

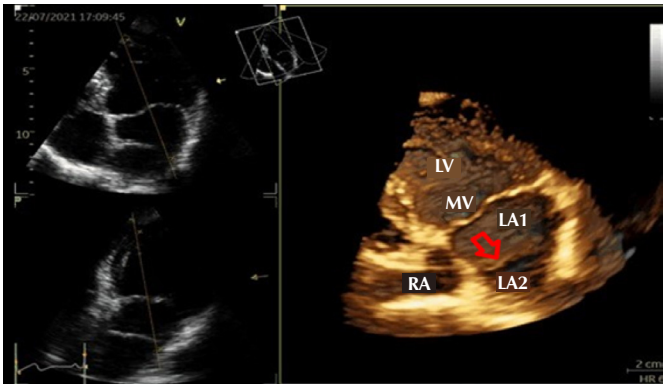

LA1: left atrium chamber 1; LA2: left atrium chamber 2; LV: left ventricle chamber; MV: mitral valve; RA: right atrium.

Figure 3 – *Three-dimensional echocardiogram. The red arrow indicates the membrane dividing the LA into two chambers (LA1 and LA2).*

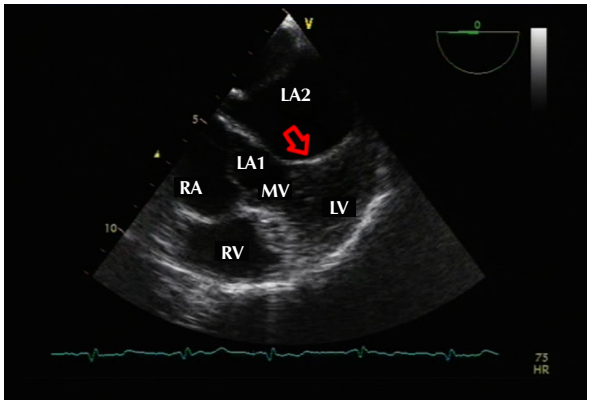

LA1: left atrium chamber 1; LA2: left atrium chamber 2; LV: left ventricle chamber; MV: mitral valve; RA: right atrium; RV: right ventricle.

Figure 4 – *Transesophageal echocardiogram. The red arrow indicates the membrane dividing the LA into two chambers (LA1 and LA2).*

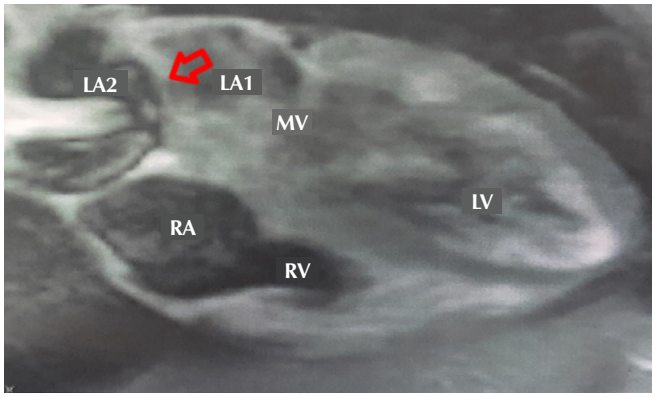

LA, left atrium; LV, left ventricle; MV, mitral valve; RA, right atrium; RV, right ventricle.

Figure 5 – *Cardiac magnetic resonance image. The red arrow indicates the membrane dividing the LA into two chambers (LA1 and LA2).*

fibromuscular band that can occur in the CTS and the right atrium. In the pediatric population, this anomaly may be associated with major congenital cardiac defects, while in adults, cor triatriatum is often an isolated and even rarer finding. The literature reports that adult patients with CTS are rarely asymptomatic.[2,5] ECHO is the most common imaging technique for diagnosing cor triatriatum, although transesophageal ECHO is also needed to precisely define membrane anatomy, its relationship to other structures, and the pulmonary venous drainage pattern.[8]

As the patient was asymptomatic with a New York Heart Association functional class I, we chose to control his systemic blood pressure with an angiotensin II AT1 receptor blocker (ARB) and to follow him up.

Conclusion

During a routine check-up visit, an asymptomatic man was diagnosed with CTS. This congenital condition is rare in adulthood. We performed several imaging tests and a functional test and performed a narrative review of the literature. We opted for conservative treatment and observational follow-up. Imaging findings classified our patient as Lam type A (Table 1). The patient signed an informed consent form allowing the publication of his data.

Authors' contributions

Alves M: study design; Amaral CSS, Morcerf FAP: data collection; Alves M: data analysis and interpretation; Alves M: manuscript writing; Alves M: critical review of the manuscript for important intellectual content; Morcerf FAP: images.

Conflict of interest

The authors have declared that they have no conflict of interest.

References

1. Church WS. Congenital malformation of the heart: abnormal septum in left auricle. Trans Pathol Soc (Lond). 1868;19:188-90.

2. Nassar PN, Hamdan RH. Cor Triatriatum Sinistrum: Classification and Imaging Modalities. Eur J Cardiovasc Med. 2011;1(3):84-7. doi: https://doi.org/10.5083/ejcm.20424884.21

3. Saxena P, Burkhart HM, Schaff HV, Daly R, Joyce LD, Dearani JA. Surgical repair of cor triatriatum sinister: the Mayo Clinic 50-year experience. Ann Thorac Surg. 2014;97(5):1659-63. doi: https://doi.org/10.1016/j.athoracsur.2013.12.046

4. Basavarajaiah S, Oxborough D, Wilson M, Sharma S. Incidental finding of cor triatriatum in an asymptomatic elite athlete. J Am Soc Echocardiogr. 2007;20(6):771.e9-12. doi: https://doi.org/10.1016/j.echo.2006.11.029.

5. Lima RP, Fonseca C, Sampaio F, Ribeiro J, Ribeiro VG. Cor triatriatum sinistrum--description and review of four cases. Rev Port Cardiol. 2010;29(5):827-36. PMID: 20866009.

6. Braulio R, Gelape CL, Figueroa CC, Ribeiro AL. Cor triatriatum with mitral insufficiency and atrial fibrillation in a 36-year-old man. Rev Bras Cir Cardiovasc. 2007;22(2):259-60. English, Portuguese. doi: https://doi.org/10.1590/s0102-76382007000200020

7. Park KJ, Park IK, Sir JJ, Kim HT, Park YI, Tsung PC, et al. Adult cor triatriatum presenting as cardioembolic stroke. Intern Med. 2009;48(13):1149-52. doi: https://doi.org/10.2169/internalmedicine.48.2148

8. Einav E, Perk G, Kronzon I. Three-dimensional transthoracic echocardiographic evaluation of cor triatriatum. Eur J Echocardiogr. 2008;9(1):110-2. doi: https://doi.org/10.1016/j.euje.2007.02.002

Use of Contrast-Enhanced Ultrasound for the Diagnosis of Endoleak After EVAR: A Case Report

Uso do Ultrassom com Contraste para Diagnóstico de Endoleak após Reparo Endovascular de Aneurisma em Ruptura

Ana Carolina N. Netto Djaló[1,2]; Glauber Lutterbach de Oliveira Pires[3,4]; Adriana Ferraz[5]; Carlos Gustavo Abath[6]; Idalécio Souto Fonseca Filho[6]; Milena O. Marques[1]

[1]Hospital das Clínicas, Recife, PE, Brazil; [2]Hospital da Restauração, Recife, PE, Brazil; [3]University Hospital of the Federal University of Vale do São Francisco (UNIVASF), Petrolina, PE, Brazil; [4]Estácio de Juazeiro College, Juazeiro, BA, Brazil; [5]Federal University of Pernambuco, Recife, PE, Brazil; [6]Angiorad, Recife, PE, Brazil.

Introduction

Abdominal aortic aneurysm (AAA), with an estimated prevalence of 4–8% and a higher incidence in men, older people, hypertensive patients, and smokers,[1] can be treated with surgical or endovascular aneurysm repair (EVAR). When well-indicated, EVAR is primarily used since it is less invasive and has lower morbidity and mortality rates.[2] However, due to possible complications, routine clinical and imaging surveillance is necessary to identify or prevent periprosthetic leaks (endoleaks) associated with aneurysmal disease progression.[3]

Accordingly, computed tomography angiography (CTA) has always been considered the gold standard for endoleak surveillance due to its high image quality and usefulness for two- and three-dimensional reconstruction; however, its use of iodinated contrast and exposure to ionizing radiation are disadvantages. Therefore, other post-EVAR control imaging methods such as contrast-enhanced ultrasound (CEUS) have been studied as an endoleak dynamic and high-quality assessment method.[4,5]

The present case report highlights the importance of CEUS as a diagnostic method for detecting endoleak after EVAR, showing its advantages and disadvantages versus those of the current gold standard method.

Case report

A 65-year-old hypertensive and diabetic man had a family history of cerebral aneurysm and AAA. In June 2014, he was diagnosed with an infrarenal AAA up to the aortoiliac bifurcation with a transverse diameter of 8.7 × 8.3 cm and a left common iliac artery (LCIA) aneurysm with a diameter of 2.1 cm.

In July 2014, he underwent infrarenal abdominal aorta EVAR with aortoiliac endoprosthesis placement and left hypogastric artery (HA) embolization (Figure 1).

Keywords

Aortic aneurysm, abdominal, Endoleak.

Mailing Address: Ana Carolina Nascimento Netto Djaló •
E-mail: ana.djalo@ebserh.gov.br
Manuscript received 6/3/2022; revised 6/22/2022; accepted 7/1/2022

DOI: 10.47593/2675-312X/20223503eabc315

CC BY

In October 2019, a follow-up CTA showed an AAA measuring 9.5 × 9.1 cm without evidence of an endoleak. A CEUS type II endoleak was diagnosed and corrected with inferior mesenteric artery (IMA) embolization (Figure 2).

The aneurysmal sac diameter transversely increased to 9.8 cm over 2020 and 2021, but no evidence of an endoleak was seen on CTA. In January 2022, spectral B-mode Doppler CEUS recorded a large infrarenal fusiform aneurysmal dilatation of 9.5 cm × 9.0 cm in transverse and anteroposteriorly, pulsatile flow inside the aneurysm sac on spectral Doppler, and, after the injection of 2.5 mL of microbubble contrast (SonoVue-Bracco), signs of leakage in a peripheral vein inside the aneurysmal sac originating from a lumbar artery (LA) from the right lateral wall and the right branch of the endoprosthesis, which aided the diagnosis of type II and III endoleaks, respectively (Figure 3).

CTA initially performed during the EVAR procedure in April 2022 (Figure 4 A) simultaneously with angiography detected an AAA with a transverse diameter of 9.58 cm, no sign of a type III endoleak, and only LA retrograde flow. Regardless, considering the CEUS findings (Figure 3), we proceeded with the therapeutic strategy, bilaterally implanting iliac endoprostheses to cover the previous endoprostheses (Figure 4B). At the end of the procedure, CTA showed correct endoprosthesis positioning with no signs of endoleak (Figure 4C, Video 1).

The patient recovered well with no recurrence and was discharged on the second postoperative day.

Discussion

Due to increasingly advanced techniques and devices for AAA treatment, most current cases can be endovascularly treated using fenestrated, branched, or even parallel stents. Constantly progressing treatments require intensified surveillance due to the possibility of several complications.[2]

Endoleak, the most frequent complication after EVAR with an incidence of 20–25% among treated patients, is defined as persistent blood flow inside the aneurysm but outside the endoprosthesis, perpetuating aneurysmal sac pressurization and all related risks.[6] Endoleaks can be anatomically classified into five types. Type I endoleaks involve a leak related to lack of endoprosthesis apposition to the healthy wall of the proximal (Ia) or distal (Ib) neck or due to lack of occlusion plug sealing in the iliac branch associated with blood flow from the crossed graft (Ic). Type II endoleaks involve aneurysmal

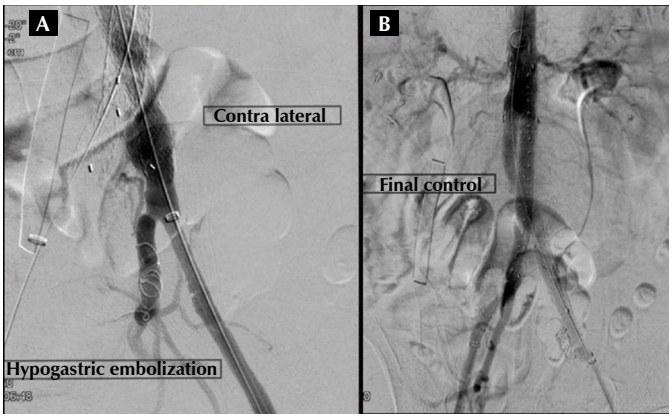

Figure 1 – *Infrarenal and left common iliac artery endovascular aneurysm repair with aortoiliac endoprosthesis placement and left hypogastric artery embolization.*

Figure 2 – *(A) B-mode ultrasound image used to take the transverse diameter measurement. (B) Color Doppler anechoic images inside the aneurysmal sac, mainly on the posterior wall, where pulsatile flow was recorded on spectral Doppler suggestive of the presence of a type II endoleak. (C) Contrast-enhanced ultrasound (SonoVue, Bracco) image showing low-pressure leakage in the anterior wall of the aneurysmal sac at the height of the proximal segment of the endoprosthesis, probably from the inferior mesenteric artery suggestive of a type II endoleak.*

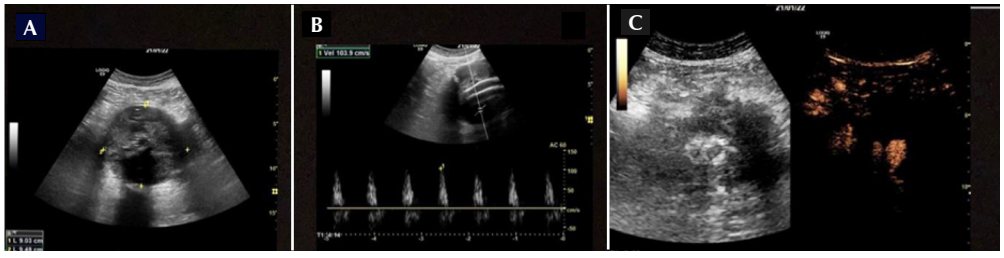

Figure 3 – *(A) B-mode ultrasound image used to take anteroposterior and transverse diameter measurements.(B) Spectral Doppler image showing high-velocity flow inside the aneurysmal sac. (C) Contrast-enhanced ultrasound (SonoVue, Bracco) image showing leakage through the right branch of the endoprosthesis.*

sac perfusion by flow from the collateral arteries such as the LA, IMA, and HA. In type III endoleaks, leakage results from the disconnection or structural failure of the endoprosthesis components. In type IV endoleaks, tissue porosity leads to leakage. Finally, type V endoleaks present as aneurysmal sac pressurization without evidence of blood flow on imaging tests, known as endotension.[2,6] Type I and III endoleaks carry an increased risk of rupture due to pressurizing more quickly and should be treated as soon as possible. Thus, frequent monitoring is imperative as this classification defines a care and action algorithm.[7]

CTA is the standard after EVAR imaging surveillance tests at 1-, 6-, and 12-month follow-up and annually thereafter. This test is fast, is reproducible, has excellent spatial resolution, and uses iodinated contrast with image acquisition through the emission of ionizing radiation.[8]

CTA disadvantages include its use of iodinated contrast, which is nephrotoxic, a limiting factor for non-dialysis-dependent kidney disease patients, and the use of ionizing radiation, which can have deleterious and cumulative effects, such as the development of cancer. An important limitation is not assessing hemodynamics or the flow direction that resulted in leakage in cases of type II endoleaks.[3]

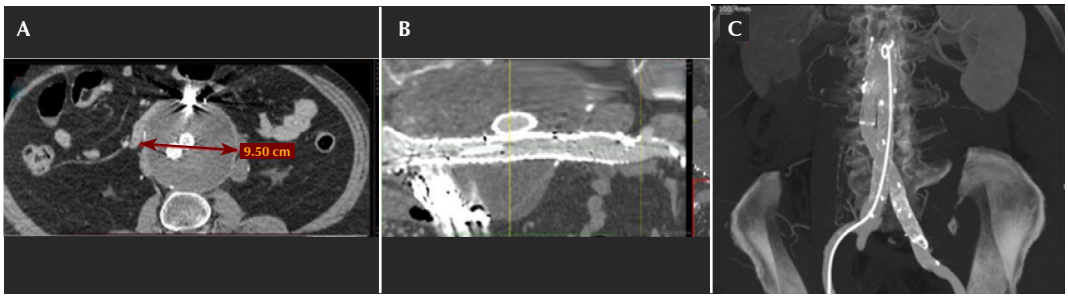

Figure 4 – *(A) Computed tomography angiography (CTA) image taken in the sagittal plane demonstrating the anteroposterior diameter of the aneurysmal sac.(B) CTA image taken in the coronal plane. (C) CTA image taken in the sagittal plane.*

Other imaging methods, such as CEUS, have been highlighted after EVAR surveillance. CEUS uses contrast agents with gas microbubbles (perfluorocarbon or sulfur hexafluoride) surrounded by a phospholipid that are injected into the bloodstream and work as intravascular reflectors of ultrasound waves. Consensus is still lacking on the ideal dose, but recommendations state 1–2.4 mL administered as a peripheral intravenous (IV) bolus. Low-frequency probe scanning is performed for about 5 min after the IV injection. The test assesses the presence of contrast in the aneurysmal sac and endoprosthesis and the perfusion time in relation to inflow and outflow vessels in addition to wave speed and shape in spectral mode.[3] This type of contrast is quickly absorbed into the bloodstream and eliminated by the respiratory system, making it safe for patients with compromised kidney function; it also has the advantage of no radiation exposure.[9]

Recent studies showed that this method has high diagnostic value and is suitable for following this complication.[7] CEUS also has higher sensitivity for detecting endoleaks than CTA, mainly due to detecting flow velocity and direction despite a lack in significant specificity differences between the two imaging modalities.[9] Another CEUS benefit reported in the literature is lower follow-up cost than CTA with high sensitivity.[7–9]

The specific analysis of CEUS for type II endoleaks can stratify cases at greatest need of additional intervention according to endoleak flow velocity and width, parameters that indicate treatment need when >80 cm/s and >4 mm, respectively. Test sensitivity and specificity were 0.62–0.83 and 0.90–0.97 for all types, respectively, and 0.40–0.97 and 0.97–1.00 for types I and III, respectively, thus demonstrating that CEUS is accurate and effective.[10]

However, despite having these advantages, CEUS is limited by being an operator-dependent technique that requires specific training and equipment and can be affected by patient-related factors such as a high body mass index, intestinal gas, aortic wall calcifications, or ascites, and the acquisition of CTA images may be necessary to better characterize the detected leaks and complete the surgical planning.[9]

In the reported case, CTA identified aneurysmal sac dilation but did not visualize the leak (Figure 4) However, CEUS classified the endoleak as type III (Figure 3), enabling safe intervention and repair due to the risk of aneurysmal sac rupture and corroborating the data in the literature about its greater sensitivity.

Therefore, the case described here highlights the importance of CEUS as an alternative to the current gold standard for following up and monitoring endoleaks after EVAR. Despite its limitations, this US method improves the detection of this complication, leading to early diagnosis and favorable outcomes.

Authors' contributions

Case introduction and presentation: Djaló ACN; literature review: Fonseca Filho IS Marques MO; discussion: Pires GLO; manuscript review: Ferraz A, Abath CG.

Conflict of interest

The authors have declared that they have no conflict of interest.

References

1. Clancy K, Wong J, Spicher A. Abdominal aortic aneurysm: a case report and literature review. Perm J. 2019;23:18.218. doi: https://doi.org/10.7812/TPP/18.218
2. Ameli-Renani S, Pavlidis V, Morgan RA. ary endoleak management following TEVAR and EVAR. Cardiovasc Intervent Radiol. 2020;43(12):1839-54. doi: https://doi.org/10.1007/s00270-020-02572-9
3. Williams AB, Williams ZB. Imaging modalities for endoleak surveillance. J Med Radiat Sci. 2021;68(4):446-52. doi: https://doi.org/10.1002/jmrs.522
4. Brown A, Saggu GK, Bown MJ, Sayers RD, Sidloff DA. Type II endoleaks: challenges and solutions. Vasc Health Risk Manag. 2016;12:53-63. doi: https://doi.org/10.2147/VHRM.S81275
5. Cassagnes L, Pérignon R, Amokrane F, Petermann A, Bécaud T, Saint-Lebes B, et al. Aortic stent-grafts: Endoleak surveillance. Diagn Interv Imaging. 2016;97(1):19-27. doi: https://doi.org/10.1016/j.diii.2014.12.014

6. Veith FJ, Baum RA, Ohki T, Amor M, Adiseshiah M, Blankensteijn JD, et al. Nature and significance of endoleaks and endotension: summary of opinions expressed at an international conference. J Vasc Surg. 2002;35(5):1029-35. doi: https://doi.org/10.1067/mva.2002.123095

7. Cantisani V, Grazhdani H, Clevert DA, Iezzi R, Aiani L, Martegani A, et al. EVAR: Benefits of CEUS for monitoring stent-graft status. Eur J Radiol. 2015;84(9):1658-65. doi: https://doi.org/10.1016/j.ejrad.2015.07.001

8. Cao P, De Rango P, Verzini F, Parlani G. Endoleak after endovascular aortic repair: classification, diagnosis and management following endovascular thoracic and abdominal aortic repair. J Cardiovasc Surg (Torino). 2010;51(1):53-69.

9. Harky A, Zywicka E, Santoro G, Jullian L, Joshi M, Dimitri S. Is contrast-enhanced ultrasound (CEUS) superior to computed tomography angiography (CTA) in detection of endoleaks in post-EVAR patients? A systematic review and meta-analysis. J Ultrasound. 2019;22(1):65-75. doi: https://doi.org/10.1007/s40477-019-00364-7

10. Uemura H, Tanaka H, Mitsuno M, Yamamura M, Ryomoto M, Sekiya N, et al. Usefulness of abdominal duplex ultrasound for detecting endoleaks after endovascular aneurysm repair. Ann Vasc Dis. 2019;12(1):30-5. doi: https://doi.org/10.3400/avd.oa.18-00108

Symptomatic Aortic Mural Thrombus in a Patient With COVID-19

Trombo Mural Aórtico Sintomático em Paciente com Covid-19

Milton Sérgio Bohatch Júnior[1], Amanda Fernandes Vidal da Silva[2], Marcelo Bellini Dálio[1], Mauricio Serra Ribeiro[1], Edwaldo Edner Joviliano[1]

[1]Hospital das Clínicas of Ribeirão Preto, University of São Paulo, São Paulo, Brazil; [2]Hospital Base of São José do Rio Preto, São Paulo, Brazil.

A 56-year-old male former smoker with a history of diabetes mellitus developed flu-like symptoms (cough, fever, and myalgia) that worsened after nine days (dyspnea and asthenia) sought medical attention in an emergency care unit. He was hospitalized with novel coronavirus (sudden acute respiratory syndrome coronavirus 2) infection confirmed by polymerase chain reaction testing. His condition progressed with sudden pain in the left lower limb, toe coldness and paresthesia without motor changes, and pain in the third finger of the left hand associated with non-fixed cyanosis. The patient was referred to the emergency room of Hospital das Clínicas of Ribeirão Preto with acute arterial occlusion. On evaluation, he presented non-fixed cyanosis in the distal phalanx of the third finger of the left hand with no pulse or neurological changes throughout the limb. The left lower limb presented no pulse of or arterial flow in the anterior and posterior tibial arteries. He underwent urgent thrombectomy (Rutherford class 2A) with thrombus removal, and limb perfusion was restored with pulsatile tibial artery flow. The patient remained on anticoagulant therapy with unfractionated heparin. Computed tomography angioplasty used to analyze the embolism demonstrated mural thrombi at the origin of the left subclavian artery and in the infrarenal aorta (Figures 1A, 1B). The patient progressed with good arterial condition (resolution of left upper limb non-fixed cyanosis and presence of pulse in the left leg), stayed in the intensive care unit for three days, and was discharged after two days of anticoagulant treatment (rivaroxaban [Xarelto®]). In outpatient follow-up, he remained asymptomatic and presented no new embolic events, and the mural thrombi resolved completely after one year of anticoagulant therapy (Figures 1C, 1D).

Coagulopathy associated with coronavirus infection has been described in a globally increased number of cases of

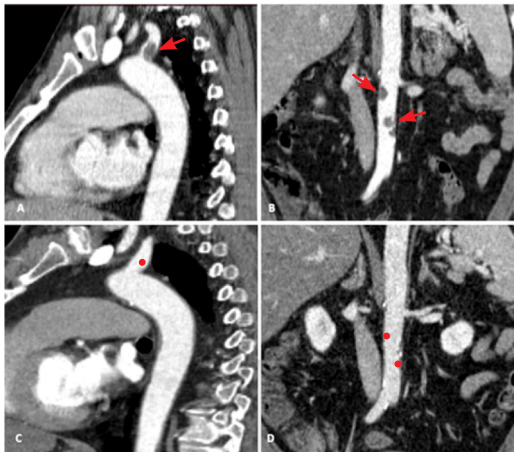

Figure 1 – *(A e B) Computed tomography angiography images showing mural thrombi at the origin of the left subclavian artery and in the infrarenal aorta. (C e D) Complete resolution of mural thrombi after one year of anticoagulant therapy.*

Keywords

SARS-CoV-2, Thrombosis, Aorta.

Mailing Address: Milton Sérgio Bohatch Júnior •
Hospital das Clínicas, Faculdade de Medicina de Ribeirão Preto, Universidade de São Paulo, Rua Tenente Catão Roxo, 3.900 – Monte Alegre.
CEP: 14015-010 – Ribeirão Preto, SP, Brazil.
E-mail: milton.jr87@hotmail.com
Manuscript received 11/9/2021; revised 3/2/2022; accepted 7/1/2022

DOI: 10.47593/2675-312X/20223503eabc270

CC BY

venous thromboembolism and arterial thrombosis, mainly acute myocardial infarction, stroke, and limb ischemia.[1] Multifactorial mechanisms involve endothelial dysfunction interacting with an intense inflammatory condition caused by cytokine storm and complement activation combined with immobilization and a hypercoagulability state.[2–4] The virus itself may directly activate the clotting cascade.[2]

Aortic mural thrombus without occlusive atherosclerotic or aneurysmal disease is an uncommon entity with potentially poor outcomes due to multiple or massive embolizations.[5] Incidental aortic thrombus has an incidence of 0.75% among infected patients with moderate to severe conditions, representing approximately 6.6% of arterial thrombosis cases. This finding highlights critical forms of the disease that are partly mediated by a hypercoagulability state characterized by macro- and microvascular thrombotic angiopathy.[6,7]

Authors' contributions

Research concept and design: Bohatch Júnior MS; data collection: Bohatch Júnior MS, Silva AFV; data analysis and interpretation: Bohatch Júnior MS, Dálio MB; manuscript writing: Bohatch Júnior MS, Silva AFV, Dálio MB, Joviliano EE; intellectual content review: Bohatch Júnior MS, Silva AFV, Dálio MB, Ribeiro MS, Joviliano EE.

Conflict of interest

The authors have declared that they have no conflict of interest.

Referências

1. Fan BE, Chia YW, Sum CL, Kuperan P, Chan SS, Ling LM, et al. Global haemostatic tests in rapid diagnosis and management of COVID-19 associated coagulopathy in acute limb ischaemia. J Thromb Thrombolysis. 2020 [cited 2022 Jul 6];50(2):292-7. Available from: https://pesquisa.bvsalud.org/global-literature-on-novel-coronavirus-2019-ncov/resource/pt/covidwho-1017011

2. Abou-Ismail MY, Diamond A, Kapoor S, Arafah Y, Nayak L. The hypercoagulable state in COVID-19: Incidence, pathophysiology, and management. Thromb Res. 2020;194:101-15. doi: https://doi.org/10.1016/j.thromres.2020.06.029

3. Woehl B, Lawson B, Jambert L, Tousch J, Ghassani A, Hamade A. 4 cases of aortic thrombosis in patients with COVID-19. JACC Case Rep. 2020;15;2(9):1397-401. doi: https://doi.org/10.1016/j.jaccas.2020.06.003

4. Ramacciotti E, Macedo AS, Biagioni RB, Caffaro RA, Lopes RD, Guerra JC, et al. Evidence-based practical guidance for the antithrombotic management in patients with coronavirus disease (COVID-19) in 2020. Clin Appl Thromb Hemost. 2020 [cited 2022 Jul 6];26:1076029620936350. Available from: https://pesquisa.bvsalud.org/global-literature-on-novel-coronavirus-2019-ncov/resource/pt/covidwho-639157

5. Karaolanis G, Moris D, Bakoyiannis C, Tsilimigras DI, Palla VV, Spartalis E, et al. A critical reappraisal of the treatment modalities of normal appearing thoracic aorta mural thrombi. Ann Transl Med. 2017;5(15):306. doi: https://doi.org/10.21037/atm.2017.05.15

6. Cheruiyot I, Kipkorir V, Ngure B, Misiani M, Munguti J, Ogeng'o J. Arterial thrombosis in coronavirus disease 2019 patients: a rapid systematic review. Ann Vasc Surg. 2021;70:273-81. doi: https://doi.org/10.1016/j.avsg.2020.08.087

7. de Carranza M, Salazar DE, Troya J, Alcázar R, Peña C, Aragón E, et al. Aortic thrombus in patients with severe COVID-19: review of three cases. J Thromb Thrombolysis. 2021;51(1):237-42. doi: https://doi.org/10.1007/s11239-020-02219-z